NEW INSTRUMENTATION TO ACCURATELY MEASURE THE FORWARD AND BACKWARD SCATTERING COEFFICIENTS

A Dissertation

by

ELEONORA DE LOS ANGELES FIGUEROA

Submitted to the Office of Graduate and Professional Studies of
Texas A&M University
in partial fulfillment of the requirements for the degree of

DOCTOR OF PHILOSOPHY

Chair of Committee,	Edward S. Fry
Committee Members,	George W. Kattawar
	Alexei Sokolov
	Jaane Laane
Head of Department,	Peter McIntyre

December 2016

Major Subject: Physics

ABSTRACT

The scattering of light is an inherent property of natural bodies of water. As such, they play a crucial role in the study and characterization of natural water. Every optical measurement done in water must take this property into account. The scattering behavior of natural body is a direct consequence of its constituents, including organic and inorganic matter, suspended and dissolved particulates and an air bubbles. In specific, these constituents have characteristic scattering coefficients.

A new optical instrument has been developed to independently determine the total scattering and backscattering coefficient of natural bodies of water. The measurement is performed by the collecting a sample of the scattered light over a large angular range, such that it introduces a $\sin\theta$ weight factor onto the detected volume scattering function of the medium. In other words, the instrument proposed consists of a total scatting coefficient (b) meter and a backscattering coefficient (b_b) meter. These meters measured the exact value of b and b_b, while not making any assumptions of the scatterers.

The measurement principle behind the instrument consists of perfectly calibrated cavity, whose signal output is proportional to the sin of incoming light, scattered light from a light source (532 nm laser). The placement of the meters' aperture is perpendicular to the direction of the laser beam. In other words, at its heart, a highly accurate cosine collector with integrating properties is described.

We present the mathematical description, design and development of each meter, along with calibration methods and results of the prototype test. In short, the backscattering coefficient meter consists of placing a 1.5 mm wide, curved aperture in a 19 mm diameter channel. The instrument's laser beam is centered about the

channel and the scattered light enters the b_b meter through the aperture, yielding and output signal. This signal can be expressed as a direct function of b_b. The b_b meter is the first instrument of its kind to make a direct measurement of b_b. The total scattering coefficient meter consists of placing a 1 cm wide, curved aperture in a 4 mm diameter channel, also centered about a laser beam. The distance of the light source from the center of the meter's aperture defines the angular resolution of the b measurement.

ACKNOWLEDGEMENTS

There are so many people who helped along my life's journey that it is impossible to name them all. Every season of my life and the people therein, have prepared for this moment, and the ones to come. That being said, there are key people whom, without their love and support, this manuscript would not have been possible.

I'd like to thank my parents, Humberto and Dilia Figueroa, for their unwavering belief in me. Since I expressed my love for Physics they have encouraged me to pursue it and done everything in their power to ensure I had access to the best education. In one case, this meant leaving my childhood home in Venezuela, and moving to Texas, USA. They have been my ongoing cheerleaders, comforting me through difficult times, and giving me words of wisdom through uncertain times. Thank you for not questioning the *why*, but instead guiding me toward the *how* to achieve my dreams. Along with them, my sisters Laura and Suzana have always been there as well, encouraging me to move on, and celebrating all my small achievements with as much enthusiasm as if it were their own. Needless to say, I love you guys.

I also have to thank Tom Broiles, my best friend and now husband, as well as as his wonderful baby, Stella, for sticking with me through my entire graduate process. Through thick and thin, hard days and good days, when nothing seemed like it was ever going to work, you were there for me. You were always by my side, pushing me to show the best of what I could be, and to never allowing me to give up. I look forward to our post-grad school life together and not having to drive 3 hours each way to see each other.

My advisor, Dr. Ed Fry, has been a great encouragement. His love for achieving the seemly impossible forces all around him to see every situation from completely

different angles. He sees opportunity when the rest of the world might see obstacles. My years under your mentorship have taught me there truly is no such thing as "impossible". Thank you for your years of guidance, friendship, enthusiasm and support.

The research presented in this manuscript would not have been possible without the entire staff in the machine shop, electronics shop and Chemistry's glass shop. In particular, Erwin Thomas, Steve Payne, Jason Caswell, and James Kirby. Without your constant help troubleshooting electrical components and designing new electrical systems, I would be lost. Tom Weimer, Ron Page, Garrick Garza, John Newkirk, and Bill Merka thank you so much for all the hours of mentorship and work you put in me and my work. Without your oversight, design help, and better judgement during every machining process, this work would have been overwhelming; not to mention, I would have broken pieces way more often! Thank you for being at my side, for being my mentors, and specially for being my friends.

This work was done with the undying support of the WET Labs team. In specific, Mike Twardowski, Alex Derr, Cris Orrico and Mike Dewey. Thank you for hours of help, discussion, ideas, instruction and insight. Thank you for all your encouragement. This task would have been incredibly daunting without your guidance and support.

My labmates David Haubrich, Michael Cone, John Mason, Xinmei Qu, and Andrei Prosvirin have each offered me different opportunities to learn and grow. They have been my mentor, and have allowed me to be theirs. Thank you for your support and advice as well as all the hours of work we spent together.

Graduate school has many challenges, the worst for me was the feeling that, despite years of hard work, I still wasn't good enough finish the degree. This is where my peers at TAMU really shined. They were quick to stand by me and remind me

that we all fear the worst on difficult days. They reminded me I hadn't failed my education, I just hadn't finished learning yet. There are many friends that I made through these last 7 years who encourage me and who I hold dear, but to name them all would be to name half of the students at the Physics and Astronomy department at TAMU and then few more! You guys are all awesome, and I have had the privilege of shaping my academic career amongst amazing peers. Andrew Traverso, Tyler Morrison, Dawson Nodurft, Elizabeth "Sooby" Wood, Heshani Jayatissa, and Lara Suntzeff, you guys were always at my core group of friends. You encouraged me through classes and research, you drank wine with me at every possible occasion, and above all, you were were always someone I could count on. My graduate experience would have been incomplete without each and everyone of you. Words cannot fully express how you helped keep me sane (believe it or not). Thank you. I am honored to have you all as friends.

This list would not be complete without acknowledging Dr. Tatiana Erukhimova. You have been an exemplary role model as a leader and a woman. You don't take no for an answer. You always have an eye on the bigger picture, while still keeping track of all the details and every person involved. I don't think any of us will ever measure up to the standard you have set. But to come close would an achievement in itself. Thanks for all your words of encouragement, every challenge you set before me, and your push to remain involved in other people's lives. You were a constant reminder that a graduate education is more than doing the research, it is investing in younger students and those to come. You allowed us to leave a living legacy through our demos. Our program is a better place for students because of you. My education is infinitely more complete because of you.

Finally, a very special thanks to my committee members. Dr. Alexei Sokolov you have seen my entire graduate career from beginning to end. I've had the honor and

privilege to have you as a mentor during these past few years. From your involvement in OSA to the AMO discussions, you have made it a point to improve and support the student's academic life at TAMU. Thank you for being there for us as someone we can trust and turn to. Also, thank you for your guidance and input, specially in the months leading up to the dissertation defense. Dr. George Kattawar, you have also seen my academic life change from my first day at TAMU. Thank you for your help and mentorship in my research project. It has been a great honor working with you and your students. Dr. John Bevan, thank you for your support. May you rest in peace. Dr. Jaan Laane, I greatly appreciate you stepping up for me when needed. Thank you so much for being someone I could count on.

CONTRIBUTORS AND FUNDING SOURCES

Contributors

This work was supported by a dissertation committee consisting of Professors Edward Fry, Alexei Sokolov, and George Kattawar of the Department of Physics and Astronomy and Professor Jaane Laane of the Department of Chemistry.

All work presented in this dissertation was completed by the student, in collaboration with Mike Twardowski from the Harbor Branch Oceanographic Institute in Florida Atlantic University and Alex Derr, Cris Orrico and Mike Dewey from WET Labs.

Funding Sources

Graduate study was supported in part by National Science Foundation (NSF) under Grant Number OCE-1333425. Its contents are solely the responsibility of the author and do not necessarily represent the official views of the NSF.

TABLE OF CONTENTS

LIST OF FIGURES

FIGURE Page

1. INTRODUCTION

When a photon interacts with a particle, the photon can be assimilated by the particle through a process called absorption or it can be redirected by a process called scattering. The absorption coefficient defines how light is absorbed and the Volume Scattering Function (VSF) describes the angular distribution of the scattered light field.

In the ocean, scattering entities including all organic and inorganic suspended particulates, as well as air bubbles, and even the water molecules themselves. When light is incident on a water sample, the VSF of the resulting light field depends on the internal composition, shape, structure, size, index of refraction, and concentration of the scatterers.[1–4] Every body of water has unique constituents, that give each of these parameters a unique value. Each combination of values exhibits an identifying VSF.

The VSF is one of the fundamental components needed to completely define the scattering behavior of a water sample. It is used as a biological and geomechanical descriptor of particle populations and is used to characterize natural waters.[5–9] It also plays an essential role in many active areas of study within oceanography, affecting areas of physics, chemistry, biology, geology and atmospheric sciences. Most studies include scattering measurements to detect changes in the environment and to understand ecological interactions and particle dynamics

The study of phytoplankton has had significant impact on our understanding of changes in natural bodies of water. Phytoplankton are found in most large, natural bodies of water, and feed manny of the existing creatures in the ocean. Additionally they convert more than 100 million tons of inorganic carbon into simple sugars and

usable O_2 per day. .

Over the past 30 years, optical remote sensing of the water surface from satellites has been a major driver for the research field of in-water optics. Satellite data is greatly relied upon for global information about the ocean. Backscattering measurements are a crucial variable in modeling the radiance leaving the ocean and are a key component of radiative transfer theory and two-flow models. Proper analysis of the data collected from satellites has facilitated the study of environmental changes induced by the climate on a global scale. Remote sensing is critical to understanding ocean biogeochemical cycles. It is the only practical means for observing the dynamic behavior of the surface waters of the ocean over a wide range of spatial scales.

The VSF is key to the study of underwater light propagation and ocean water modeling.[8,10] However, complete VSF measurements are not possible. Near zero degree scattering is difficult to separate from the main beam, and hence difficult to measure. and hence, total scattering coefficient, b, via empirical methods. In contrast, remote sensing methods depend on analyzing backscattered light; knowledge of the spectral backscattering is crucial to expanding the quality and quantity of information that can be extracted from remote observations. These subjects also play an important role in the development of ocean color remote sensing algorithms, particularly for coastal regions. An accurate estimate of the scattering and attenuation characteristics of the upper layer ocean may provide insight into the nature of the particles in suspension.[11]

Improved methods will enhance scientists' understanding of the changes in optical properties of ocean water. The information gained from this data can be given to policymakers, environmental engineers, defense specialists and any agency with an interest in optical water quality to make decisions that affect us worldwide.

Originally, the water sample was observed via microscopes. This was the primary

method to determine the overall particle concentration and provide estimates for the distribution of particles. This method was not favored for its labor-intensiveness. It was impractical to routinely analyze high number of samples with enough particles to make the measurement statistically significant.

In 1880, Ludwig Valentin Lorenz developed and published the first theoretical treatment of particle scattering[12] which he later expanded to make more inclusive.[13] By 1908, Gustav Mie expanded the theory using Maxwell's equations. This gave a complete analytical VSF of the suspended particles.[14] This combined theory is known today as the Lorenz-Mie Theory or Mie Theory for short. With a better understanding of the scattering behavior of small particles, the ocean optics scientific community created new instruments and techniques to improve the VSF measurements and particle characterization methods. In 1972, Petzold et al published a complete set of data on the VSF of three types of natural waters (deep clear oceanic water, nearshore ocean water and very turbid harbor water), as well as in-lab water samples. Eight water samples total.[15] His data is still used as reference sets today.

Thus far, ocean optics researchers have developed many techniques to study ocean waters. One straightforward method is to measure the VSF and calculate the desired scattering coefficients from the value. By knowing the VSF with high resolution, b_b can be easily calculated. Several Volume Scattering Function (VSF) meter designs are employed both on table tops and in *in situ* to obtain these values. Most setups consist of a collimated beam of light which interacts with a small volume sample. Outside the volume is a detector which rotates about the sample collecting scattered light at small angle intervals.

This setup has inherent limitations. For starters, at small forward scattering angles, it is difficult to collect the scattered light without the interaction of the unscattered collimated beam. At large backscattered angles, the detector casing

might block part of the incoming beam. Furthermore, because of the VSF profile (with the forward scattered light up to six orders of magnitude more intense than backscattered light), the detector must have a very large dynamic range. In addition to these complications, in the case of low levels of scatterers present (e.g.: deep ocean waters), the sample size necessary to accurately make a measurement representative of the bulk sample might be too large to allow high resolution of VSF measurements. Finally, these designs are clearly made with tabletop applications in mind, making it difficult to use *in situ*.

Many designs have been used to measure the scattering coefficient of water samples, including integrating spheres (a cavity with inner walls coated with a highly reflecting material) to assist in measuring the backscattered light.[16–18] Where a beam of light enters the sphere through a small opening, it traverses through the entire cavity, and then encounters the cell containing the liquid sample. The design of the integrating sphere acts as a diffuser and light trap for the back scattered light, eventually leading the light to a detector where it is measured. However, the flat cuvette window where the sample is located reflects some of the scattered light, keeping it out of the integrating cavity. Kim *et al.* found a way to minimize this effect[6] but their publication was only a theoretical model. These setups rely on taking a small sample of the water and placing it in a tabletop machine. Although there are some advantages to being able to test the sample in comfort of a personal laboratory, there are huge drawbacks to consider.

The main consequence of the tabletop approach is the necessity to remove water samples from their natural environment - this process can potentially contaminate the sample, changing the physical composition of the sample before it is analyzed. The storage and displacement process may also disrupt the particle assemblage from their natural state. In fact, the very act of removing the sample from the water has

the potential of altering the physical structural qualities of the sample components. In addition, the organic nature of the majority of particulate matter in these samples disintegrate quickly once removed from their natural environment, making these measurements time-sensitive. To measure b and b_b, an instrument capable of *in situ* measurements is preferable.

The most popular method to obtain the scattering coefficients involves the use of inversion models which provide empirical relationships between specific scattering angles to the total VSF of the sample.[5,19,20] With these models it is possible to predict the backscattering coefficient. Unfortunately, the models rely on additional information, such as particle size distribution and concentrations. In other words, prior information is needed to complete the analysis. When this information is unknown, they are assumed depending on the sampled water type. As a result, the calculated values can be considered an educated best estimate of the actual scattering coefficient value. This means also means that cases where the VSF does not follow the standard expected behavior cannot properly studied since they will have the highest measurement errors.

To avoid the inversion problem, Haubrich *et al.*[21] developed a prototype for a backscattering meter which showed more promise as compared with other designs. Their design was expected to directly measure the backscattering coefficient, without any prior knowledge of the VSF. However, their prototype is not well suited for long *in situ* measurements. Without constant oversight particles can easily be trapped at the indentation in the 45° window, blocking the incoming (backscattered) light from entering the detector, rendering the instrument useless. The suggested prototype might create too much turbulence, destroying delicate structures before any measurements are taken.

A limited number of b_b meters exist commercially, all based on the inversion model

technique (including the Hydroscat series from HOBI Labs, Inc, the ECO BB series from WETLabs, Inc). Their accuracy vary in the range of 10% to a few percent, and, in many cases, also depend on the prior knowledge of the VSF of the sample. To date, there is no instrument that *directly* measures b_b. To our knowledge, there is currently no commercial instrument capable of measuring or estimating b or b_f *in situ*, either. Despite years of study, characterizing and predicting variability in the ocean's optical properties is still a challenge. Better, more accurate, instrumentations capable of consistently measuring b and b_b are needed in the field.

This document describes an instrument designed to measure the total scattering coefficient, b, and the backscattering coefficient, b_b, with unprecedented accuracy. In addition, the design will satisfy the size restrictions needed to be used on autonomous underwater vehicles, and be simple enough for any user to get the necessary information desired out of every aquatic environment. Our final instrument consists of two meters: a b_b meter and a b meter. The completion of this instrument will fundamentally revolutionize autonomous optical measurements, impacting light scattering studies for any remote sensing application, as well as in-water bio-optical applications.

2. BACKGROUND

The behavior of light as it interacts with an aqueous sample is strongly defined by the constituents suspended in the sample. In this section I will describe the difference between inherent and apparent optical properties of water. Please note that these properties define a bulk sample, and should not be used for individual molecules. I will also define most of the fundamental concepts used throughout the dissertation.

2.1 Optical Properties of Water

2.1.1 Inherent Optical Properties VS. Apparent Optical Properties

Inherent optical properties, or IOPs, are characteristics of the sample and do not depend on the ambient light. They are affected by materials that make up the particle or dissolved substance, including the index of refraction of that material relative to that of the surrounding water, the size and shapes of these particles, and the number of particles present.

In other words, these properties are particular to the sample of the sample, whether or not there is any light present. The IOPs more easily tested since they can be measured in the laboratory environment, as well as in situ in the ocean.

As mentioned in the introduction, the energy of the photons can be assimilated water sample through a process called absorption. The absorption coefficient $a(\lambda)$ describes how far into the sample light can travel before it is absorbed. Low values of absorption coefficients indicate low absorption of light.

Similarly, the Volume Scattering Function (VSF) $\beta(\lambda, \theta, \phi)$ describes how the medium redirects unpolarized light. It characterizes the intensity of the scattered light as a function of angle. In mathematical terms it can be expressed as the differential scattering cross section per unit volume.

Once the absorption coefficient and the VSF are known, other optical properties can be derived (e.g.: index of refraction n, total, forward and back scattering coefficients - $b(\lambda), b_f(\lambda)$ and $b_b(\lambda)$ respectively).

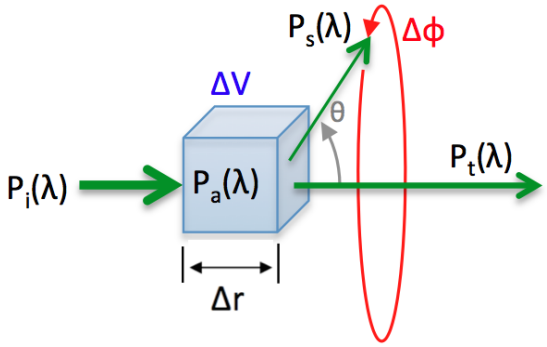

Figure 2.1: Geometry used to define inherent optical properties

A visual interpretation would help define the IOPs. Consider Fig. 2.1. A collimated beam illuminates a small volume ΔV of water. The beam comes from a monochromatic source of wavelength lambda and has an incident power of $P_i(\lambda)$. We define the power to be absorbed as $P_a(\lambda)$, the power to be scattered as $P_s(\lambda)$ and the total power transmitted through ΔV (a distance of Δr) as $P_t(\lambda)$. At this point, we assume no photons are reemitted at a different wavelength, such that

$$P_i(\lambda) = P_a(\lambda) + P_s(\lambda) + P_t(\lambda). \tag{2.1}$$

We define the absorptance $A(\lambda)$, scatterance $B(\lambda)$, and transmittance $T(\lambda)$ as the fraction of incidence power absorbed, scattered and transmitted in ΔV as

$$A(\lambda) = \frac{P(\lambda)_a}{P(\lambda)_i} \tag{2.2}$$

$$B(\lambda) = \frac{P(\lambda)_s}{P(\lambda)_i} \tag{2.3}$$

$$T(\lambda) = \frac{P(\lambda)_t}{P(\lambda)_i} \tag{2.4}$$

such that

$$A(\lambda) + B(\lambda) + T(\lambda) = 1 \tag{2.5}$$

It is more common to describe these IOP in terms of the absorption and scattering coefficients, which is the absorptance and scatterance per unit distance in the sample. Therefore, we define the absorption coefficient as

$$a(\lambda) \equiv \lim_{\Delta r \to 0} \frac{A(\lambda)}{\Delta r} \qquad [m^{-1}] \tag{2.6}$$

and the scattering coefficient as

$$b(\lambda) \equiv \lim_{\Delta r \to 0} \frac{B(\lambda)}{\Delta r} \qquad [m^{-1}] \tag{2.7}$$

In addition to these values, there is equal interest in how much total power is lost in the transmission of the beam. By adding all losses (absorption and scattering of light) we can describe the extinction of the beam by defining the beam attenuation coefficient

$$c \equiv a(\lambda) + b(\lambda). \tag{2.8}$$

The Bouger-Beer-Lambert Law describes the exponential decrease of power through a scattering material. At some distance x we can expect the remaining power to be

$$P(x) = P(x = 0)e^{-(a,b,c)x} \tag{2.9}$$

We return attention to the VSF taking into account the angular distribution of the scattered power. We define the VSF as

$$\beta(\lambda,\theta,\phi) \equiv \lim_{\Delta r\to 0}\lim_{\Delta\Omega\to 0}\frac{B(\lambda,\theta,\phi)}{\Delta r\Delta\Omega} \qquad [m^{-1}sr^{-1}] \tag{2.10}$$

where $B(\lambda,\theta,\phi)$ is the fraction of the incident power scattered from the beam into a solid angle $\Delta\Omega$ centered about the scattering sample as shown in Fig. 2.1.

At this point, it is important to consider our medium. For the purposes of this paper, we shall assume that particles are oriented randomly due to turbulence in the medium. This is an acceptable assumption since we are interested in the behavior of natural waters. Integrating $\beta(\lambda,\theta,\phi)$ over all direction gives the total scattered power per unit incident irradiance and unit volume of water. Hence, we can also express the scattering coefficient as

$$b(\lambda) = \int_{4\pi}\beta(\lambda,\theta,\phi)d\Omega = 2\pi\int_0^{\pi}\beta(\lambda,\theta)\sin\theta d\theta. \tag{2.11}$$

It is useful to categorize the scattered light into forward scattered light (where the scattering angle is deflected from its original path by θ less than $\pi/2$) and backward scattered light (for scattering angle of $\pi/2 \le \theta \le \pi$). We describe these values with the forward scattering coefficient

$$b_f(\lambda) \equiv 2\pi\int_0^{\pi/2}\beta(\lambda,\theta)\sin\theta d\theta \tag{2.12}$$

and the backward scattering coefficient

$$b_b(\lambda) \equiv 2\pi\int_{\pi/2}^{\pi}\beta(\lambda,\theta)\sin\theta d\theta. \tag{2.13}$$

Another useful quantity frequently used is the volume scattering phase function $\widetilde{\beta}(\lambda, \theta)$

$$\widetilde{\beta}(\lambda, \theta) \equiv \frac{\beta(\lambda, \theta)}{b(\lambda)} \qquad [sr^{-1}] \tag{2.14}$$

which allows us to rewrite the VSF as

$$\beta(\lambda, \theta) = \widetilde{\beta}(\lambda, \theta) b(\lambda). \tag{2.15}$$

This description allows us to separate the scattering magnitude, $b(\lambda)$, and the total scattering angular distribution, $\widetilde{\beta}$. In addition, we can combine equations 2.11 and 2.14 to obtain the normalization condition for the phase function:

$$\int_{4\pi} \widetilde{\beta}(\lambda, \theta) d\Omega = 1 \tag{2.16}$$

Thus far, we have explicitly stated the λ dependence of every optical property. From this moment on, we will assume the λ dependance it is understood as a dependent variable, and not mention it explicitly. For example:

$$A(\lambda) \rightarrow A$$

$$B(\lambda, \theta, \phi) \rightarrow B(\theta, \phi)$$

In contrast, apparent optical properties, or AOPs, are properties that depend on both the medium and the geometric structure of the ambient light. In the early days of optical oceanography, it was difficult to measure the previously described IOPs *in situ*, therefore, early ocean optics scientists were forced to relay on more easily accessible measurements to study and characterize the bodies of water.

The first commonly used parameter we define is the radiant flux F, which is the

amount of power (or energy) P, per time t

$$F = \frac{dP}{dt} \qquad [W \rightarrow Watt]. \tag{2.17}$$

It is equally important to define intensity I at some angle γ to the incoming beam as the radiant flux over the solid angle $d\Omega$

$$I(\gamma) = \frac{dF(\gamma)}{d\Omega(\gamma)} \tag{2.18}$$

The radiance L can be defined as I emitted by a surface at an angle γ by some infinitesimally small area dA through $d\Omega$. In other words, it refers to the average power which goes through a surface per unit solid angle per unit projected area. L can also be expressed in terms of power, P,

$$L(\gamma) = \frac{dI(\gamma)}{dA\cos\theta} = \frac{dP}{dA\cos\theta d\Omega dt} \qquad [Wm^{-2}sr^{-1}], \tag{2.19}$$

where θ is the angle between the normal and the direction of γ. This parameter is particularly useful because it indicates how much of the power emitted by a surface will be received by an optical system positioned at γ

In contrast, the irradiance E is the radiant flux received by a surface per unit area. We define it as

$$E = \int_{4\pi} L(\gamma)\cos\theta d\Omega \qquad [Wm^{-2}.] \tag{2.20}$$

Now, when making oceanic measurements, the irradiance is divided into upwelling and downwelling. In this case, the integration in Eq. 2.20 is only done over the upper half of the hemisphere when calculating the upwelling irradiance E_u, or the lower

half of the hemisphere for the downwelling irradiance E_d

To be of any use, AOPs used must display enough regular features to be considered good descriptors for different bodies of water. However, it is clear that using only E_u or E_d to describe a particular lake is not useful. Their values would vary significantly depending on the time of day, time of year, and cloud cover, and choppiness of the water. In fact, E_u could change by orders of magnitude within seconds if a thick enough cloud momentarily blocks the sun. By taking the ratio of E_u and E_d, the ambient effects are minimized, since ambient fluctuations would affect both quantities, and, in most cases, cancel out. We have described the irradiance reflectance R_D

$$R_D = \frac{E_u}{E_d} \tag{2.21}$$

as an AOP. Most AOPs rely on taking ratios or derivatives to "cancel out" the ambient effects as much as possible, and giving a quantity which is relayable.

2.1.2 Optical Properties of Natural Waters

2.2 Scattering Theory

Scattering theory is a framework for studying and understanding the redirection of light after its interaction with some a sample (e.g.: light in water interacting with a suspended particle). Specifically, scattering consists of the study of how light interacts at some boundary, and then defines how it propagates afterwards.

In the study of scattered light, a dimensionless parameter, χ, is often used to describe the scatterer. This parameter is called the size parameter and is expressed as

$$\chi = \frac{2\pi r}{\lambda}. \tag{2.22}$$

Here, r represents the radius of the particle and λ the wavelength of incident light.

The scattering from molecules and very small particles ($\chi << 1$) is described by Rayleigh scattering, whereas larger particles are best described by Lorenz-Mie scattering. The resulting scattering pattern strongly depends on both the scatterer and the sampling incident wavelength. See Fig 2.2.

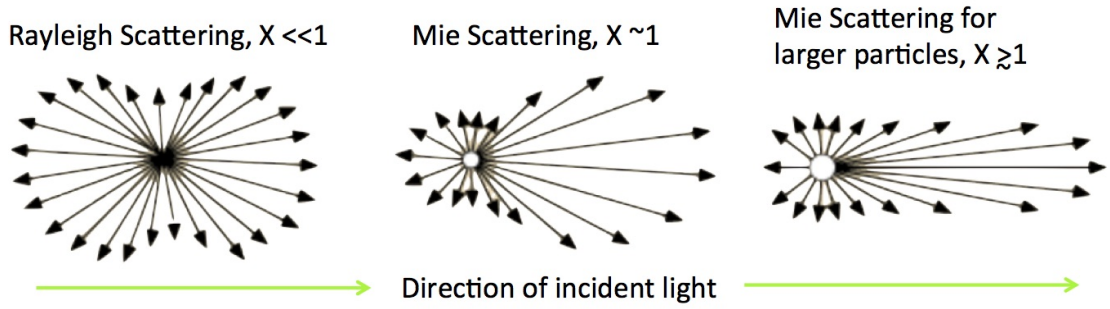

Figure 2.2: Example of scattering patterns produced by incident light on different particle sizes

There are many approaches and techniques dedicated to describing light scattering of any arbitrary sample developed since 1871. We briefly summarize the two leading theories.

2.2.1 Rayleigh Scattering

Rayleigh scattering was named after Lord Rayleigh (John William Strutt), a British physicist. He presented his original work in 1871 and continued to refine his theory through 1899.[22–24] Rayleigh scattering is considered the dominant form of scattering for particles or molecules with sizes up to one tenth of the wavelength of the radiation. Although it is best used to describe light traveling through gasses, it is also loosely valid for light traveling through transparent solids and liquids.

Lord Rayleigh treated the scattering molecules as dipoles. The oscillating electric field of oncoming radiation acts on the dipole, causing the scatterer to move in sync. This results in the particle becoming a small radiating dipole whose radiation we see as scattered light. To ensure the electric field of incoming radiation is homogenous across the dipole, we allow the particle to be no larger than one tenth of the wavelength of radiation. Lord Rayleigh found the intensity of unpolarized light, I, scattered by a small sphere of diameter d is given by

$$I = I_o \frac{1 + \cos^2\theta}{2R^2} \left(\frac{2\pi}{\lambda}\right)^4 \left(\frac{n^2 - 1}{n^2 + 2}\right)^2 \left(\frac{d}{2}\right)^6, \tag{2.23}$$

where I_0 is the intensity incident on the isotropic particle, R is the distance to the particle and θ is the angle of scattering. With equation 2.22 we can rewrite the Rayleigh scattering as

$$I = I_o \frac{1 + \cos^2\theta}{2R^2} \chi^4 \left(\frac{n^2 - 1}{n^2 + 2}\right)^2 \left(\frac{d}{2}\right)^6, \tag{2.24}$$

From here, Lord Rayleigh noticed that the scattering intensity, and therefore the VSF, was symmetric about $\theta = 90°$. Specifically, he found that

$$\beta(\theta) = \beta_{90}(1 + \cos^2\theta). \tag{2.25}$$

Integrating this equation over the solid angle to obtain b we get

$$b = \int_0^{2\pi} d\phi \int_0^{\pi} \beta_{90}(1 + \cos^2\theta) \sin\theta d\theta = \frac{16\pi}{3}\beta_{90}. \tag{2.26}$$

Lord Rayleigh's theory initially assumed isotropic molecules. Once the effects of

anisotropic molecules were taken into account[25–27] Eq. 2.25 was modified to

$$\beta(\theta) = \beta_{90}\left(1 + \frac{1-\delta}{1+\delta}\cos^2\theta\right), \tag{2.27}$$

and Eq. 2.26 was modified to

$$b = \frac{8\pi}{3}\beta_{90}\frac{2+\delta}{1+\delta}, \tag{2.28}$$

where the depolarization ratio, δ, is defined as the ratio of the s-wave and p-wave at 90°,

$$\delta = I_{\perp}(90)/I_{\parallel}(90) \tag{2.29}$$

2.2.2 Lorenz-Mie Scattering

A better different approach to was developed by Gustav Mie.[14] In trying to understand the color effects connected with colloidal gold particles, he published the first analytical solutions of the scattering of small particles using Maxwell's electromagnetic equations. It is important to note that his treatment assumes single, homogeneous, isotropic spherical scatterers, and additionally assumes single particle scattering. A complete treatment of this method can be found in many books describing scattering of light (e.g.: "Absorption and Scattering of Light by Small Particles" by Bohren and Huffman[2]). Here only a brief overview is presented.

Begin with Maxwell's equations

$$\begin{aligned} \nabla \cdot \overrightarrow{E} &= 0 & \nabla \times \overrightarrow{E} &= iw\mu\overrightarrow{H} \\ \nabla \cdot \overrightarrow{H} &= 0, & \nabla \times \overrightarrow{H} &= -iw\epsilon\overrightarrow{E} \end{aligned} \tag{2.30}$$

such that $\nabla^2\overrightarrow{E} + k^2\overrightarrow{E} = 0$ and $\nabla^2\overrightarrow{H} + k^2\overrightarrow{H} = 0$ or alternatively,

$$\nabla^2\psi + k^2\psi = 0. \tag{2.31}$$

Define a vector function such that

$$\overrightarrow{M} = \nabla \times (\overrightarrow{c}\psi)$$

and

$$\overrightarrow{N} = \frac{\nabla \times \overrightarrow{M}}{k}.$$

Vectors $\overrightarrow{M}$ and $\overrightarrow{N}$ satisfy all previous requirements. Now, since we are assuming spherical scatterers, we describe ψ in terms of spherical polar coordinates, such that Eq. 2.31 is rewritten as

$$\underbrace{\frac{\partial^2\psi}{\partial r^2} + \frac{2}{r}\frac{\partial\psi}{\partial r}}_{\frac{1}{r^2}\frac{\partial}{\partial r}\left(r^2\frac{\partial\psi}{\partial r}\right)} + \frac{1}{r^2\sin\theta}\frac{\partial}{\partial\theta}\left(\sin\theta\frac{\partial\psi}{\partial\theta}\right) + \frac{1}{r^2\sin^2\theta}\frac{\partial^2\psi}{\partial\phi^2} + k^2\psi = 0. \tag{2.32}$$

The solutions of Eq. 2.32 can be written in terms of Legendre functions of the first kind with degree n and order m for the even and odd function form of ψ,

$$\psi_{emn} = \cos(m\phi)P_n^m(\cos\theta)z_n(kr)$$

$$\psi_{omn} = \sin(m\phi)P_n^m(\cos\theta)z_n(kr),$$

where z_n is any of the four special Bessel functions

$$\begin{aligned} j_n(\rho) &= \sqrt{\frac{\pi}{2\rho}} J_{n+1/2}(\rho) \\ y_n(\rho) &= \sqrt{\frac{\pi}{2\rho}} Y_{n+1/2}(\rho) \\ h_n^{(1)}(\rho) &= j_n(\rho) + i y_n(\rho), \quad \text{and} \\ h_n^{(2)}(\rho) &= j_n(\rho) - i y_n(\rho). \end{aligned} \tag{2.33}$$

Once the solution to the scalar wave equation is obtained, the solutions to the vector $\overrightarrow{M}$ and $\overrightarrow{N}$ wave equations are expressed as

$$\begin{aligned} \overrightarrow{M}_{emn} &= \nabla \times (\overrightarrow{c}\psi_{emn}), \\ \overrightarrow{M}_{omn} &= \nabla \times (\overrightarrow{c}\psi_{omn}), \\ \overrightarrow{N}_{emn} &= \frac{\nabla \times \overrightarrow{M}_{emn}}{k}, and \\ \overrightarrow{N}_{omn} &= \frac{\nabla \times \overrightarrow{M}_{omn}}{k}. \end{aligned} \tag{2.34}$$

such that the electromagnetic field is express as an infinite series of spherical harmonics. This makes it possible to describe the scattering field with the series expansions as well as boundary conditions.

2.2.3 Fluctuation Theory

In 1905 Einstein published his findings on Brownian motion,[28] where he showed that, thermal energy allowed molecules to move randomly. In cases were light is scattered because of moving water molecules, the scattered light is depolarized. A few years later, Smoluchwski[29] and Einstein[30] had developed a new theory of scattered light in dense materials, taken into account the depolarization of light. This theory accurately described small fluctuations in liquids.

If applied to pure liquids, we find that the VSF is described as

$$\beta_w(\theta) = \beta_w(90)\left(1 + \frac{1-\delta}{1+\delta}\cos^2(\theta)\right), \tag{2.35}$$

where δ represents the depolarization ratio, S-polarization divided by P-polarization at $\theta = 90°$. The $\beta_w(90)$ is commonly referred to as the Rayleigh ratio. By 1974, Morel published his work on optical properties of water,[31] where he experimentally calculated the Rayleigh ratio as:

$$\beta_w(90, \lambda) = \beta_w(90, 450nm)\left(\frac{\lambda}{450nm}\right)^{-4.32} = 2.18 \cdot 10^{-4}. \tag{2.36}$$

With the aid of Einstein and Smoluchwsi's statistical fluctuation treatment of liquids, Morel also calculated the backscattering coefficient of pure water, $b_b = 8.95 \cdot 10^{-4} m^{-1}$ using the real size and shape of the water molecules. His b_b value of pure water is still considered the standard today.

3. THE INSTRUMENT DETAILS

To address the issues found in the previous instruments, this design will focus on maximizing the light transmissivity through the entrance aperture of the detector, ensuring azimuthal symmetry in the signal collected by the detector, and encouraging laminar flow of the surrounding water being sampled.

The designed instrument will be composed of two parts: a backscattering coefficient meter and a total scattering coefficient meter. These instruments will measure the scattering coefficients of any aquatic sample, without having any prior knowledge of particle kind, shape, size, quantity or distribution. In addition, the only assumption made about the volume scattering function is that it is azimuthally symmetric − a belief held within the ocean optics community.

By having a detector on the same surface as the outgoing laser beam, with the detector aperture normal parallel to the direction of the laser beam, the solid angle integrated by the meter will be $\beta(\theta)\cos(\theta)d\theta$. However, if the position of the detector aperture was placed such that the normal of its surface was perpendicular to the direction of propagation of the laser, we would collect instead $\beta(\theta)\sin(\theta)d\theta$ of the scattered light. In other words, by carefully considering the placement of the detector aperture we can ensure that the meter collects scattered light in such a way as to satisfy equations 2.12 and 2.13, measuring the exact value of b_b and b_f for arbitrary $\beta(\theta)$.

For our instrument, we designed an cosine collector − a meter that outputs a value proportional the cosine of the intensity of incoming light beams relative to the surface normal of the meter. Traditional cosine collectors consist of some diffusing material (usually PTFE or Spectralon) at the entrance port, an empty cavity, and

a photodiode receptor. In addition, the cavity of the cosine collector was made to behave as an integrating cavity.

In addition, instead of using a fixed-angle meter in the traditional sense, the design will include a "fixed-angle" which wraps around the laser (remaining at a distance R_1 from the outgoing laser). To date, there is no cosine collector with the accuracy necessary for our instrument nor the desired shape.

3.1 Backscattering Coefficient Meter (b_b meter)

The basic concept of the b_b meter design has been thoroughly analyzed and modeled in the literature, and significant sources of error have been discussed.[21] Fig. 3.1 shows a cross-section of the instrument. It is a half cylinder centered about the z-axis. A laser beam of cross-sectional area A and irradiance E_0 propagates along the z-axis (toward the right of the page). Light exits the instrument through a quartz rod centered with the detector's aperture. A small opaque tube of radius r surrounds the quartz rod such that light cannot escape through the sides of the tube. At $z = 0$ the quartz rod and metal tube end, and light enters the scattering medium. The aperture that defines the directions of the scattered light to be detected is an opening in the form of a cylindrical ring of radius R extending from $z = -Z_0$ to $z = +Z_0$.

Consider a scattering volume ΔV of length Δz and cross-sectional area A at position z. For a volume scattering function $\beta(\theta)$, the power dP scattered at an angle θ into the detector aperture in the solid angle defined by $\theta_1(z) \leq \theta \leq \theta_2(z)$ is then given by

$$dP = 2\pi A E_0 \int_{\theta_1(z)}^{\theta_2(z)} \beta(\theta) \sin\theta d\theta dz, \tag{3.1}$$

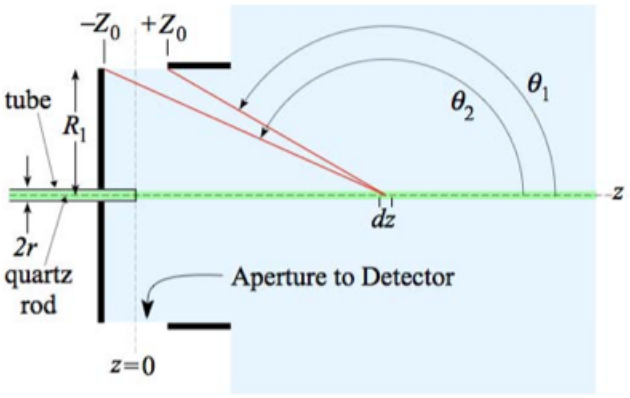

Figure 3.1: Geometry used to define inherent optical properties

such that the total power scattered into the detector is given by

$$P = 2\pi AE_0 \int_0^{\infty} dz \int_{\theta_1(z)}^{\theta_2(z)} \beta(\theta) \sin\theta d\theta dz. \tag{3.2}$$

As described by Haubrich *et al*,[21] P can be re-written, without any approximations, as

$$P' = 2\pi \int_{\pi/2}^{\pi} \beta(\theta) \sin\theta d\theta + \pi \int_{\theta_{10}}^{\pi/2} \beta(\theta) \sin\theta d\theta - \pi \int_{\pi/2}^{\theta_{20}} \beta(\theta) \sin\theta d\theta - \frac{\pi R_1}{Z_0} \int_{\theta_{10}}^{\theta_{20}} \beta(\theta) \cos\theta d\theta \tag{3.3}$$

where P' is related to P by an instrument calibration constant, $P' = \frac{P}{2Z_0 AE_0}$. After close inspection of Eq. 3.3, we notice that the first term is the exact definition of b_b as defined in Eq. 2.13, and the remaining three terms represent systematic measurement errors in its determination. This leads us to write

$$P' = b_b(1 + \rho_0) \tag{3.4}$$

where the fractional error, ρ_0, is expressed as

$$\rho_0 = \frac{1}{b_b}\pi \int_{\theta_{10}}^{\pi/2} \beta(\theta)\sin\theta d\theta - \frac{1}{b_b}\pi \int_{\pi/2}^{\theta_{20}} \beta(\theta)\sin\theta d\theta - \frac{1}{b_b}\frac{\pi R_1}{Z_0} \int_{\theta_{10}}^{\theta_{20}} \beta(\theta)\cos\theta d\theta. \tag{3.5}$$

Given a volume scattering function, $\beta(\theta)$, the theory suggests that the ρ_0 in a measurement of b_b can be evaluated to a few tenths of a percent.

3.2 Total Scattering Coefficient Meter (b meter)

The inner design for this cavity will be similar to the b_b meter. To properly measure forward scattered light, the laser must be placed a distance z away from the aperture. In addition, the space between the laser and the aperture, R_2, needs to be minimized. The distance should be comparable to the laser beam's radius. See Fig. 3.2. As light approaches and goes past the aperture, scattered light in the backward direction will also be collected, allowing for this meter to singlehandedly measure the total scattering coefficient.

Consider a scattering volume ΔV of length Δz and cross-sectional area A at position z with a characteristic $\beta(\theta)$. The power dP scattered scattered by this volume at angle θ which reaches into the detector aperture is defined by

$$dP = \pi A E_0 \int_{\theta_3(z)}^{\theta_4(z)} \beta(\theta)\sin\theta d\theta dz \tag{3.6}$$

when θ is limited by $\theta_3(z) \leq \theta \leq \theta_4(z)$ and ϕ covers a 180° range. When we integrate over z, the total power detected is

$$P = \pi A E_0 \int_0^{\infty} dz \int_{\theta_3(z)}^{\theta_4(z)} \beta(\theta)\sin\theta d\theta. \tag{3.7}$$

After some mathematical manipulation (worked out in Appendix A), Eq. 3.7 can

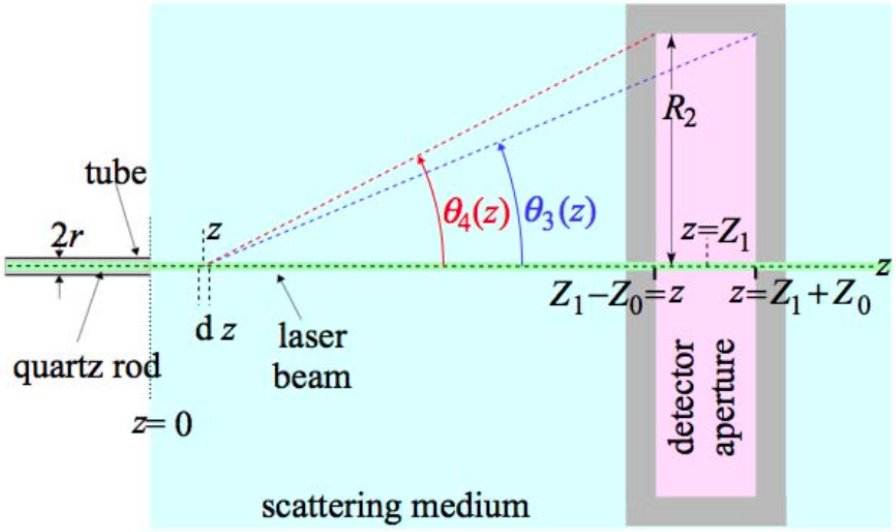

Figure 3.2: Cross-section of b meter. The detector aperture is defined by a half cylinder of inner radius R_2

be expresses as

$$P' = b(1 - \rho_I - \rho_{II}) \tag{3.8}$$

where

$$P' = \frac{P}{AE_0Z_0},$$

ρ_I corresponds to the scattering at angles completely missed by the detector aperture (i.e: $\theta < \theta_3(0)$)

$$\rho_I = \frac{2\pi}{b} \int_0^{\theta_3(0)} \beta(\theta) \sin\theta d\theta,$$

and ρ_{II} corresponds to the small fraction of light which partially misses the window of the detector

$$\rho_{II} = \frac{2\pi}{b} \frac{\sin\big(\theta_3(0)\big)}{\theta_4(0) - \theta_3(0)} \int_{\theta_3(0)}^{\theta_4(0)} \beta(\theta) \sin\big(\theta_4(0) - \theta\big) d\theta.$$

To properly grasp the magnitude of ρ_I and ρ_{II} the expected $\beta(\theta)$ of 4 μm and 40 μm polystyrene spheres was found by using Mie theory. The 4 μm diameter particles have a ρ_I value of 1.39% and a ρ_{II} value of 0.056%. For the 40 μm diameter particles $\rho_I = 41.9\%$ and $\rho_{II} = 0.173\%$. All values were calculated with $Z_1 = 100$ mm, $Z_0 =$ 2mm and $R_2 = 1$ mm, such that $\theta_3(0) = 0.562^\circ$ and $\theta_4(0) = 0.585^\circ$.

The large deviation in the value of ρ_I arrises from the small angle scattered light that misses the detector. For very strongly peaked forward scattering, this is an appreciable source of error. A few geometric tricks can be used to maximize the amount of forward scattered light which can be detected. Placing the aperture as close to the beam as possible, and allowing for a large distance between the laser source and the detector aperture.

4. THE EXPERIMENTAL SETUP

The main goal of the scattering coefficient meter design is to ensure $I \sin\theta$ is collected as accurately as possible for every scattered beam. To understand the effectiveness of each cavity, we simulate a collimated scattered beam, and allow it to be incident on the cavity aperture at specific scattering angles, θ, and azimuthal angles, ϕ.

4.1 The Optical Setup

The optical setup to test the backscattering and total scattering meter via the cosine collector is shown in Fig. 4.1. Two different views of the same setup are provided to fully explain the laser behavior through the optical components of the setup.

The setup ensures that the light incident on the cosine collector (integrating cavity) was a well-collimated homogeneous beam. Every lens was placed to maximize this result. The step-by-step setup is described below.

First, the 532 nm Sapphire SF laser was aligned with the beam parallel to the table's surface. Then, three irises were placed and aligned to the laser. The irises were used to ensure that the laser beam remains aligned, even after the addition of optical components. To spread the beam out horizontally we decided to have the beam pass through a 2 μm slit and make use of the diffraction effects. To maximize the fraction of light going through the slit, the beam was focused onto the center of a slit with a 400 mm focal point spherical lens. After the slit, the horizontal divergence of the beam was significantly different than its vertical divergence, and cylindrical lenses were needed from proper collimation. A 100 mm focal point cylindrical lens was placed collimating the beam in the horizontal direction. Then a combination of

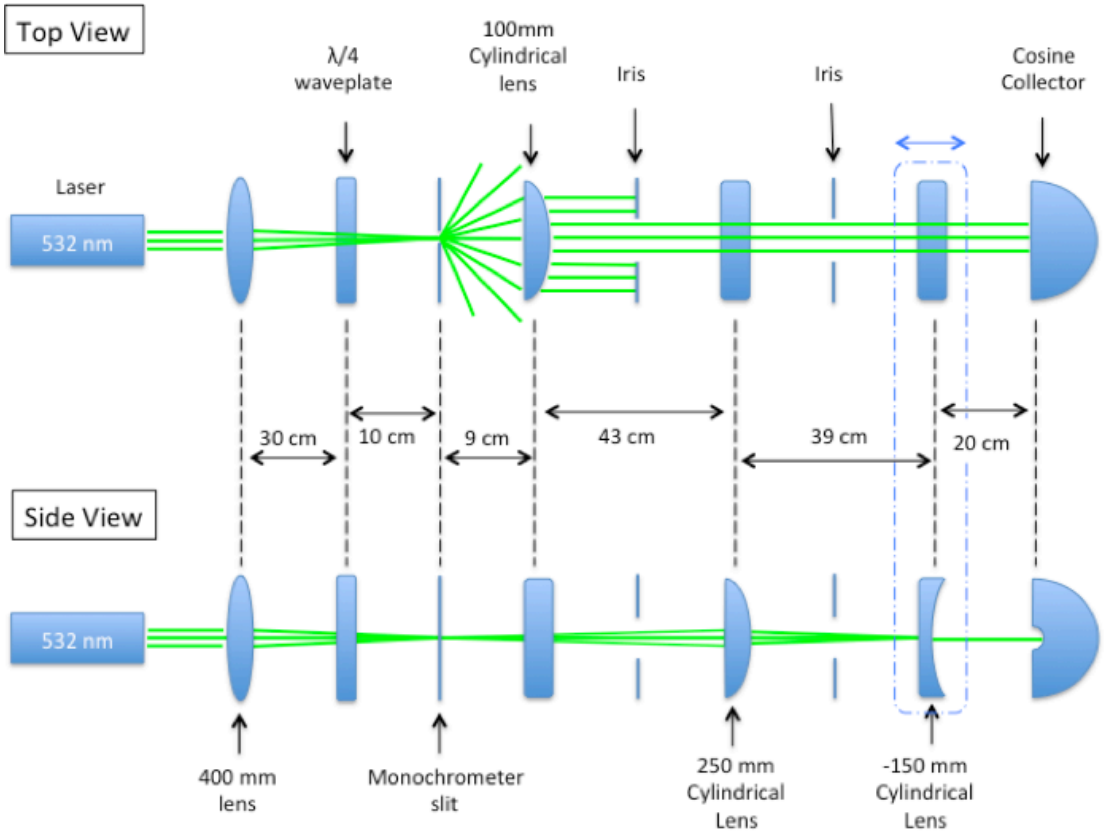

Figure 4.1: Shows effects of optical components on laser from top and side view. This setup collimates the light into a 1mm x 25mm beam.

cylindrical lenses were used to tighten the beam cross-section. By carefully combining a 250 mm focal point lens and a -150 mm focal point (diverging) lens, the beam profile was collimated. The cross-sectional height was 1 mm, and the intensity of the beam remained roughly homogeneous. See Fig. 4.2

Finally, to minimize the s and p polarization effects of the laser on the cavity surface, a quarter waveplate was placed in the beam's path before the slit changing all linearly polarized light into circularly polarized light.

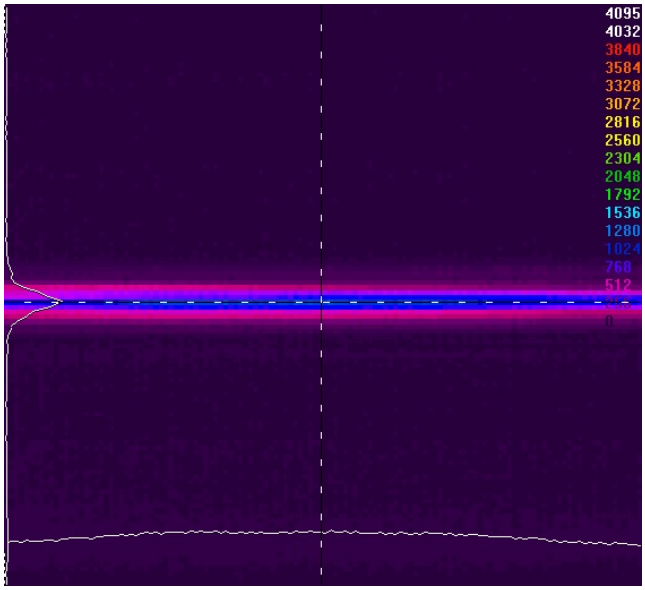

Figure 4.2: Beam profile as viewed by a CCD camera

4.2 The Cavity Holder

Simulation of the incoming scattering beams at different angles was done by designing a detector holder which would independently rotate the cosine collector about two perpendicular axis, simulating incident scattered light at different angles tested. This way, the incoming laser beam's profile and its collimation remain constant at every angle. A holder was designed such that the azimuthal response of the cavity could be tested. When placing the holder on a rotating stage, the angle of light incidence on the cavity could be changed.

The holder consists of two pieces: the black polyvinyl chloride (PVC) clamp placed around the cavity and the aluminum base, which supported the clamp and the cavity. The angular ϕ resolution was obtained by rotating the clamp relative to the base (as allowed by the channels) and inserting a pin through the 0.07" diameter hole in the aluminum base and into one of the side holes in the PVC clamp. See

Appendix B. The PVC material was picked to ensure the clamp would be sturdy enough to properly hold the cavity in place, while being soft enough to not crush or scratch the cavity. The metal base has 1/4" deep circular channel where it mates with the PVC piece, allowing the PVC piece to glide about the ϕ axis. In practice, this rotation allows us to test the response of the cavity when light is incident upon different points along the cavity's aperture window.

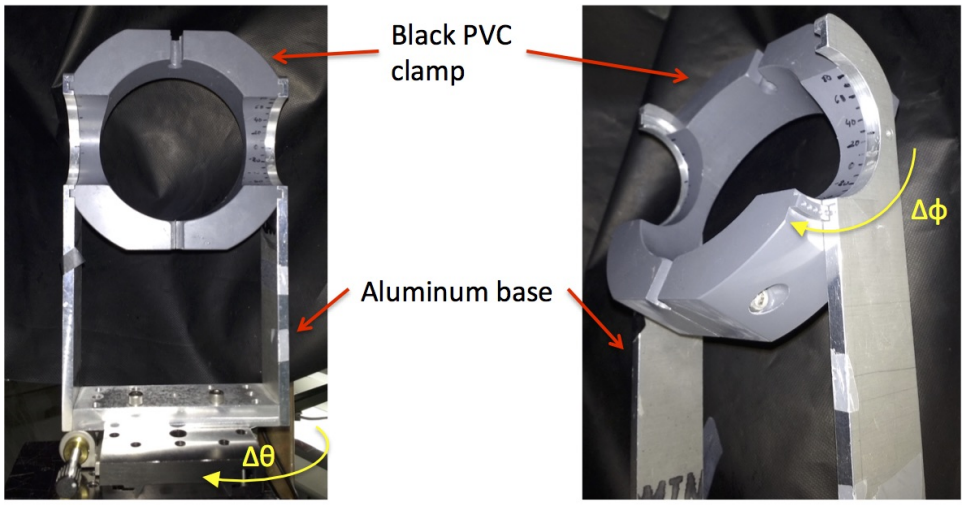

Figure 4.3: Components of the detector holder. The metal part which supports the Black PVC, allowing it to rotate only about the ϕ axis.

4.3 The Setup Alignment

Before every run, the setup must be properly aligned. The following the following three steps helps ensure that the setup is centered to the laser. Each step should be repeated until the desired outcome is achieved.

First, the rotation stage axis must be aligned with the laser beam. For these steps it is best if the iris closest to the cavity setup is minimized, such that only a

small circular profile is obtained, as opposed to a rectangular one. One way to align the rotation stage is by placing an iris off-center on the stage and rotating the stage until the laser beam goes through the center of the iris. Then rotating the stage by 180° and ensuring the iris is still aligned with the laser. If it is not, the rotation stage needs to be moved closer to the laser and this step repeated. Once the rotation stage is centered to the laser, the translation stage should not be moved again.

Second, the detector holder needs to be aligned vertically to the laser. For this, the detector holder and the cavity are placed on an x-y translation stage and positioned on top of the rotation stage. The height of the holder is adjusted in the z axis such that the center of the black PVC (and hence the center of the cosine collector) intersect with the laser. Once this is achieved the location of the rotation stage should not be changed.

Third, ensure the aperture normal is aligned with the direction of the laser at $\theta = 90°$. Rotate the cavity holder on the translation stage until its surface normal seems antiparallel to the direction of the laser beam. Adjust the x-y translation stage in the x direction (perpendicular to the direction of the laser beam) until the beam is incident on the center of the aperture. Then, slowly rotate the translation stage. At every angle, the laser should still be centered around the aperture. If needed, move the x-y translation stage in the y direction to align the laser beam to the aperture. At some angle, the beam should appear completely parallel to the cosine collector's surface (the beam of light will be spread as a line covering the entire surface). This angle will be considered $\theta = 180°$ on the rotation stage. Move the rotation stage by 90° to $\theta = 90°$ and confirm that the laser is still centered about the aperture. If not, adjust the x direction on the translation stage once again. Then slowly rotate stage towards $\theta = 0°$. As it rotates, the beam should remain centered about the cosine collector's aperture and, once the rotation is complete, the beam should be parallel

to the cosine collectors surface.

For cosine collector cavities which are perfectly symmetric on the inside and have a detector positioned on the at $\theta = 0^\circ$ for any ϕ angle, the cavity can be rotated (via the rotation stage) to $\theta = \pm 45^\circ$. The value collected by the detector should be the same for both of the θ values.

When testing the experiment in water, the entire setup was turned upside down and was suspended from a tall fixture, then submerged into the water tank. The alignment steps for remained the same.

5. INSTRUMENT DEVELOPMENT

In this section we describe the development and evolution of our design. Our instrument relies on a highly accurate cosine collector. As described in the previous chapter, most cosine collectors do not have the accuracy needed for our instrument. In hopes of adapting existing cosine collector designs to our specific needs, it was important to understand how cosine collectors behave given our application. Most commercial cosine collectors can be generalized to a tube, with a dispersing medium on one end of the tube (usually PTFE or Spectralon) and a photodiode detector on the other. Incident light goes through the dispersing media and then is detected by the photodiode detector.

5.1 Transmission Through Diffusing Materials

In this section we examine the behavior of transmitted light through diffusing materials. Diffuse reflectors of different thicknesses were tested, and the effects of the presence of a slit (entrance aperture for light) on the surface of the diffuse reflector was examined.

For this experiment, a simple prototype was setup. A collimated laser was incident on the sample. A fiber coupled to a photodiode detector collected the transmitted light through the material. The incident angle of the laser beam on the sample ranged between 0° and 80° relative to the sample's surface normal.

The setup consisted of placing a 1 mm slit centered around the beam on the sample itself. The slit was defined by 2 pieces of electric tape placed on the surface of the sample with a 1mm gap between them. The laser beam was then expanded to achieve a profile of 1 mm width by 1.5 cm length. The diffusing materials used included Spectralon, PTFE, white quartz and fumed silica were compared. Figure

5.1 compares the results of each tests on a single graph. The materials investigated are color coded as follows: Spectralon samples are red, teflon samples are green, white quartz is purple and pressed fumed silica powder is blue. Every curve has been scaled such that it's maximum value is unity. In addition, a theoretical sin θ is indicated with the dashed black line.

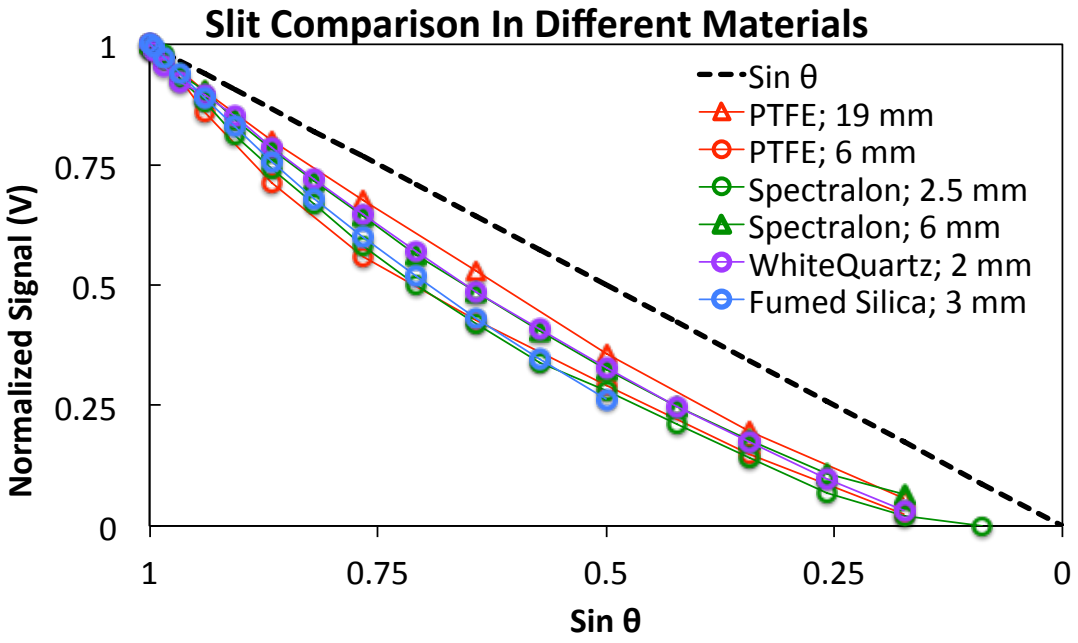

Figure 5.1: Relative behavior of multiple dispersing media with the presence of a 1mm aperture on the surface.

We find that none of the samples viewed behave as sin θ for incoming angles. To better understand the effect of the aperture, we observe the behavior of transmitted light through a 6 mm thick piece of Spectralon when changing the slit size. See Fig. 5.2.

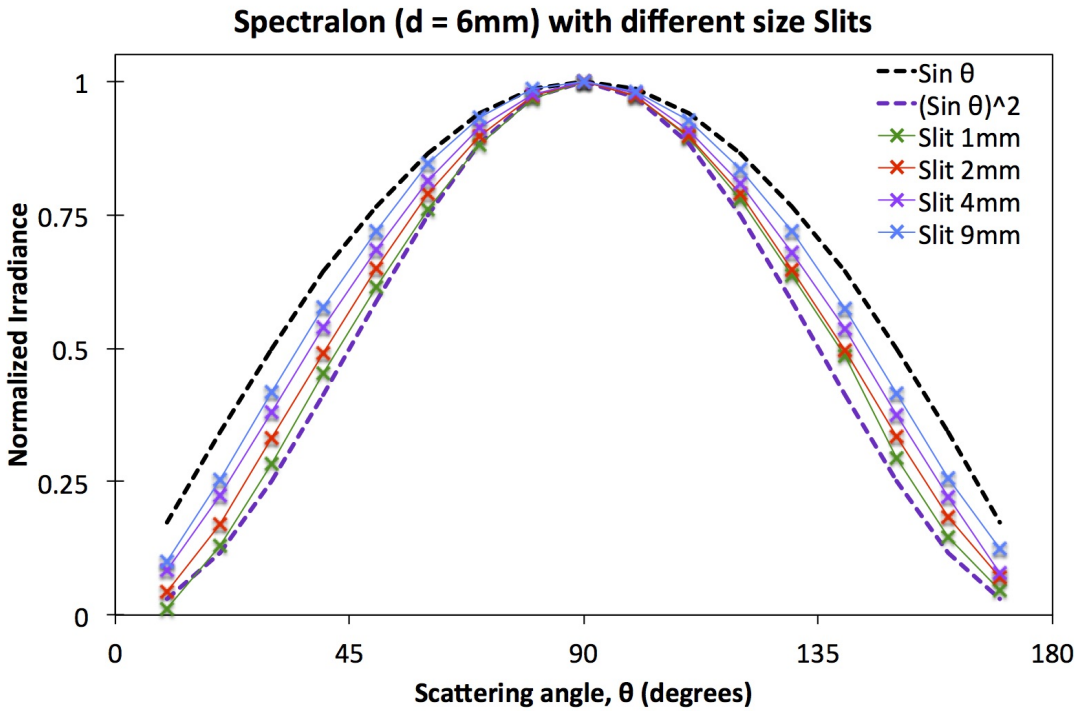

Figure 5.2: Signal transmitted perpendicularly through a Spectralon piece with fiber 6mm from surface as a function of incident angle and slit size. The smaller the slit, the closer the transmitted light's behavior approaches a $\sin^2\theta$ curve.

From figures 5.1 and 5.2 we notice that light does not disperse evenly around the point of incidence, but instead, has a stronger forward scattering envelope. This envelope gives preferential directional illumination to the photodiode receptor, such that some directions are detected with greater intensity than others. As a consequence, the dispersing light as a function of incident angle on the dispersing media has a loose $\sin\theta$ behavior. When placed in conjunction with the limiting effects of the detector's aperture, the angular dependence of incoming light seems to behave as $\sin^2\theta$ for small apertures. In contrast, as the aperture width increases, the photodiode response shows a more $\sin\theta$-like behavior. Although it is possible to find the exact geometry needed to achieve this curve, there is no guarantee that it would

work for every type of water. Additionally, the aperture size also determines the resolution of the scattering coefficient measurements, Having an aperture of greater than 1 cm wide would negatively impact the detector's reliability. In summary, since small aperture is desirable, it is necessary to use a detector setup which allows the scattered light to enter some cavity, disperse, and then be sampled by a detected.

5.2 Entrance Window

As described in the previous section, the detector aperture must be positioned with its normal perpendicular to the direction of the laser beam (z axis). This will ensure that the scattering meter measures the integral of $\beta(\theta)\cos\theta d\theta$.

As light enters the cavity, it must go through a well defined entrance aperture (an opening) in the cavity. Also, to ensure the cavity does not get contaminated, it must also be well sealed from the surrounding medium. In other words, the entrance window must be a clear window with well defined edges.

Reflectivity at the entrance window is a major concern for our instrument, if light is reflected away from the instrument, then the instrument cannot properly measure the total scattered light. As light is incident upon a flat surface, the total transmission varies with incident angle. The transmission through an air/quartz interface can be as high as 99.8% for normal incidence or approach zero for beams near grazing angles.

Haubrich's design consists of a cylindrical cavity with a flat quartz window tilted at 45° to the direction of the laser beam. See Fig. 5.3. This design is beneficial because the light scattered from the laser beam is incident on the window at angles smaller than 45°, where the transmission through the aperture window is relatively independent of the angle of incidence. However, a 45° angle window is undesirable for true *in situ* instruments. The region between the aperture and the window is exposed

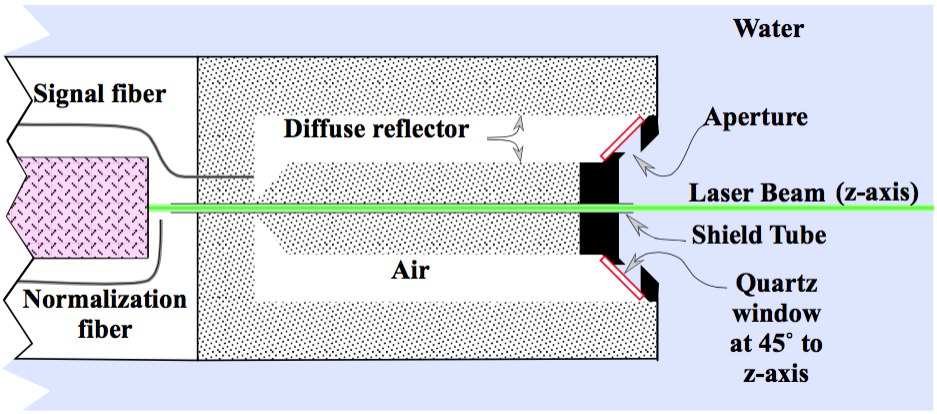

Figure 5.3: Cross-section (cylindrical symmetry around the z-axis) of the prototype b_b instrument showing the window (outlined in red) at 45°.

to the underwater environment and would trap contaminants. These contaminants would obscure the light path and quickly render the instrument useless.

The solution to this problem is to modify the entrance aperture such that it has a slight depression in it. The depression decreases the angle of incidence relative to the quartz, increasing the total transmission through the aperture. Furthermore, it allows for reflected rays to hit the quartz surface multiple times before being fully reflected away from the detector. See Fig. 5.4.

Figure 5.5 compares the effective transmission of light incident at various angles as a consequence of different apertures. The width of the aperture remains constant while radius of curvature of the groove change. The graph shows that for deeper grooves, the total transmission increases. Therefore, although deep grooves are desirable mathematically, the final design must have a groove which is shallow enough to not trap contaminants. The sharp dips in each curve figure 5.5 indicate where the transmission caused by multiple reflections start dominating. See Appendix C.1 for the source code used to calculate the transmission through the window.

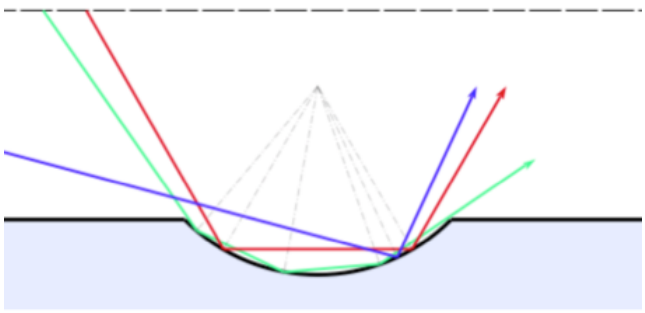

Figure 5.4: Scattered rays from laser at various angles showing multiple reflection effect of depressed surface on red and green ray.

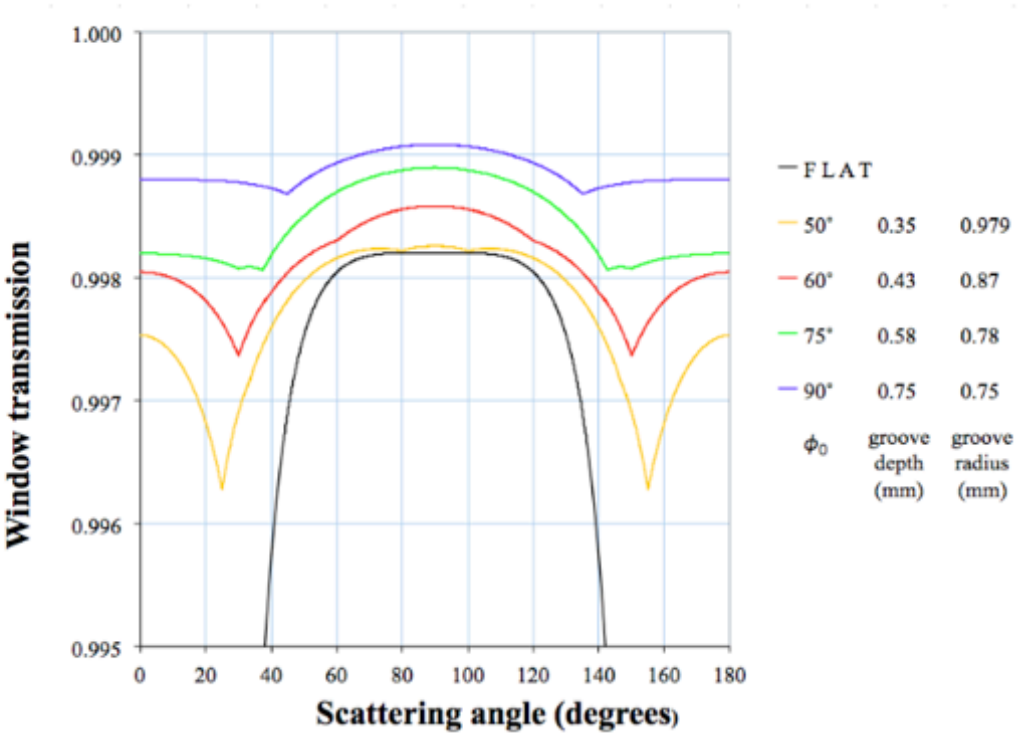

Figure 5.5: Average transmission of the curved quartz window as a function of scattering angle. In every case, the aperture is set at 1.5 mm.

5.3 Side Cavity

To minimize turbulence caused by the instrument, and since oceanic water is understood to have a VSF which is azimuthally symmetric, the cosine collector was designed to detect only the lower hemisphere of the scattered light. To test the new indented entrance window, a replica of Haubrich's design was made. The inside of the cavity was clear quartz. The surrounding diffuse reflecting material was pressed quartz powder. The aperture was designed with an 0.46 mm deep curved indentation and a width of 1.52 mm.

By looking at the effect of individual scattering angles and the cavities signal detection, it became apparent that the cavity was more sensitive to larger scattering angles than at normal incidence. Therefore the detector design had to be changed.

See Fig. 5.6.

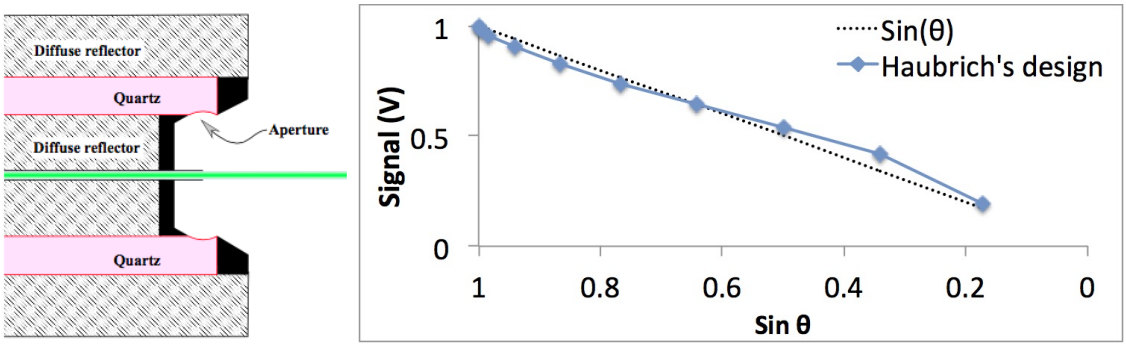

Figure 5.6: Side cavity. Simulating Haubrich's design

5.4 Inner Quartz Piece Geometry

The defining aperture of the cavity is a quartz window. In our cavities, we used a small quartz piece to help define the aperture. This quartz piece was used in multiple shapes of cavity to ensure that the aperture did not change from one test to another. Because the shapes of the cavities examined varied greatly, small quartz pieces were made to fit in each cavity. This quartz piece can take several shapes. The end result of using these quartz pieces is that the inside of the cavity was comprised of both quartz and air. To study the effect of the presense of the quartz, a few geometries were examined. Figure 5.7 shows the signal detected by the photodiode when only the exterior geometry of the quartz pieces were changed. In particular we used a spherical Teflon cavity with a teflon top. The teflon top had fibers coming out of the side of the top cavity (both top and bottom). By changing only the quartz piece (from a round bottomed piece to a cylindircal, flat bottomed piece) we measured the difference in ϕ behavior. Both sets were averaged and then normalized to one and graphed together with the expected sin θ curve. Changing the quartz piece had a minimal effect on the shape of the average, but it affected the intensity of individual phi curves. We decided to use the round piece of quartz to limit internal reflections and difractions from the quartz into the cavity.

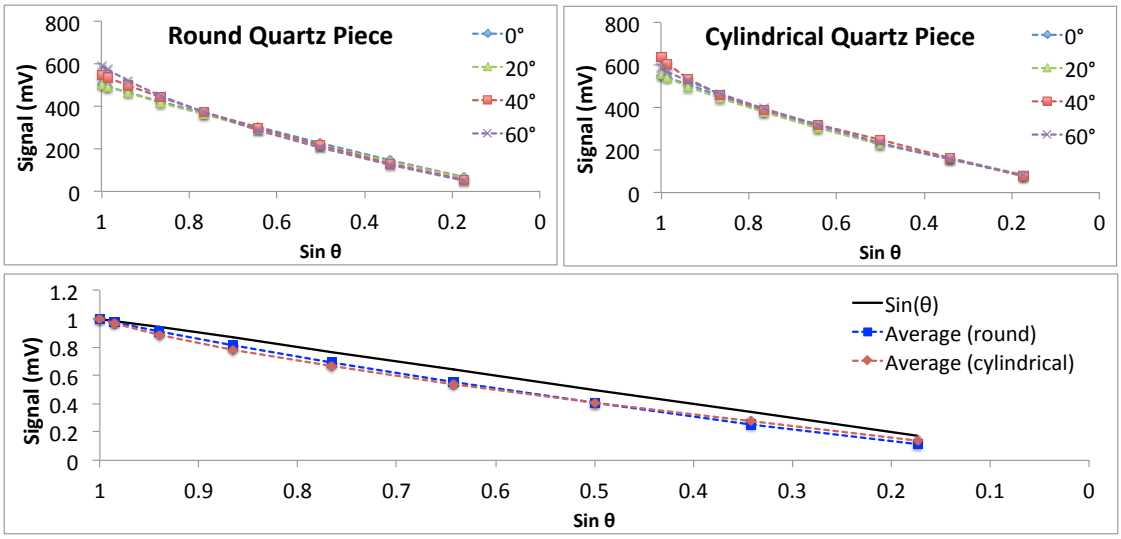

Figure 5.7: The theta dependence of different phi curves is shown. The average of both situations is shown on the bottom graph.

5.5 Presence Of Baffles

Many integrating cavities relay on the presence of baffles to limit stray beams of light from saturating the detector. This issue was investigated with different kinds of cavities and shapes of baffles.

5.5.1 Cylindrical Cavities

Using a large cylindrical PTFE cavity with a hole on the bottom. We introduced a cone shaped baffle inside the cavity, blocking transmitted light in the integrating cavity from exiting without first hitting a PTFE surface and being dispersed. The baffle was held in place, and separated from the bottom surface of the cavity, by a thin quartz ring. The detector was placed outside of the cavity, on the opposite end of the baffle. Figure 5.8 shows the detector response at three different ϕ angles to a TPFE cavity with a "large cone" (48 mm tall and 35.6 mm in diameter), a "small cone" (38.1 mm tall and 28 mm in diameter) and the small cone with a ring around

the top portion.

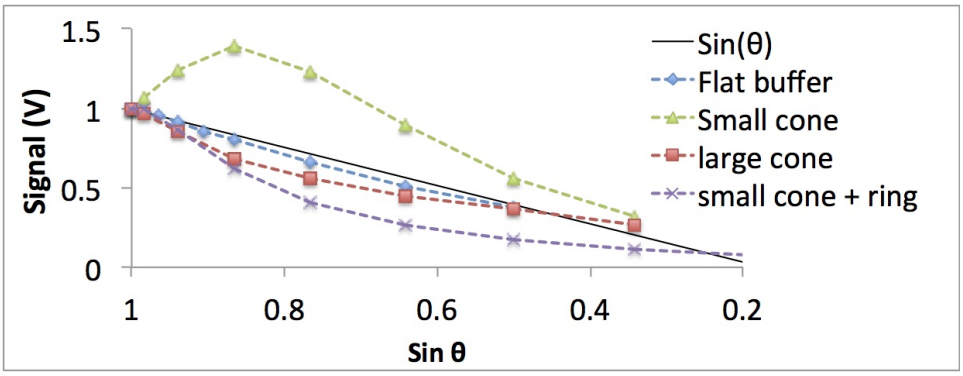

Figure 5.8: Effect of baffles on cylindrical cavities.

Additionally, the azimuthal symmetry is almost non-existent when extra geometries are added into the cavity. For example, figure 5.9 shows the cavity response when the light is incident at $\phi = 0°$, $20°$, and $40°$.

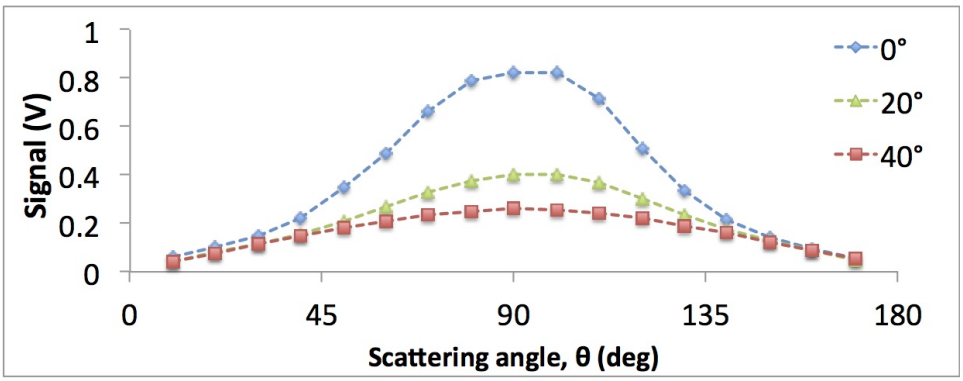

Figure 5.9: Different ϕ curves showing the azimuthal behavior of the cavity with a cone shape buffer plus a ring.

5.5.2 Hemispherical Cavities

The presence of baffles in hemispherical PTFE cavities was also observed. Using small PTFE cylindrical baffles (plugs) to block direct access to the detector hole. For this experiment, the PTFE top had two through holes make on opposite ends of the piece. Each hole was ∼1 cm diameter. FDS1010 photodiodes sampled the light through those holes.

Figure 5.10 shows the added signal from the photodiodes for each ϕ angle as the θ is changed. The top panel displays the raw data as a function of $\sin\theta$. The middle panel shows the averaged ϕ values in addition to the raw data. Here we confirm that this cavity has a high degree of azimuthal symmetry between ϕ values of -40° and 40°. The bottom panel compares the average value of the ϕ curves normalized to $\sin(90°) = 1$ with the expected $\sin\theta$ behavior. The bottom panel also shows the slope of the average ϕ values, showing close agreement between the behavior of the the overall signal collected from the cosine collector with this setup and the expected $\sin\theta$ response.

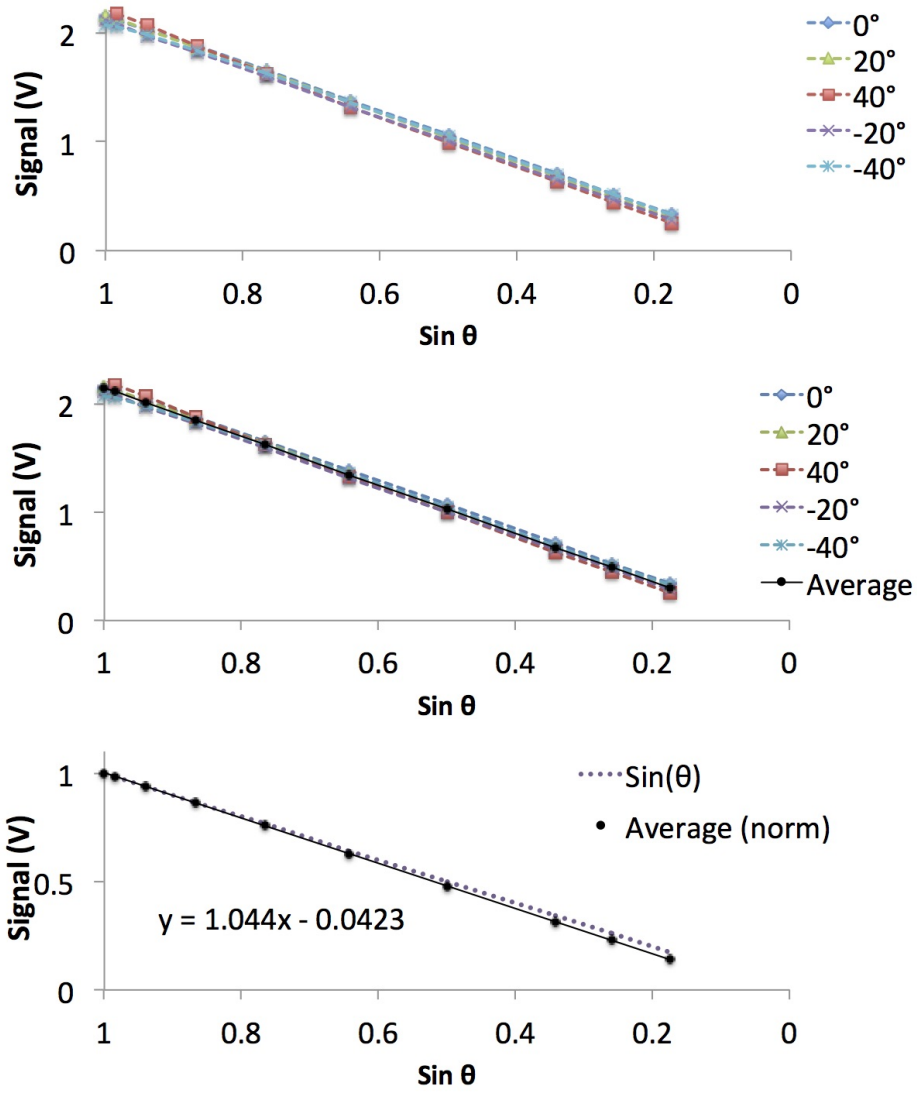

Figure 5.10: Cavity response to incident light when a cylindrical baffle blocks direct light from being sampled by the photodiode. The top panel shows the raw data collected by the photodiodes. Each curve is the sum of two detectors on opposite end of the cavity. Each curve represents scattered light entering the detector at a specific ϕ (labled), and the cavity response at different θ angles. The top panel shows the raw data collected at each ϕ and θ angle. The middle panel shows the same data, while adding the averaged sum of the curves showed. The bottom panel compares the normalized averaged sum to the expected $\sin\theta$ response.

5.6 Position Of Detectors

5.6.1 Teflon Concave Cavity

By placing fibers around the surface of the PTFE cavity we can easily determine the light sampled by each fiber as the laser light is incident upon the cavity window. Detector 1 was placed on the side of the cavity near the front face, perpendicular to the beam (ϕ = 90°, θ = 0°). Detector 2 was placed on the opposite end of the incoming beam (ϕ = 0°, θ = 0°). Detector 3 was placed on the side of the cavity along the horizontal axis of laser propagation (ϕ = 0°, θ = 45°) and Detector 4 was placed on the opposite side (ϕ = 0°, θ = -45°). All other aspects of the experiment were held constant. The signal collected by each detector is shown in Fig. 5.11.

Detector 1 shows all the curves between ϕ = -50° and ϕ = 40° being highly linear, as well as being of relatively constant in intensity per every angle sampled. Detector 2 shows the effect of having a detector in a location accessible by incoming beams. Detector 3 and detector 4 display non-linear relationships with respect to sinθ. Clearly, the best option is Detector 1, if the widest ϕ angles are ignored (i.e ϕ = $\pm$ 60°)

To further study the effects of the cavity position, 3 fibers were placed in the same cavity relatively near eachother. One fiber was placed on the cavity top piece, closest to the cavity's inner top surface. Two 1 mm diameter through holes were drilled in the cavity base for other two fibers. The holes were made such that the first hole was parallel to the hole for Fiber 1, and the second hole was mad at a 15° angle as compared to the hole for fiber 2. This angle was intended to give the fiber a better viewing area of the inside of the cavity. All fibers were placed into the cavity and made flush with the inner wall. The cavity response was then tested at five different ϕ angles. There is little observable difference between the Fiber 1

and Fiber 2. Fiber 3 starts showing deviations in the intensity as the laser incidence approaches the fiber location. The results of the signals are shown in figure 5.12. The ϕ values of each fiber were averaged and then normalized to 1. The bottom panel, labeled "Averaged values", shows all three averaged values on the same graph. The deviations between the values of each curve are almost imperceptible.

5.6.2 The Medusa Experiment

In an attempt collect all of the light going through the aperture, 150 fibers were added around the entrance window. This had huge intensity issues. The aperture was defined with aluminum foil held onto the teflon nail polish (used as adhesive). Radially outward of the window were 150 polished fibers which bunched into 3 sets and coupled to detectors. The values of the detectors were added together and are shown in figure 5.13. Note that most of these curves are very straight, displaying a very good $\sin\theta$ behavior, but the intensity spread over different ϕ values is too wide to be practical.

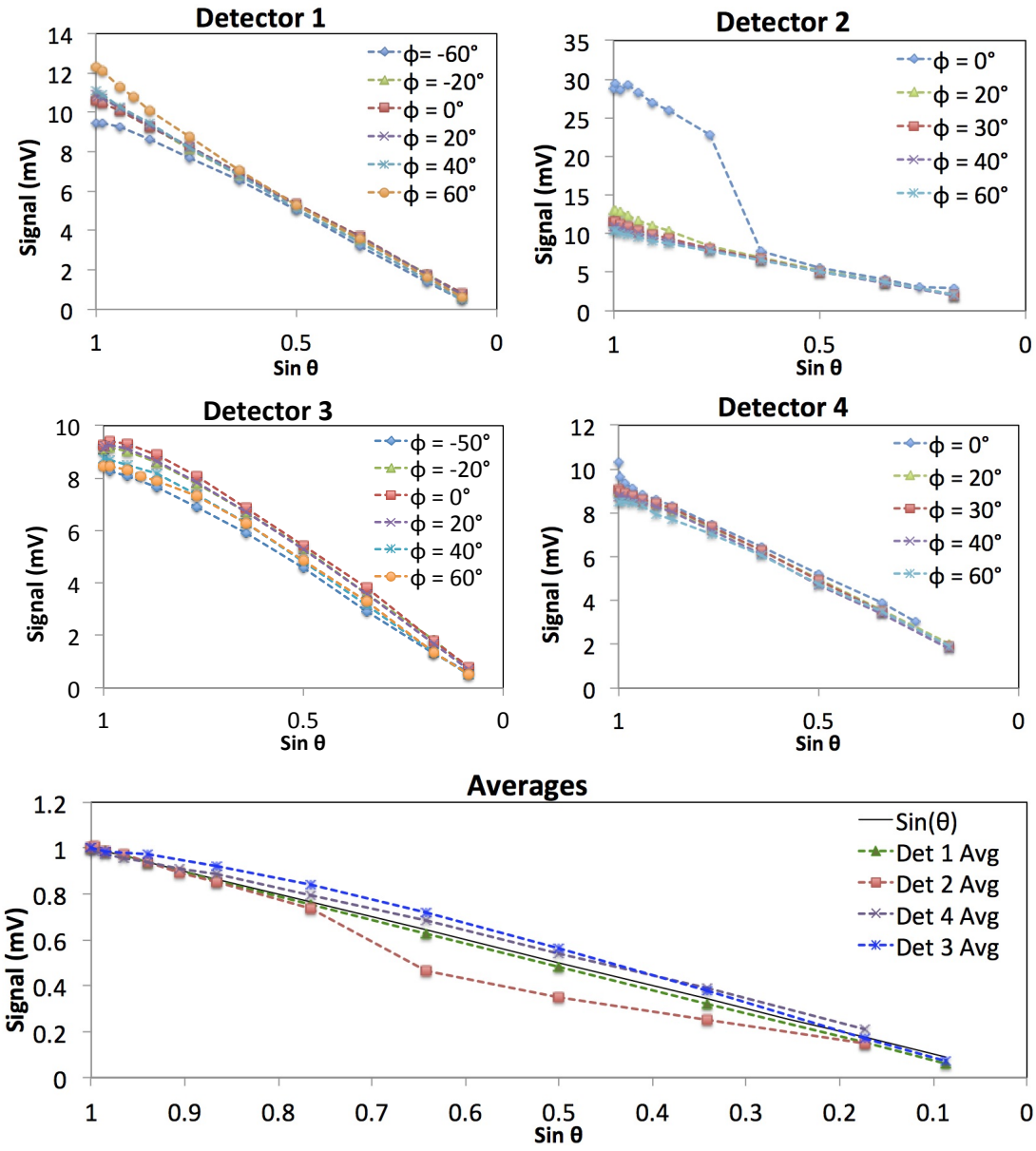

Figure 5.11: Detector position comparison. Four detectors where placed in the same cavity, and the response of each detector is compared relative to the same incoming light beam. The bottom graph shows the average signal collected by each detector.

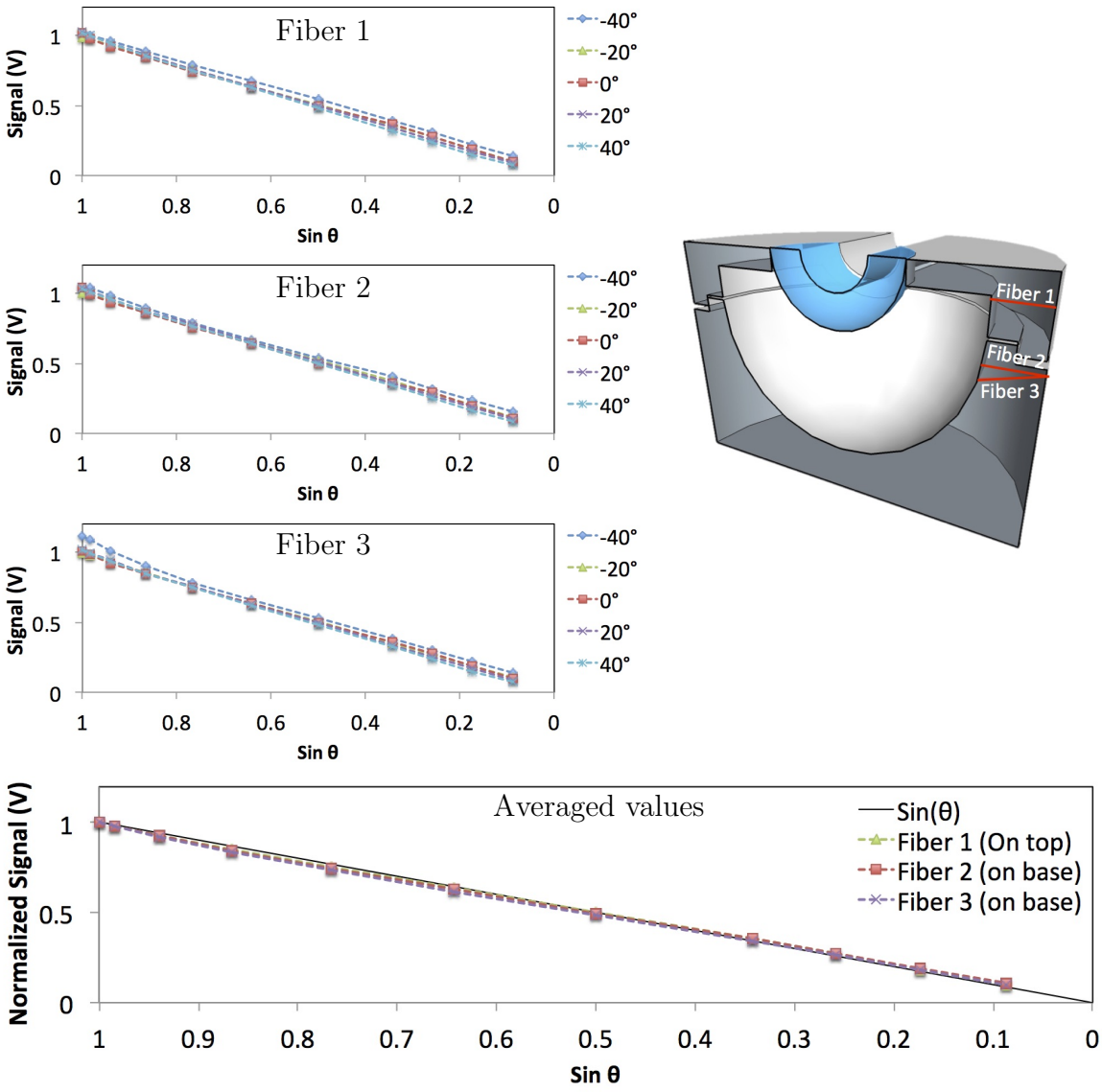

Figure 5.12: Test of fiber location near cavity top. Fibers 1 and 2 were placed parallel to the top surface of the integrating cavity. Fiber 3 was placed with at a 15° angle into the cavity. The bottom curve shows the average value of each fiber after normalization and compares them to the expected $\sin\theta$ curve.

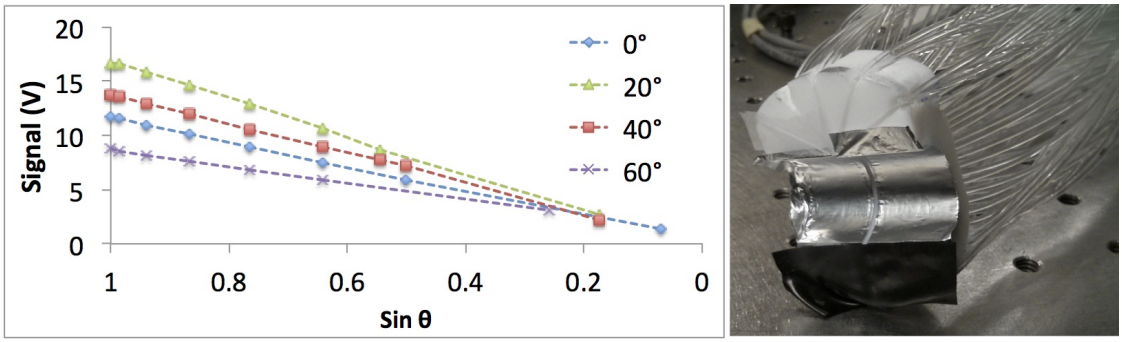

Figure 5.13: Medusa picture plus data.

5.7 Size Of Cavity

To better understand the effect of the cavity size, cylindrical Spectralon cavities of different heights were observed. The inner diameter of each cavity was 76.2 mm and the height, H, ranged from 39 mm to 141 mm in 25.5 mm increments. The laser light was incident on each cavity at $\phi = 0°$. The photodetectors were placed on the top face of the PTFE top which had two 1cm diameter through holes (one on each side of the quartz piece, perpendicular to the direction of travel of the laser beam). Then the setup was rotated to view the total signal from detector at different incident (θ) angles. Figure 5.14 a) shows the signal from the photodiode as a function of the sine of the simulated scattered angle. For $\phi = 0°$ and $\theta = 0°$, the photodiode signal was 12V with a cavity of H = 39 mm. However, this signal decreased as the cavity size increased. When H = 141 mm, the detector signal was 8.72V, 72% of it's original value.

To better compare the decay of each curve, figure 5.14 b) shows each curve normalized by their respective maximum value. Additionally, the expected $\sin\theta$ curve from the scattered light is also plotted (dotted purple line). The curves all show a similar decay, regardless of the cavity size, however, none of the curves match the expected $\sin\theta$ behavior very well.

Let us take a closer look at the cavity behavior at each cavity volume extreme. Figure 5.15 shows the behavior of the Spectralon cavity with H = 25.4 mm (right side) and 141 mm (left side). The top graphs show the signal collected from the photodiode detectors at multiple ϕ angles. From panel a) we note that as the ϕ angle changes, the intensity per scattering angle is affected. Specifically, the values at $\phi = 0°$ is considerably lower than the rest of the ϕ curves. Further, panel b) shows the average of the ϕ curves as compared to the expected $\cos\theta$ values, and, there are

a)

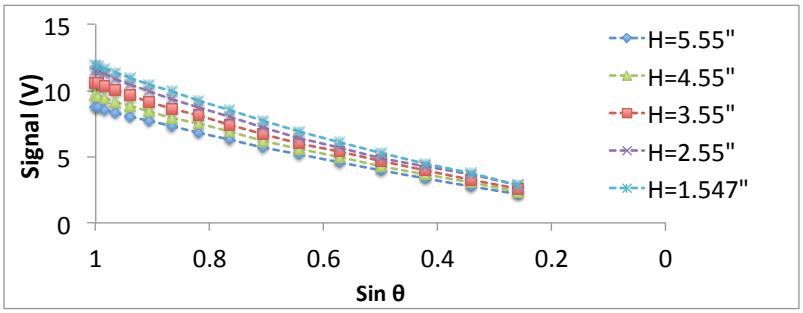

b)

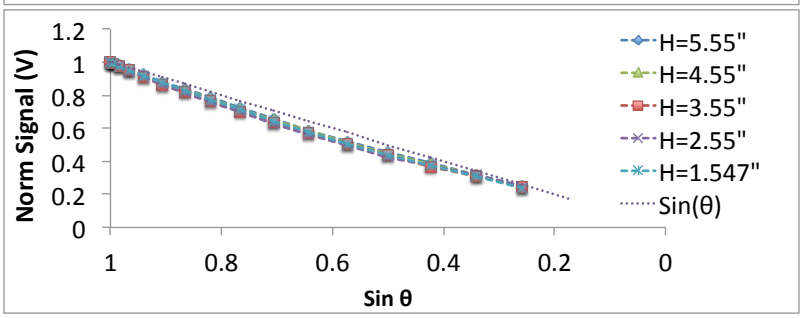

Figure 5.14: Effect of Spectralon cavity height on transmitted light. a) Shows the intensity detected by the photodiode increasing as the cavity volume decreases. b) Shows the same data normalized and compares the decay to the expected $\sin\theta$ curve.

still discrepancies between both values. Panel 5.15 c) shows a smaller cavity (H=25.4 mm). Similarly to panel a) $\phi = 0°$ is the detected with the lowest intensity. However, the $\phi = 60°$ curve is greatly affected, causing the average of these curves (shown in panel d)) to move further away from the expected $\sin\theta$ values.

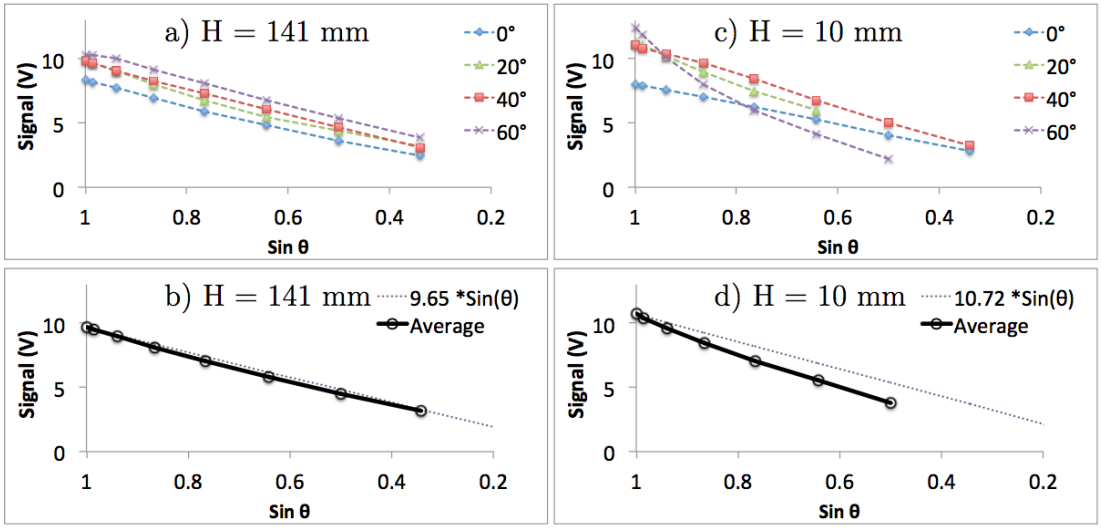

Figure 5.15: Effect of Spectralon cavity height on ϕ curves. The top figures a) and c) show the signal from the photodiode detector two different cavity sizes (H = 141 mm and 10 mm, respectively). The bottom figures b) and d) show the average value of different ϕ curves as compared with the expected $\sin\theta$ behavior (dotted line).

5.8 Aperture Wall Thickness

As described in Chap 4, to study the sine-like angular response from light scattered from the laser beam, I simulated the scattered light by shinning a well-collimated laser upon the collector's entrance aperture. The total incident light through the aperture should be proportional to $I_0 \sin(\theta)$, where I_0 is related to the total irradiance of the scattered ray and θ is the scattering angle from the laser beam.

Now, consider an the entrance window as defined by an aperture of width w, with walls of thickness t. To focus on the effects of the aperture itself, let all incident light be the compliment of the scattering angle. At normal incidence (when θ'=0°, representing the scattered light at $\theta = 90°$), the wall thickness has no effect on the total incoming light through said aperture. However, when the incoming beam is at an incidence angle $\theta' \neq 0°$, the effective width of the aperture is reduced by $t\tan\theta'$,

as represented by the greyed out section. In other words, the effective width of the slit is $w - t\tan\theta'$. See Fig. 5.16.

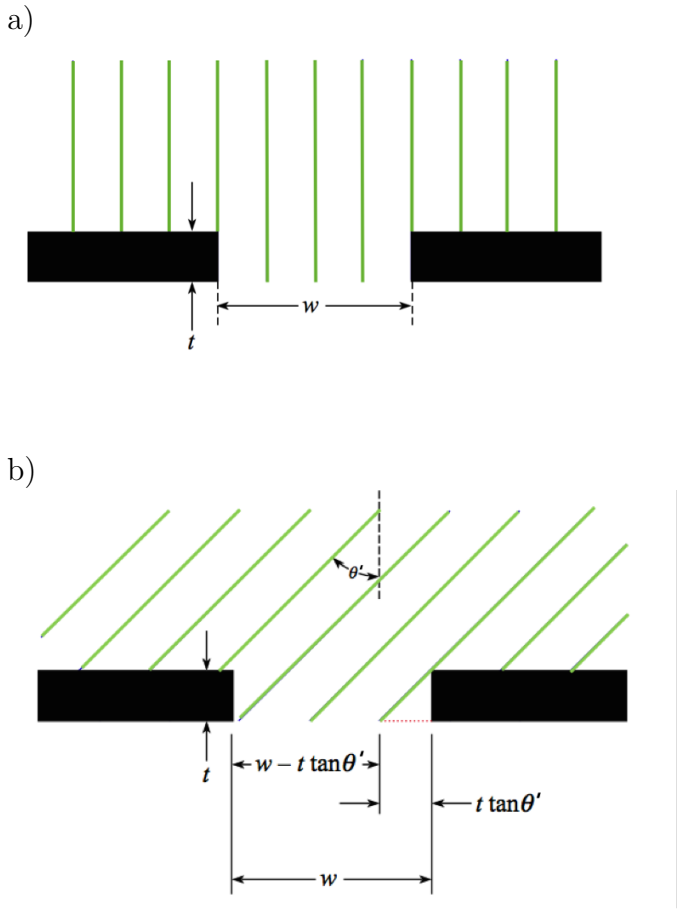

Figure 5.16: a) Cross-section of an aperture with a collimated beam at normal incidence. b)Cross-section of an aperture with a collimated beam at θ incidence angle

It follows that instead of a cosine like response to the incident beam, the response to uniform, collimated light is proportional to

$$(w - t\tan\theta')\cos\theta' = w\left(\cos\theta' - \frac{t}{w}\sin\theta'\right) = w\left(\sin\theta - \frac{t}{w}\cos\theta\right) \tag{5.1}$$

With carefully chosen parameters, the t/w term can be minimized. After some consideration, we selected $w = 1.52\ mm$ as our slit width. Figure 5.17 shows the effect of different wall thicknesses with this aperture size. The dashed lines represent the percent deviation from the expected $\sin\theta$ values. Clearly, as the wall becomes thinner, the effect lessens.

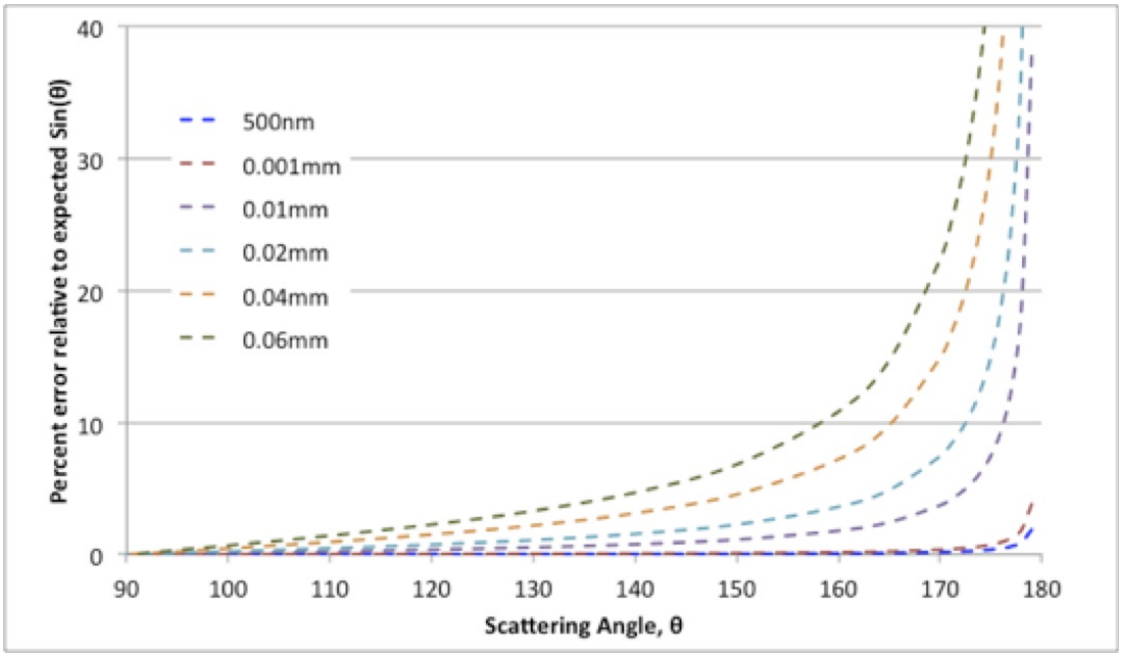

Figure 5.17: Theoretical percent deviation from $\sin(\theta)$ for various aperture wall thicknesses

5.9 Sampling Hole Size

To understand the effect of the viewing aperture, the the viewing hole of the instrument was changed from 1 mm to 8 mm diameter. In the case of a 1 mm diameter hole, the signal inside the meter was collected via a 1 mm diameter optical

fiber. The fiber was coupled to a PMT for the measurement. For the 8 mm diameter hole, a silicon photodiode detector was placed immediately above the hole. The signal collected with a wider viewing aperture for the photodiode was more azimuthally symmetric than the signal collected by the fiber, seen in Fig. 5.18. However, if we normalize the average signal collected by each detector, we see that there is very good agreement in both cases. See Fig. 5.19.

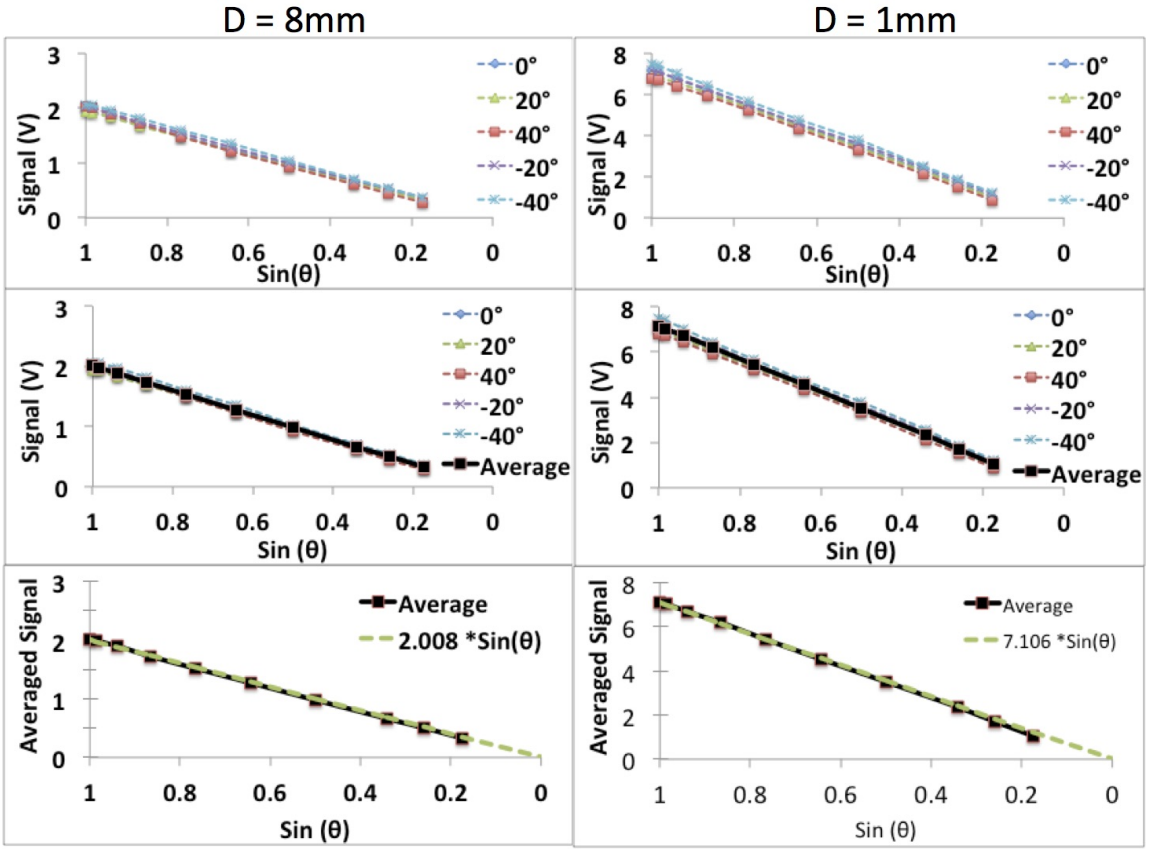

Figure 5.18: Comparison of detector behavior for different sized sampling holes

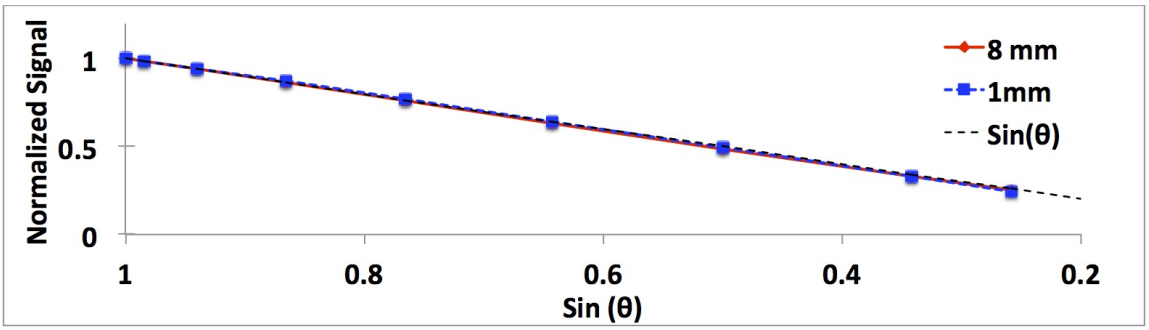

Figure 5.19: Normalized average signal of detector behavior for different sized sampling hole

6. INSTRUMENT DESIGN AND CHARACTERIZATION

6.1 The Backscattering Coefficient Meter

The backscattering meter prototype consists of a highly calibrated cosine collector with light integrating properties. The entire design is made of Polytetrafluoroethylene or PTFE (commonly known as virgin Teflon), used for its high bulk reflectivity and low absorption coefficient. The design consists of three parts: a quartz piece delimiting the entrance window, a hemispherical PTFE hollow base and a machined PTFE top. Together, they form an integrating cavity as shown in Fig. 6.1. Appendix B shows the technical drawings of each piece. The quartz piece is a 38.1 mm

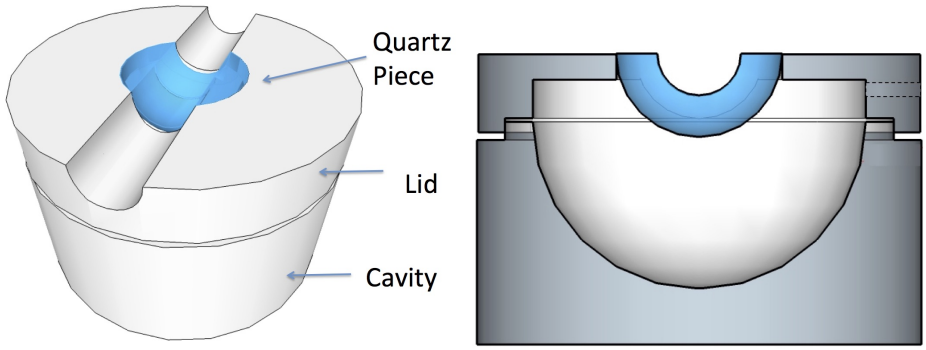

Figure 6.1: Schematic of the backscattering meter design. The left image shows a 3D sketch of the integrating cavity once it is put together. The right image shows a cross-section of the integrating cavity

diameter quartz hemisphere, selected because of it's strength, low thermal expansion coefficient, durability, and inertness. It has a 19 mm diameter channel on it's otherwise flat surface. Light enters the integrating cavity via the grooved aperture

inside the quartz channel. The entire channel (with the exception of the aperture) is covered in aluminum foil to ensure that incident light is reflected away from the cavity's aperture. The shiny side of the aluminum foil is placed facedown (facing the inside of the integrating cavity) on the quartz since it is found to have the highest reflectivity of both sides (88%). The dull face of the aluminum foil on the exterior side of the cavity is spray painted flat black to maximize stray light absorption. Straight edges of the aluminum foil are used to define the aperture window for the incident light in the center of the channel. Consequently, the aperture walls are defined by the thickness of the aluminum foil, the spray paint used on the top surface, and the thickness of the adhesive used to keep the aluminum strip in place. In our prototype, the total thickness of the aperture walls is 50 μm. The aperture window has a radius of curvature of 0.43 mm, a depth of 0.87 mm from the channel, and an width of 1.5 mm. The aperture itself will be positioned 9.5 mm away from the laser. The expected average transmission of all light incident upon the aperture is 99.8% as described by the red curve in Fig. 5.5.

The top piece of the cavity was made entirely of PTFE with a wall thickness no less than 6.35 mm. It has a 1 cm diameter through hole on the side for the detector placement. No baffles were used. All seams between the quartz piece and the top were covered with PTFE tape. The inner surface of the bottom cavity was hemispherically shaped to maximize symmetry in detection over all incoming ϕ and θ angles. Both the top and bottom pieces were designed to fit together tightly and minimize light losses through seams. The outer surface of the cavity was covered in silver tape to minimize losses due to light transmission through the PTFE.

The detector used to sample the signal in the cavity is a FDS1010 silicon photodiode sold by Thorlabs. The photodiode was connected to a homemade variable-gain amplifier (see Appendix D).

The aperture window is wide enough to detect light from $\phi = -90°$ to $90°$, to ensure the azimuthal behavior remains constant, we will limit the detector range between $\phi = -40°$ to $40°$. The optical setup and the cavity were aligned as described in Chap 4. The integrating cavity's response to simulated scattered light in air is shown in Fig. 6.2 where panel a) shows the cavity response at different ϕ angles, panel b) shows the ϕ angles with the average data of the values at each θ angle (in black), and panel c) shows the averaged data with it's maximum value normalized to unity (labeled as "Avarage (norm)") as compared to the expected sin θ. The trendline of the average normalized data has a slope of 1.015, showing good comparison with the expected $\sin\theta$ response. All data is found in Appendix E.1.

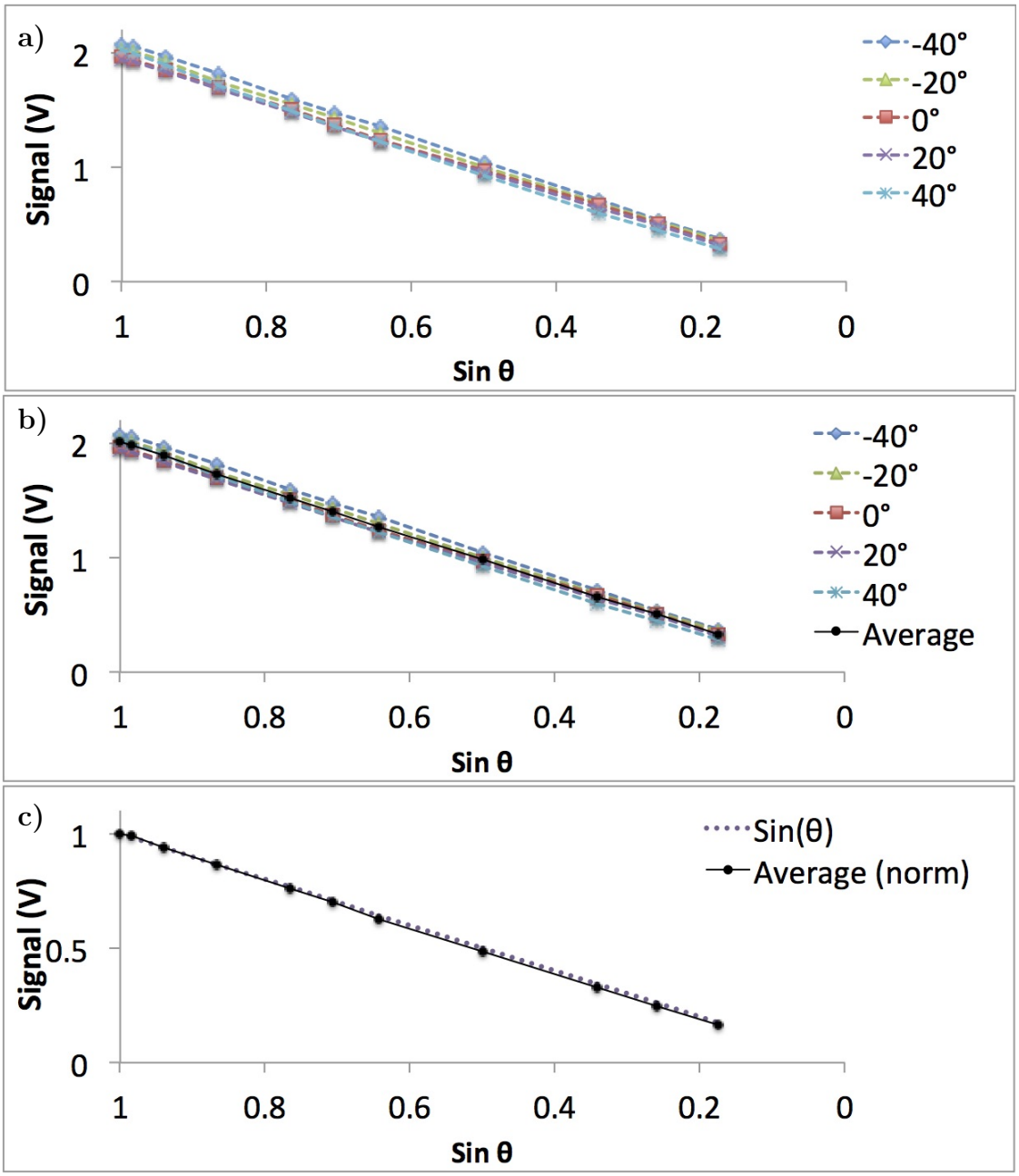

Figure 6.2: b_b meter response in air to simulated scattered light. Panel a) shows the cavity response for specific ϕ curves. Panel b) shows the average value of the ϕ curves in black. Panel c) compares the normalized average cavity response with the expected sin θ behavior.

6.2 The Total Scattering Coefficient Meter

The total scattering meter (b meter) prototype consist of a carefully calibrated cosine collector with light integrating properties. Similar to the b_b meter, the entire design is made of PTFE and has a custom made quartz piece defining the entrance aperture. The quartz piece has a 2 mm radius channel (covered in aluminum foil with the dull side spray painted matte black facing up) and a 1 cm wide aperture window. The aperture window size was selected to maximize the amount of scattered light which could enter the cavity at small (grazing) angles, and minimize the errors caused by the wall thickness. See section 5.8. To achieve 99.8% transmission over all incoming angles, the aperture depth was machined to 2.9 mm, with a curvature of radius of curvature of 5.77 mm. The final wall thickness of the aperture is 0.05 mm.

The PTFE top was designed to have a minimum thickness of 6.35 mm on every surface, with a 2 mm radius channel going through the center of the top piece (matching the quartz piece). It has a 1 cm diameter through hole on the side (perpendicular to the direction of incoming scattered light entering in normal to the instrument's front face). All seams were blocked with PTFE tape. The bottom cavity is hemispherical of 38.1 mm radius. The cavity was wrapped in aluminum foil tape to reflect otherwise lost light back into the cavity. See Appendix B for technical drawings of all pieces.

A FDS1010 silicon photodiode connected to a variable gain amplifier circuit was used to sample the signal from the 1 cm through hole on the rim of the top PTFE piece. The amplifier was set to increase the signal by a factor of 50, and filters were used in the laser beam's bath to control the intensity of the laser beam incident on the cavity.

Because of the geometry of the top piece, the measurable ϕ range is limited (the

top itself blocks the incoming simulated scattered light because of the small area and depth of the channel). All tests done with the total scattering meter were performed only at $\phi = 0°$.

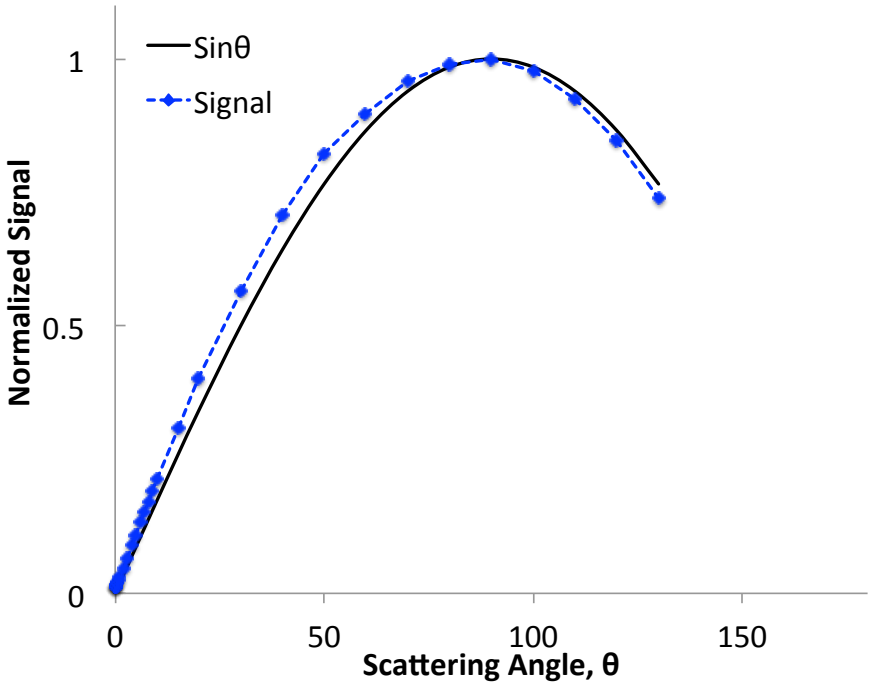

Figure 6.3: Normalized b meter response data at $\phi = 0°$

6.3 Mathematical Corrections

As discussed in previous chapters, it is important to ensure that cavity has a sine-like detector response to incident light. Let us take a step back to consider the optical setup. The cavity is aligned such that light incident upon the aperture window enters the cavity perpendicular to the photodiode's field of view. The light then spreads throughout the cavity. The cavity's rotation axis is centered to the

point of incidence between the laser and the cavity (at the aperture window). This rotation is described by θ.

Imagine the cavity is placed such that the incident laser is perpendicular to cavity's top face. Recall that the photodiode detector is placed perpendicular to the front face of the detector, such that it has no angular (θ) bias. Assuming the inside of the cavity is perfectly symmetric, there should be no difference between the detected signal of the photodiode once the cavity is rotated clockwise or counter-clockwise.

Possible explanations for the asymmetric values:

1. Cavity behavior is actually not symmetric about θ.

2. Outer-cavity interference localized to one side of the cavity.

3. Cavity not aligned properly.

Examining these reasons in more detail:

1. The cavity behavior is not symmetric. In other words, there is something inside the cavity which would cause one side to reflect more light than other, or some area that is more absorbing that other. The inner cavity is made of.

Because the cavity pieces being used were machined to be symmetric, it is unlikely that one side is more reflective (or more absorptive) than the other side. The cavity pieces were cleaned before they were put together in an effort to minimize contamination, and as far as can be observed, there is no difference in the inner parts of the cavity. For this reason it is unlikely that we should expect the backscattering meter cavity to not behave symmetrically. In the case of the total scattering meter, asymmetries were allowed to maximize light entering the cavity at grazing angles, therefore, preferential deviations in the cavity's response could be attributed the inherent design.

2. Outer-cavity interference. There are multiple situations which can occur outside of the cavity affecting the incoming light at some specific angles. For example, uneven thickness of the material covering the groove on the quartz piece and improper placement of the aluminum foil defining the aperture window on the quartz piece will have negative impacts on the expected $\sin\theta$ curve. The quartz piece and the setup is checked carefully to ensure that all wrinkles are minimized and do affect the laser beam's path until $\sim 170°$, and the area near the aperture window is as thin as possible (0.05 mm including nail polish as adhesive, aluminum foil and spray paint). In addition, both sides of the cavity have the same amount of material (implying that they should have roughly the same thickness), and visually the aperture edges of the quartz piece seem straight and well defined. Both sides of the aperture were made in a similar fashion, and errors on both sides of the quartz piece are to be expected, it is unlikely that one side of the cavity would have negligible effects on the incoming light, while the other one, which is visually the same, seems to affect the laser light dramatically.

3. Cavity not aligned properly. There are many ways in which the cavity can be misaligned for these tests. In general, misalignment issues fall into one of 3 categories:

a) The axis of rotation of the cavity is slightly off from the laser beam, giving preferential behavior to one side as over the other.

b) The center of the incoming beam might not be perfectly centered on the detector's entrance window.

c) The assumed angle of incidence of the laser is off by some $\delta\theta$ value.

Thinking back to the optical setup, the incoming beam is 2.5 cm wide and roughly homogenous. Cases a) and b) display a shift from the center of beam for

different reasons. But if the beam is homogenous and considerably wider than the aperture hole (which it is) then this small shift should have a minimal effect on total light.

On the other hand, it is reasonable to believe that the alignment process has errors associated with it. Considering the alignment was done "by eye", small angle deviations from the true incidence of light are expected. In other words, case c) is very likely.

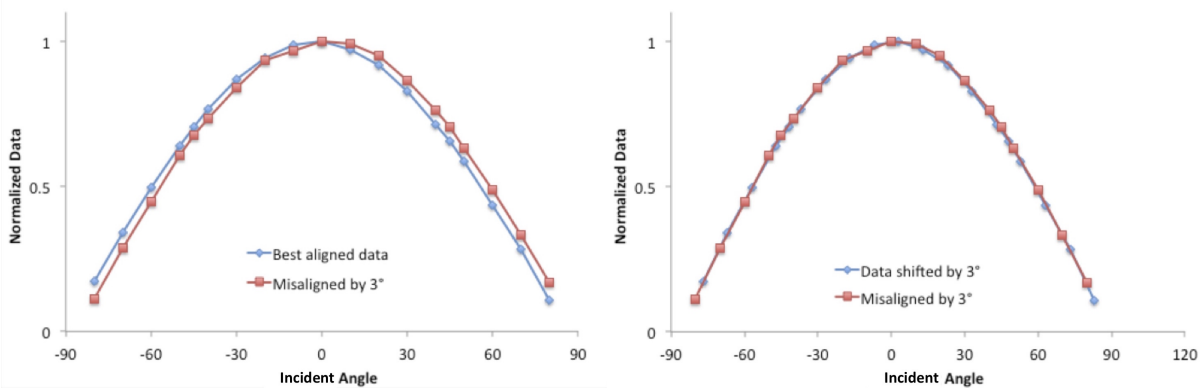

Figure 6.4: Small angle mathematical correction is comparable to realignment procedures.

Figure 6.4 shows data taken from a standard cavity at $\phi = 0°$ with light incident on the cavity from -80° to 80° with respect to the normal axis of the detector's face. The cavity was aligned as explained in the Optical Setup document sent previously, and then misaligned by $\theta = 3°$ (shown on the left). Then the aligned data curve was mathematically shifted by $\theta = 30°$ and compared to the curve obtained by when the cavity was misaligned by 3°. The figures show almost perfect agreement between the curves. In summary, small angle misalignments of the cavity can be corrected

mathematically, yielding the same cavity response curve as a correction to the cavity alignment itself.

This mathematical adjustment is crucial for finalizing the small angle alignment for the total scattering meter, where accurate incident angle measurements are imperative. Figure 6.5 shows the data aligned by eye of the total scattering meter with a 1 cm aperture. The data is plotted relative to the scattered angle of light from the laser beam. The signal was normalized to a maximum value of 0.9 to better match the sine curve in the small angle interval. The asymmetric behavior of the curve is expected to be the cause of the asymmetric inner design of the cavity top. The inset shows a zoomed version of $\theta = 0^\circ$ - 10° on a log-log scale. From the inlet it is easy to see that the cavity does not properly measure the expected sine curve at small angles. The bottom image of the figure shows that by applying a mathematical shift of $\theta = -0.58^\circ$ the cavity response shows perfect agreement with the expected cavity behavior at small angles. Corrected data values are presented in Appendix E.2

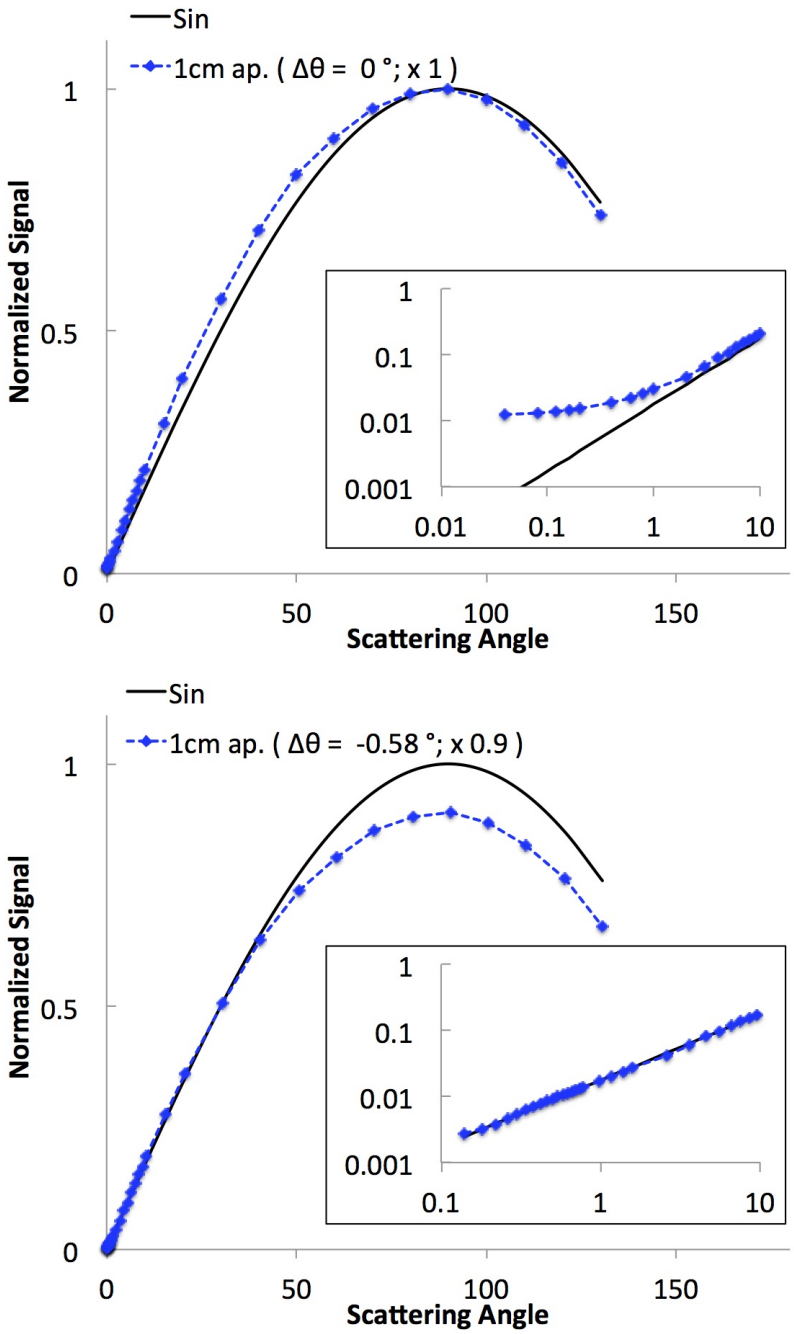

Figure 6.5: The top figure shows cavity response of the 1cm aperture width total scattering meter aligned by eye (dashed blue curve). The inset graph is a zoomed version on a log-log plot of the first 10 degrees. In addition the sine curve (solid black curve) is also shown. The bottom figure shows the same data mathematically displaced by 0.58° and renormalized to 90% of its previous value. The inset graph shows the improved agreement with the sine curve.

6.4 Water Characterization

To ensure the instrument characterization in air is representative for underwater experiments, the cavity's response to simulated scattered light was done in the presence of water. For this test, the backscattering meter cavity was submerged in a tank filled with water. To accomplish this, the b_b meter cavity holder was hung from a beam above the table and aligned as explained in Chap. 4. The water tank was filled with 14 L of water and placed the on a jack on the optical table. The water tank was then elevated until the cavity was completely submerged. To minimize water leaking into the cavity, the PTFE top had a 1mm through hole, which was plugged with a fiber optics cable. The fiber carried the sampled cavity signal from outside of of the water tank to a PMT. The meter was tested for different θ and ϕ angles. The cavity characterization results are shown in Fig. 6.6. They show that the averaged signal over ϕ all angles has very good agreement with the expected $\sin\theta$ behavior.

To adequately compare the cavity response to scattered light, the averaged normalized signal from the different ϕ curves have been plotted in Fig. 6.7. It is important to note that small deviations in the slope of the curve can easily be attributed to alignment differences between experimental runs, as explained in the previous section. In addition, the air tests were done with a 8 mm through hole were the detector is positioned. Whereas the water experiments are done with a 1 mm through hole and a fiber which carries the sampled signal to a the detector.

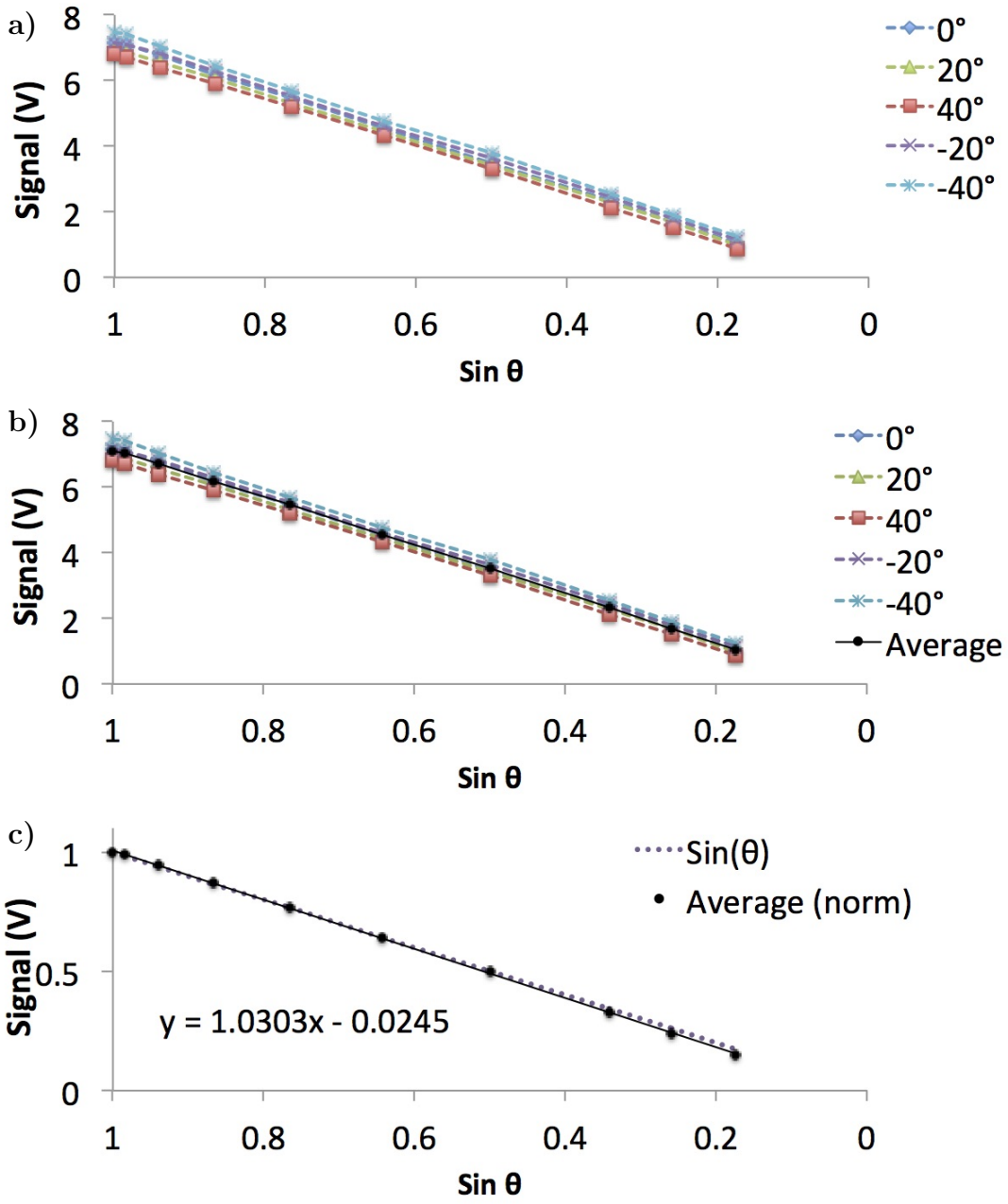

Figure 6.6: b_b meter response submerged in a tank with 14L of water to simulated scattered light. Panel a) shows the cavity response for specific ϕ curves. Panel b) shows the average value of the ϕ curves in black. Panel c) compares the normalized average cavity response with the expected sin θ behavior.

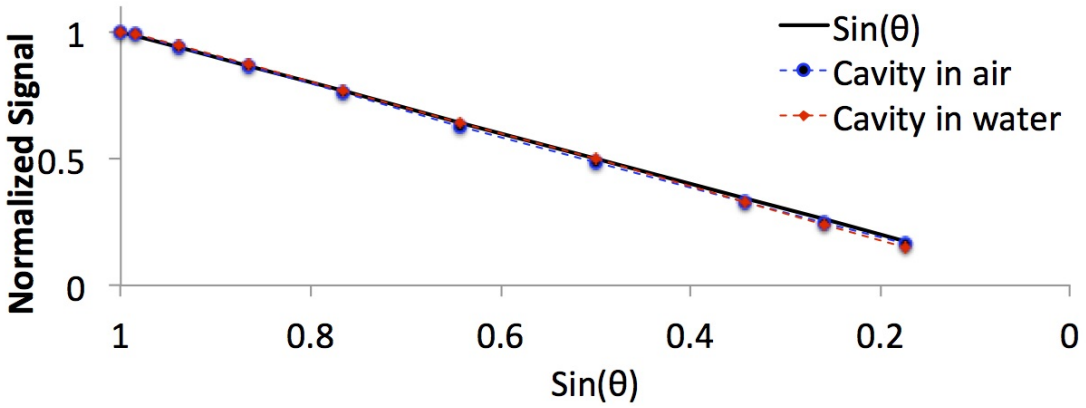

Figure 6.7: Comparison of cavity behavior in air (blue circular points) and water (red diamonds). Both curves strongly match the expected Sin(θ) behavior.

6.5 Instrument Validation

Once the meter is properly aligned, it is possible to calculate the expected overall instrument response *in situ*. As previously described, the strength of the instrument is that it directly measures the desired scattering coefficient. In reality, the instrument measures

$$P \propto \int_{\theta_1}^{\theta_2} \beta(\theta) f(\theta) d\theta,$$

where θ_1 and θ_2 depend on the meter's field of view and the location of the laser source relative to the aperture window, and f(θ) is the cavity's weight function (signal detected by the photodiode as the simulated scattered light is incident at different angles). When $f(\theta)$ approaches sin(θ), the value measured by the instrument approaches the true scattering coefficient value. However, if there are small deviations in $f(\theta)$ from sin(θ), then there will also be deviations in the measured scattering coefficient.

To understand the effects of the weight function's deviation from the expected sin(θ) on the scattering coefficient measurement, we compare the real b and b_b values for 7 different water samples (provided by National Research Laboratories (NRL)[32] and shown in Appendix F) and compare them to the expected scattering coefficient values as expected from the b meter and the b_b meter. First, we use Eqs. 2.11 and 2.13 to calculate the true b and b_b, respectively, for each NRL water sample. Then, the backscattering coefficient measurement is calculated for the b_b meter by following Eq. 3.3, where the weight function of the cavity is described by the"Average (norm)" data presented in Fig. 6.2. Because of the resolution needed for the perform the integration exceeds the resolution of our experimental setup, a cubic interpolation was used on the data to estimate the instrument's weight function at every angle

provided by the VSF data. Therefore,

$$P_b' = 2\pi \int_{\pi/2}^{\pi} \beta(\theta) f(\theta) d\theta + \pi \int_{\theta_{10}}^{\pi/2} \beta(\theta) f(\theta) d\theta - \pi \int_{\pi/2}^{\theta_{20}} \beta(\theta) f(\theta) d\theta - \frac{\pi R_1}{Z_0} \int_{\theta_{10}}^{\theta_{20}} \beta(\theta) \cos\theta d\theta \tag{6.1}$$

With an R_1 value of 9.5 mm and the laser centered about the aperture where $Z_0 =$ 0.762 mm, $\theta_1(0) = 89°$, and $\theta_2(0) = 91°$.

Similarly, the total scattering coefficient measurement was calculated for the b meter by following Eq. 3.8, where the cubic spline interpolation was used on the data presented in Fig. 6.5 to calculate all θ values outside of the setup's resolution abilities. We find

$$P' = 2\pi \int_0^{\pi} \beta(\theta) f(\theta) d\theta - 2\pi \int_0^{\theta_3(0)} \beta(\theta) f(\theta) d\theta - 2\pi \frac{f\Big(\theta_3(0)\Big)}{\theta_4(0) - \theta_3(0)} \int_{\theta_3(0)}^{\theta_4(0)} \beta(\theta) f\Big(\theta_4(0) - \theta\Big) d\theta. \tag{6.2}$$

Our b meter design has a value of $R_2 = 2$mm. The minimum angle of scattered light accepted by the instrument is directly related to the z distance (from the center of the aperture to from the laser source). The smallest angle the b meter can resolve is 0.14°, which exceeds the resolution of every commercial instrument to date. The smallest angle provided in the VSF data sets (θ_{min}) are in the range from 0.5° (for the Lingurian Sea) and 0.952° (for all other samples). The distance z can be selected such that the minimum angle of acceptance of the b meter ($\theta_3(0)$) matches (θ_{min}) for each VSF set. As a consequence, the second term of Eq. 6.2 cannot be calculated from the VSF measurements provided without added assumptions about the VSF's shape and composition. In addition, the θ_{min} required to perform the trapezoidal

integration of the first term (determined by the VSF values for each water sample) does not provide enough information for us to determine the third term the equation. Hence, to measure the expected P' for known samples of water, we can only perform the first integral in Eq. 6.2, starting at the first $\beta(\theta)$. This value will give us a good first order approximation of how accurate we can expect the meter to be. We found the b meter's measurement shows total scattering coefficient deviations smaller than 1.5% with respect to the real value for every sample, and the b_b meter had measurement errors in the backscattering coefficient measurements less than 0.7%. Values are presented in Fig. 6.8. This conclusively shows that our instrument should be capable of outperforming every commercial instrument to date.

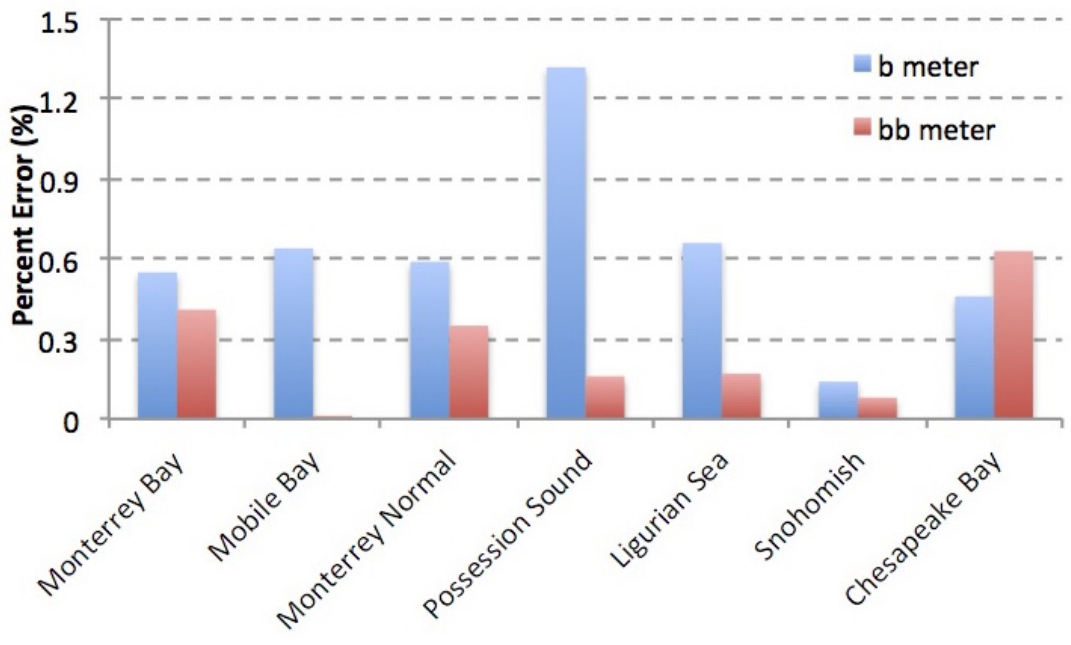

Figure 6.8: Percent error between expected scattering coefficient value and expected scattering coefficient value for the b meter and b_b meter in different water samples. The different error values come from the characteristic $\beta(\theta)$ of each sample.

7. INSTRUMENT RESULTS, CALIBRATION AND DISCUSSION

7.1 The b_b Meter

To obtain a proper calibration of the instrument, the resulting signal from the instrument at known backscattering values need to be examined. As described in Chap. 3, the power which enters the instrument due to scattered light from the laser source is defined as:

$$P = 2Z_0AE_0\Big(b_b(1+\rho_0)\Big), \tag{7.1}$$

where $2Z_0AE_0$ is a proportionality factor introduced by the geometry of the cavity. In our instrument, the parameters are defined as $Z_0 = 0.030$", $A = \pi(0.5\ mm)^2$, and $E_0 = 3.14$, as described in Section 6.1.

The scattered light enters the instrument through the aperture and, via multiple reflections, illuminates the entire cavity. The illumination is detects via a photo-multiplier tube (PMT) positioned at the 8 mm diameter hole on the top piece of the cavity. The total power detected by the PMT is proportional to the b_b of the scattering medium, as described in Chap. 3. This is true even after limiting the acceptance ϕ angle of the aperture as described in Section 6.1. The PMT in turn outputs a signal as a function of voltage, proportional to the power sampled in the cavity.

Under laboratories conditions, it is possible for the signal to be contaminated and biased. In other words the signal detected by the meter can be expressed as:

$$S_{back} = S_{electric} + S_{equip} + K_b b_{b\ water} + K_b b_{imp} + K_b b_{b\ PSL} \tag{7.2}$$

where $S_{electric}$ is the bias in the measurements due to electronic noise; S_{equip} is the

fraction of light detected by the instrument because of unwanted reflections of the laser beam into the cavity aperture (e.g.: reflections due to the water tank walls and the glass rod leading the laser beam); $K_b b_{b\ water}$ is the signal detected from light scattering off the molecules; $K_b b_{imp}$ is the signal detected from scattered light off pure water molecules; and $K_b b_{b\ PSL}$ is the signal scattered off the polystyrene spheres in the water.

As the particle concentration in the water changes, we expect only the b_{PSL} term in Eq 7.2 to be affected. In addition, by knowing the change of particle concentration and the size of the particles, we can use Mie theory to calculate the corresponding scattering coefficents. That is, by plotting the signal change (dS_{back}) as compared to the change in expected backscattering coefficient of the water caused by the particle concentration (db_{PSL}), we can easily obtain the slope resulting graph and determine the meter's scaling factor. For the backscattering meter, this scaling factor is called the calibration constant, K_b, and is unique to the designed meter.

$$K_b = \frac{dS_{back}}{db_{b\ PSL}} \tag{7.3}$$

To properly calibrate the meter, we measured the backscattering coefficient of increasing concentrations of two different particle sizes (1 μm and 4 μm in diameter). The goal is to find the relationship between the signal measured by the PTM and the b_b due to the particles. To accomplish this, the b_b meter needs to be water sealed. This was accomplished by adding RTV along all the seams between the quartz piece and the teflon top. Then hot glue was used to seal the bottom cavity to the top piece. In addition, the entire cavity was wrapped in aluminum tape, and spayed with liquid acrylic. To ensure the laser source entered the medium centered on the aperture, a 1/4" diameter glass rod was secured to the cavity, with it's edge aligned

to the center of the aperture. See Fig. 7.1.

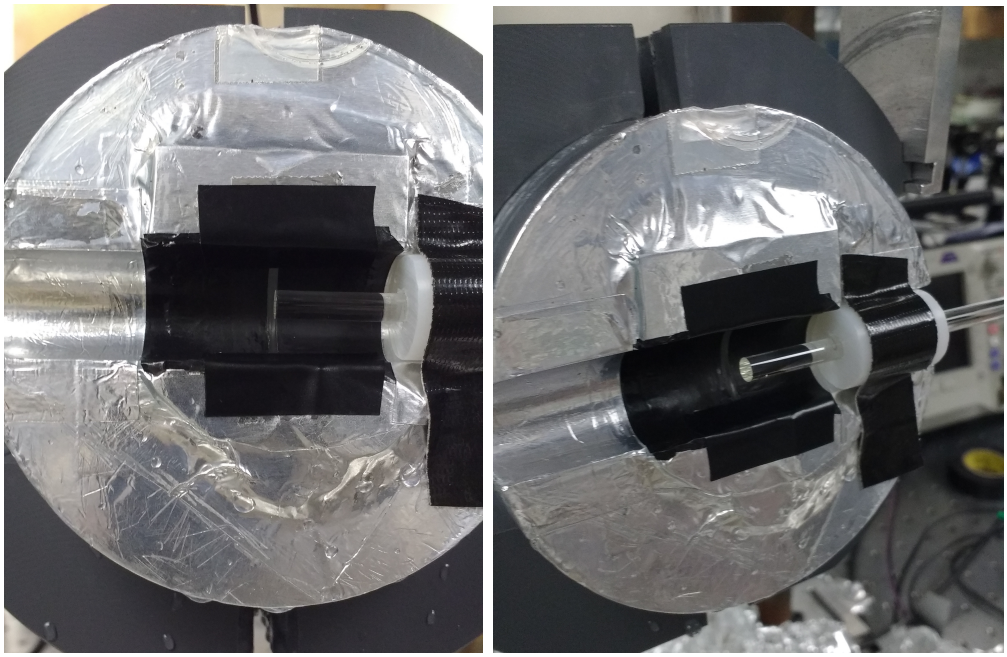

Figure 7.1: Picture showing the placement of the glass rod being centered with the aperture of the b_b meter

We filled a water tank with 22.8 L of highly purified water, free of organic elements, filtered through a with a 0.2 μm filter. The cavity was submerged until the top of the meter, where the PMT was positioned, barely reached the water. The meter was positioned such that the opposite end of the glass rod was in contact with the water tank, and aligned with the laser source, such that the laser traveled through the center of the rod. At this point the signal collected by the PMT was recorded and labeled as background. Then measured amounts of a polystyrene latex microsphere solution were added to the tank. The signal from the b_b meter was recorded for each new microsphere concentration.

Two different microsphere sizes were selected to calibrate and validate the meter. In each case, a solution was prepared such that, in its entirety, the microspheres would change the backscattering coefficient of the water in the tank by about 0.05 m^{-1}. An aquarium pump was placed in the tank to ensure the added particles were well mixed and remained suspended. In addition, WETLabs' C-Star Transmissometer (CST) was also placed in the water tank to confirm the particles are homogeneously distributed in the water, as well as obtain an accurate measurement of the concentration of particles. Between sample sizes, the tank was emptied and rinsed several times, and the water pump and CST were thoroughly washed to avoid cross-contamination between particle sizes.

The first solution was made by adding 1230 μl of a 1% concentration of 1 $\pm$ 0.011 μm diameter polystyrene latex microspheres to 10 ml of water. The second solution was made by adding 5 ml of a 1% concentration of 4 $\pm$ 0.043 μm diameter particles to 10 ml of water. Small amounts of each concentration were pipetted into the water tank. NIST traceable microspheres were used, with well known size distribution and mean diameter of the particles. Data details are found in Appendix G.1

The recorded signal of each measurement was plotted against the calculated microsphere b_b at each concentration. The background measurement of each curve was subtracted from every point, such that at the signal plotted shows 0 V in the absence of particles. The standard deviation of each data point was calculated and are also shown in Fig. 7.2. Linear fits to the data were used to calculate the slope and slope error. The K_b values, as defined by the slopes are $K_{b\ 1\mu m} = 2.78 \pm 0.0077$ and $K_{b\ 4\mu m} = 2.71 \pm 0.0084$.

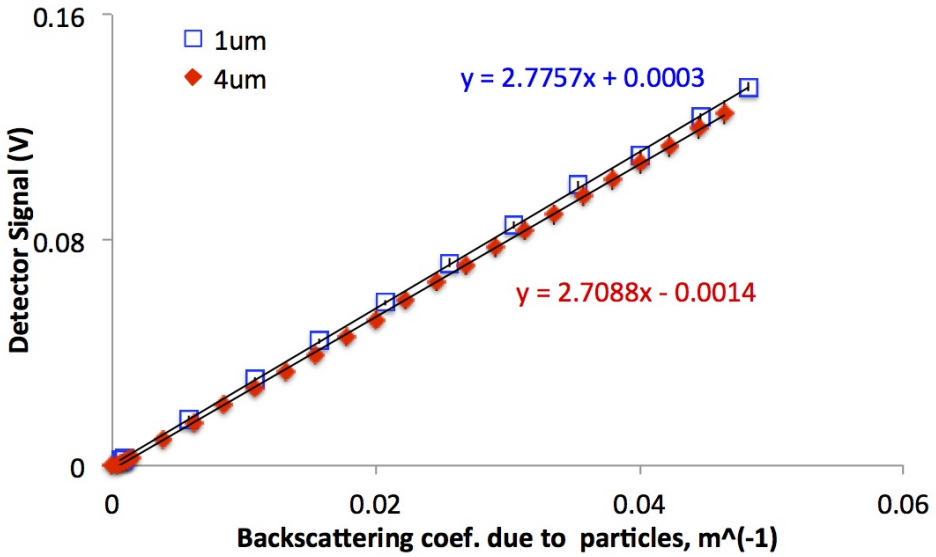

Figure 7.2: Measured signal for microparticle concentrations of particles with 1μm (blue) and 4 μm (red) in diameter plotted against the expected b_b. Linear fit also shown.

7.2 The b Meter

To calibrate the b meter it is necessary to revisit Eq. 3.8. As described in Section 6.2, the characteristic parameters of the instrument are $Z_0 = 1$ cm and $r = 2$ mm. To minimize the error values, the source needs to as far away as possible from the aperture of the b meter. In our setup, we positioned the b meter on the opposite end of the water tank, allowing for the laser beam to travel 39 cm in the water before it reached the center of the aperture. In addition, the laser beam was aligned such that it remained centered with the instrument's channel, 2 mm away from the surface. This setup allows us to define the field of view of the b meter, where the angles of integration in the error values of Eq. 3.8 correspond to $\theta_3(z = 0) = 0.29°$ and $\theta_4(z = 0) = 0.30°$. Here, θ_3 describes the smallest angle

As with the b_b meter, the laboratory environment has the potential to further

bias the data, such that

$$S = S_{electric} + S_{equip} + Kb_{water} + Kb_{imp} + Kb_{PSL} \tag{7.4}$$

where $S_{electric}$ is the bias in the measurements due to electronic noise; S_{equip} is the fraction of light detected by the instrument because of unwanted reflections of the laser beam into the cavity aperture (e.g.: reflections due to the water tank walls and the glass rod leading the laser beam); Kb_{water} is the signal detected from light scattering off the molecules; Kb_{imp} is the signal detected from scattered light off pure water molecules; and Kb_{PSL} is the signal scattered off the polystyrene spheres in the water.

As the particle concentration in the water changes, we expect only the b_{PSL} term in Eq. 7.4 to be affected. With Mie theory we calculate the expected total scattering coefficient for each concentration. Then, by plotting the signal change (dS) with respect to the expected b caused by the microsphere particles (db_{PSL}), we can determine the meter's calibration constant, K,

$$K = \frac{dS}{db_{PSL}} \tag{7.5}$$

where K is the calibrating constant of the backscattering meter, and is unique to the designed meter. In practice, $K = Cf(1 - \rho_I - \rho_I I)2Z_0E_0A$, where C is the proportionality constant which converts detected power to a voltage, f is the fraction of total power detected by the instrument, and ρ_0 is the geometric error of the cavity (defined in Eq 3.5).

The setup and procedure used for calibrating the total scattering meter followed similar steps as the b_b meter. A tank was filled with 22.8 L of high purity filtered

water and placed on a jack. The meter was water sealed and submerged in the water by lifting the water tank until the PMT was close to the surface of the water. The signal detected by the b meter was recorded and labeled as background signal. Then small concentrations of microsphere particles were added to the tank, and the corresponding meter response measured. The same sized microspheres were used to calibrate the b meter (1 μm and 4 μm), however the concentration was such that the final change of the total scattering coefficient was estimated to be 0.2 m^{-1}.

The recorded signal of each measurement was plotted against the calculated microsphere b, at each concentration. The standard deviation of each data point was calculated, and the errors are also shown. Data points can be found in Appendix G.2. The background measurement of each curve was subtracted from every point. Linear fits to the data were made and the resulting equation is also shown. See Fig. 7.3. The K values, as defined by the slopes of the curves are $K_{1\mu m} = 1.20 \pm 0.0062$ and $K_{4\mu m} = 1.26 \pm 0.0062$.

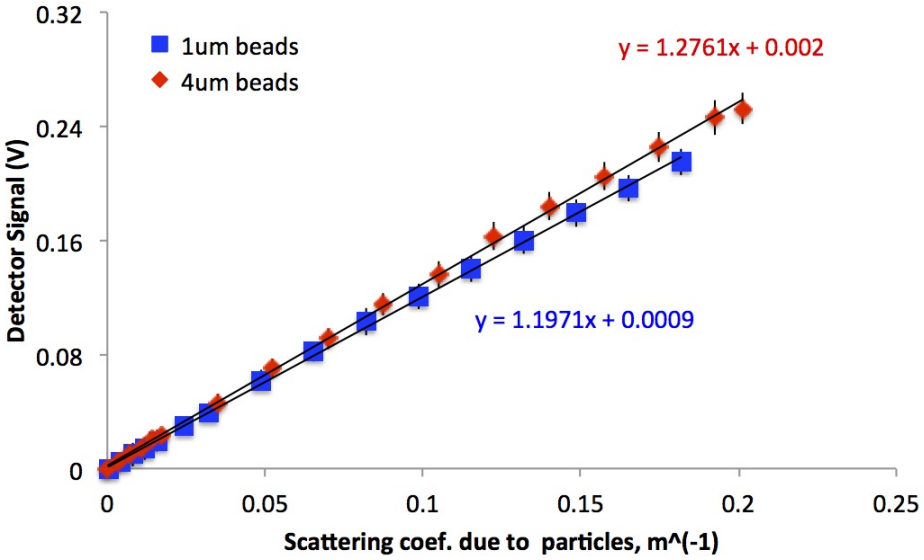

Figure 7.3: Measured signal for microparticle concentrations of particles with 1μm (blue) and 4 μm (red) in diameter with respect to expected b value. Linear fit also shown.

7.3 Additional Sources of Errors

It is important to note that the change of concentration of particles in the water tank could potentially have a small effect on other terms in Eqs. 7.2 and 7.4. For example, increased scattering in the water tank will also change the direction of the reflected light from the tank walls and other equipment in the tank, potentially biasing the signal from the detector. However, these effects are expected to be very small in comparison to the main signal detected. In addition, these changes are nearly impossible to completely isolate. As a result, great care was taken to minimize all other sources of optical and particulate contamination in the water.

8. CONCLUSION AND FUTURE WORK

We have presented two new instruments: a the total scattering coefficient meter and the backscattering coefficient meter. Both these instruments measure the desired coefficient directly and with an unprecedented accuracy. The mathematical theory for both instruments has been presented, and the physical characteristics and design process was discussed. The theoretical expectation of the finalized prototype has been derived and tested with VSF information of six different locations. The calibration of each meter was done by observing the meter's response when submerged in a tank under a changing, controlled microparticle polystyrene latex concentration.

Overall, both of the instruments presented make use of the exact definition of the scattering coefficient they measure, and present an instrument which, instead of making assumptions about the scatterers, collect the scattered light and applies the necessary weight function to obtain the desired scattering coefficient.

These prototypes were built was a proof of concept. Future iterations should consider broadening both instrument's ϕ range to further minimize scattering effects from ordered structures. In addition, the use of aluminum foil and spray paint is unsuited for open water. The meters should have proper enclosure, and the aperture walls should be made of a sturdy yet equally thin material as the aluminum foil. In addition, the material used must be perfectly opaque, with a high absorption coefficient on one side and a high reflection coefficient on the other side. The inside of the cavity should be one solid material, such that the quartz piece which defines the entrance aperture for scattered light, also extends to the hemispherical walls of the integrating cavity.

REFERENCES

[1] M. I. Mishchenko, J. W. Hovenier, and L. D. T. (editors), "Light scattering by nonspherical particles: Theory, measurements, and applications," Measurement Science and Technology **11**, 1827 (2000).

[2] C. F. Bohren and D. R. Huffman, *Absorption and Scattering of Light by Small Particles* (Wiley-VCH Verlag GmbH, 2007).

[3] H. C. van de Hulslt, *Light Scattering by Small Partilces* (Wiley, 1957).

[4] M. Kerker, *Scattering of Light, and Other Electromagnetic Radiation* (Academic, 1969).

[5] H. R. Gordon, M. R. Lewis, S. D. McLean, M. S. Twardowski, S. A. Freeman, K. J. Voss, and G. C. Boynton, "Spectra of particulate backscattering in natural waters." Opt. Express **17**, 16192–16208 (2009).

[6] M. Kim and W. D. Philpot, "Development of a laboratory spectral backscattering instrument: design and simulation," Appl Opt **44**, 6952–6961 (2005).

[7] R. A. Maffione and D. R. Dana, "Instruments and methods for measuring the backward-scattering coefficient of ocean waters," Appl Opt **36**, 6057–6067 (1997).

[8] C. D. Mobley, L. K. Sundman, and E. Boss, "Phase function effects on oceanic light fields," Appl Opt **41**, 1035–1050 (2002).

[9] M. S. Twardowski, E. Boss, J. B. Macdonald, W. S. Pegau, A. H. Barnard, and J. R. V. Zaneveld, "A model for estimating bulk refractive index from the optical backscattering ratio and the implications for understanding particle composition in

case I and case II waters," Journal of Geophysical Research: Oceans **106**, 14129–14142 (2001).

[10] G. R. Fournier and J. L. Forand, "Analytic phase function for ocean water," in "Proc. SPIE," , vol. 2258 (1994), vol. 2258, pp. 194–201.

[11] J. Chen, W. Quan, G. Yao, and T. Cui, "Retrieval of absorption and backscattering coefficients from HJ-1A/CCD imagery in coastal waters," Opt. Express **21**, 5803–5821 (2013).

[12] L. Lorenz, "Ueber die refractionsconstante," Annalen der Physik **247**, 70–103 (1880).

[13] Ludvig, "Lysbevaegelsen i og uden for en af plane lysbolger belyst kugle," Det Kongelige Danske Videnskabernes Selskabs Skrifter **6**, 1–62 (1890).

[14] G. Mie, "Beiträge zur optik trüber medien, speziell kolloidaler metallösungen," Annalen der Physik **330**, 377–445 (1908).

[15] T. Petzold, "Volume scattering functions for selected ocean waters," Scripps Institution of Oceanography Reference pp. 72–78 (1972).

[16] A. Bricaud, A. Morel, and L. Prieur, "Optical efficiency factors of some phytoplankters1," Limnology and Oceanography **28**, 816–832 (1983).

[17] A. Morel and Y.-H. Ahn, "Optical efficiency factors of free-living marine bacteria: Influence of bacterioplankton upon the optical properties and particulate organic carbon in oceanic waters," Journal of Marine Research **48**, 145–175 (1990).

[18] Y.-H. Ahn, A. Bricaud, and A. Morel, "Light backscattering efficiency and related properties of some phytoplankters," Deep Sea Research Part A. Oceanographic Research Papers **39**, 1835 – 1855 (1992).

[19] G. C. Boynton and H. R. Gordon, "Irradiance inversion algorithm for absorption and backscattering profiles in natural waters: improvement for clear waters," Appl. Opt. **41**, 2224–2227 (2002).

[20] H. R. Gordon and G. C. Boynton, "Radiance—irradiance inversion algorithm for estimating the absorption and backscattering coefficients of natural waters: homogeneous waters," Appl. Opt. **36**, 2636–2641 (1997).

[21] D. Haubrich, J. Musser, and E. S. Fry, "Instrumentation to measure the backscattering coefficient bb for arbitrary phase functions," Appl Opt **50**, 4134–4147 (2011).

[22] J. Strutt, "On the scattering of light by small particles," Philosophical Magazine **41**, 447–454 (1871).

[23] J. Strutt, "On the electromagnetic theory of light," Philosophical Magazine **12**, 81–101 (1881).

[24] J. Strutt, "On the transmission of light through an atmosphere containing small particles in suspension, and on the origin of the blue of the sky," Philosophical Magazine **47**, 375–394 (1899).

[25] J. Strutt, "The light scattered by gaes: its polarization and intensity," Proceedings of the Royal Society London A **95**, 129–142 (1920).

[26] J. Strutt, "A re-examination of the light scattered by gases in respect of polarization. i. experiments on the common gases," Proceedings of the Royal Society London A **97**, 435–450 (1920).

[27] J. Cabannes, "Relation entre le degré de polarisation et l'intensité de la lumiére diffusée par des molécules anisotropes. nouvelle détermination de la constante davogadro," Le Journal de Physique et le Radium **6**, 129–142 (1920).

[28] A. Einstein, "Uber die von der molekularkinetischen theorie der warme geforderte bewegung von in ruhenden flussigkeiten suspendierten teilchen," Ann. Phys **17**, 549–560 (1905).

[29] M. von Smoluchowski, "Molekular-kinetische theorie der opaleszenz von gasen im kritischen zustande,sowie einiger verwandter erscheinungen," Annalen der Physik **330**, 205–226 (1908).

[30] A. Einstein, "Theorie der opaleszenz von homogenen flussigkeiten und flussigkeitsgemischen in der nahe des kritischen zustandes," Ann. Phys. **33**, 1275–1298 (1910).

[31] A. Morel, *Optical properties of pure water and pure sea water* (Academic Press, 1974), pp. 1–24.

[32] D. Grey, personal communication.

APPENDIX A

TOTAL SCATTERING COEFFIECIENT DERIVATION

Consider a laser beam with cross-sectional area A and irradiance E_o propagating along the z axis. The laser emerges from a transparent rod into the scattering medium at point $z = 0$. See figure A.1. Scattered light can only be detected if it enters the aperture in the detector (pink area in the Fig. A.1). The aperture itself is in the form of a half cylinder, extending from $\phi = -90°$ to $\phi = 90°$, and has a radius of R_2. The width of the aperture is centered about $z = Z_1$, and extends from $z = Z_1 - Z_0$ to $z = Z_1 + Z_0$

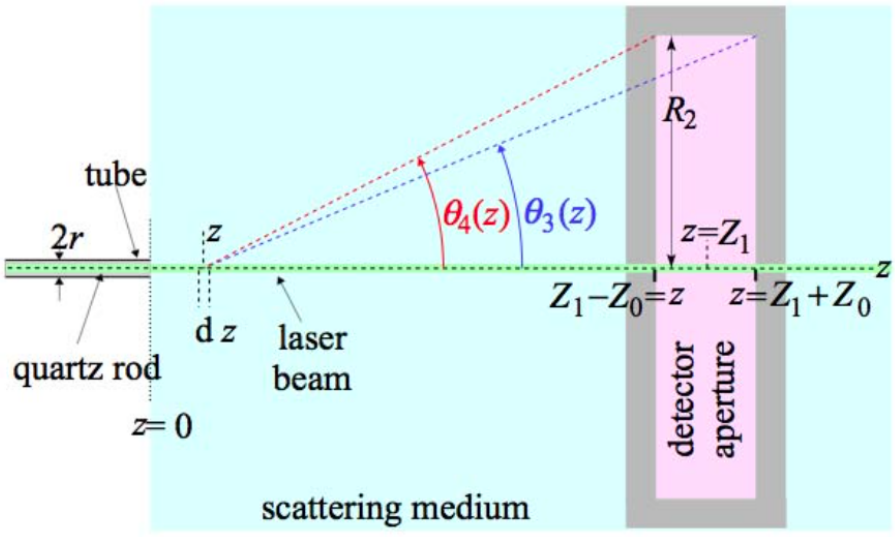

Figure A.1: Cross-section of b meter. The detector aperture is defined by a half cylinder of inner radius R_2

Consider a scattering volume (length dz and cross-sectional area A) at some point z on the axis. The power dP scattered scattered at an angle θ and capable of reaching the detector aperture can be expressed as

$$dP = \pi A E_0 \int_{\theta_3(z)}^{\theta_4(z)} dz \beta(\theta) \sin\theta d\theta \tag{A.1}$$

where θ is limited by $\theta_3(z) \leq \theta \leq \theta_4(z)$ and ϕ covers a 180° range. Therefore, the total power scattered into the detector (when taking every z location into account) is expressed as

$$P = \pi A E_0 \int_0^{\infty} dz \int_{\theta_3(z)}^{\theta_4(z)} \beta(\theta) \sin\theta d\theta. \tag{A.2}$$

To solve this equation, reverse the order of integration, i.e: integrate over z first. Consider the following variables

$$\theta_3(z) = \tan^{-1} \frac{R_2}{Z_1 + Z_0 - z} \ , \qquad \theta_4(z) = \tan^{-1} \frac{R_2}{Z_1 - Z_0 - z}. \tag{A.3}$$

For any z, only light scattered at $\theta_3(z) \leq \theta \leq \theta_4(z)$ (as defined by equation A.3) can enter the cavity through the aperture. Similarly, for any θ, z must be between $z_3(\theta)$ and $z_4(\theta)$ if the scattered light is to enter the cavity through the aperture. These limiting z values are defined as

$$z_3(\theta) = Z_1 + Z_0 - \frac{R_2}{\tan\theta} \tag{A.4}$$

$$z_4(\theta) = Z_1 - Z_0 - \frac{R_2}{\tan\theta}. \tag{A.5}$$

where $z_3(\theta) > z_4(\theta)$.

Reversing the order of integration of Equation A.2 we get

$$P = \pi A E_0 \Bigg\{ \int_{\theta_4(0)}^{\pi} \beta(\theta)\sin(\theta) d\theta \int_{z_4(\theta)}^{z_3(\theta)} dz \; + \; \int_{\theta_3(0)}^{\theta_4(0)} \beta(\theta)\sin(\theta) d\theta \int_{0}^{z_3(\theta)} dz \Bigg\}. \quad \text{(A.6)}$$

After integrating over z and using equation A.4 we get

$$P = \; (\pi A E_0) \Bigg\{ 2Z_0 \int_{\theta_4(0)}^{\pi} \beta(\theta)\sin\theta d\theta + \left(Z_1 + Z_0 - \frac{R_2}{\tan\theta} \right) \int_{\theta_3(0)}^{\theta_4(0)} \beta(\theta)\sin\theta d\theta \Bigg\} \quad \text{(A.7)}$$

which can be rewritten as

$$\begin{aligned} P = \; (\pi A E_0) \Bigg\{ & 2Z_0 \int_{\theta_4(0)}^{\pi} \beta(\theta)\sin\theta d\theta \; + \; Z_1 \int_{\theta_3(0)}^{\theta_4(0)} \beta(\theta)\sin\theta d\theta \\ & + \; Z_0 \int_{\theta_3(0)}^{\theta_4(0)} \beta(\theta)\sin\theta d\theta \; - \; R_2 \int_{\theta_3(0)}^{\theta_4(0)} \beta(\theta)\cos\theta d\theta \Bigg\}. \end{aligned} \quad \text{(A.8)}$$

Rearranging Eq A.8 while adding and subtracting equal terms (highlighted in red) with the goal of obtaining an expression in which one of the terms is the scattering

coefficient b gives

$$
\begin{aligned}
P &= (\pi A E_0)\Bigg\{\Bigg(2Z_0\int_{\theta_4(0)}^{\pi}\beta(\theta)\sin\theta d\theta + 2Z_0\int_{\theta_3(0)}^{\theta_4(0)}\beta(\theta)\sin\theta d\theta\Bigg) \\
&\quad + Z_1\int_{\theta_3(0)}^{\theta_4(0)}\beta(\theta)\sin\theta d\theta - R_2\int_{\theta_3(0)}^{\theta_4(0)}\beta(\theta)\cos\theta d\theta \\
&\quad + \Bigg(Z_0\int_{\theta_3(0)}^{\theta_4(0)}\beta(\theta)\sin\theta d\theta - 2Z_0\int_{\theta_3(0)}^{\theta_4(0)}\beta(\theta)\sin\theta d\theta\Bigg)\Bigg\} \\
P &= (\pi A E_0)\Bigg\{2Z_0\int_{\theta_3(0)}^{\pi}\beta(\theta)\sin\theta d\theta + Z_1\int_{\theta_3(0)}^{\theta_4(0)}\beta(\theta)\sin\theta d\theta \\
&\quad - R_2\int_{\theta_3(0)}^{\theta_4(0)}\beta(\theta)\cos\theta d\theta - Z_0\int_{\theta_3(0)}^{\theta_4(0)}\beta(\theta)\sin\theta d\theta\Bigg\} \\
P &= (\pi A E_0)\Bigg\{\Bigg(2Z_0\int_{\theta_3(0)}^{\pi}\beta(\theta)\sin\theta d\theta + 2Z_0\int_{0}^{\theta_3(0)}\beta(\theta)\sin\theta d\theta\Bigg) \\
&\quad - 2Z_0\int_{0}^{\theta_3(0)}\beta(\theta)\sin\theta d\theta + \Bigg(Z_1\int_{\theta_3(0)}^{\theta_4(0)}\beta(\theta)\sin\theta d\theta \\
&\quad - R_2\int_{\theta_3(0)}^{\theta_4(0)}\beta(\theta)\cos\theta d\theta - Z_0\int_{\theta_3(0)}^{\theta_4(0)}\beta(\theta)\sin\theta d\theta\Bigg)\Bigg\} \\
P &= (\pi A E_0)\Bigg\{2Z_0\int_{0}^{\pi}\beta(\theta)\sin\theta d\theta - 2Z_0\int_{0}^{\theta_3(0)}\beta(\theta)\sin\theta d\theta \\
&\quad + \int_{\theta_3(0)}^{\theta_4(0)}\beta(\theta)\Big(\big(Z_1 - Z_0\big)\sin\theta - R_2\cos\theta d\theta\Big)d\theta\Bigg\} \\
\frac{P}{AE_0Z_0} &= 2\pi\int_{0}^{\pi}\beta(\theta)\sin\theta d\theta - 2\pi\int_{0}^{\theta_3(0)}\beta(\theta)\sin\theta d\theta \\
&\quad + \frac{\pi}{Z_0}\int_{\theta_3(0)}^{\theta_4(0)}\beta(\theta)\Big(\big(Z_1 - Z_0\big)\sin\theta - R_2\cos\theta d\theta\Big)d\theta.
\end{aligned}
$$

Setting $P' = \frac{P}{AE_0Z_0}$ and using the definition of the total scattering coefficient, $b = 2\pi\int_0^{\pi}\beta(\theta)\sin\theta d\theta$, we obtain

$$
P' = b + \Bigg[-2\pi\int_{0}^{\theta_3(0)}\beta(\theta)\sin\theta d\theta + \frac{\pi}{Z_0}\int_{\theta_3(0)}^{\theta_4(0)}\beta(\theta)\Big(\big(Z_1 - Z_0\big)\sin\theta - R_2\cos\theta\Big)d\theta\Bigg] \quad \text{(A.9)}
$$

The quantity P' is just proportional to the voltage signal measured. The two terms in the square brackets identify the deviation from the ideal b measurement by the instrument. The first of these is the largest; it corresponds to scattering at angles $< \theta_3(0)$. These scattered beams completely miss the detector aperture. The second term accounts for the small fraction of light scattered at angles between $\theta_3(0)$ and $\theta_4(0)$ and which partially misses the detector aperture.

Not only is the second term very small when compared with the first term in the square brackets, but, when the integrand is evaluated at the upper limit ($\theta = \theta_4(z)$) or equivalently $z_4(\theta) = 0$, then Eq. A.5 shows the integrand is zero,

$$R_2 \cos\theta_4(0) - (Z_1 - Z_0)\sin\theta_4(0) = 0. \tag{A.10}$$

The last integral in the brackets in Eq. A.9 can be simplified if we allow the arc length to be equated to one leg of a right triangle whose hypotenuse is $2Z_0$. See blue triangle figure A.2. From the yellow section in Fig. A.2

$$\frac{R_2}{\sin\theta_4(0)}(\theta_4(0) - \theta_3(0)) \approx 2Z_0 \sin\theta_3(0) \tag{A.11}$$

We can use Eq. A.10 to eliminate the explicit dependence on R_2, followed by Eq. A.11 to eliminate the explicit Z_0 and Z_1, such that Eq. A.9 takes the form

$$P' = b - \left[2\pi \int_0^{\theta_3(0)} \beta(\theta)\sin\theta d\theta + \frac{\pi}{Z_0}\int_{\theta_3(0)}^{\theta_4(0)} \beta(\theta)\frac{2Z_0\sin\theta_3(0)}{\theta_4(0) - \theta_3(0)}\Big(\sin\theta_4(0)\cos\theta - \cos\theta_4(0)\sin\theta\Big)d\theta\right]$$

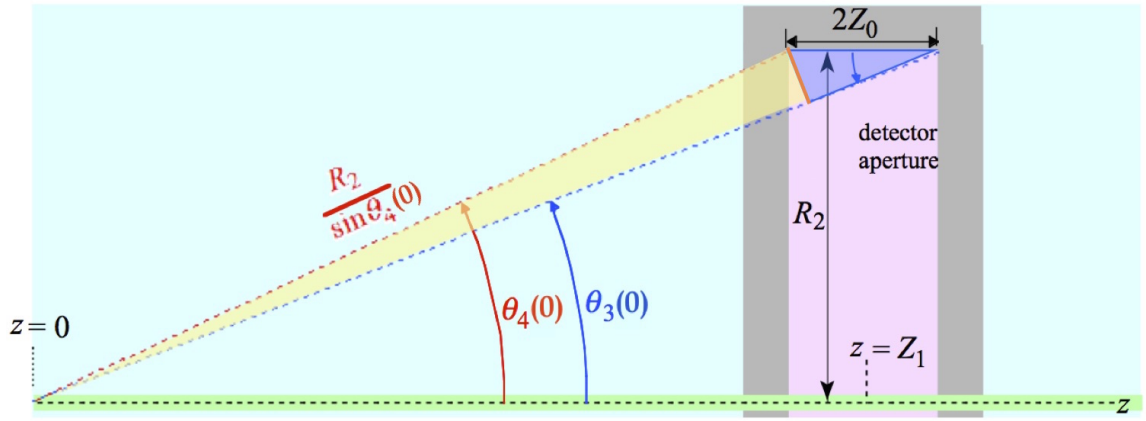

Figure A.2: Graphic representation of approximation used for error term simplification. The orange segment is the arc length being equated to one leg of a right triangle

which can be further simplified to

$$P' = b - 2\pi \int_0^{\theta_3(0)} \beta(\theta)\sin\theta d\theta - 2\pi \frac{\sin\theta_3(0)}{\theta_4(0)-\theta_3(0)} \int_{\theta_3(0)}^{\theta_4(0)} \beta(\theta)\sin\big(\theta_4(0)-\theta\big)d\theta. \tag{A.12}$$

In other words, we can write the total power collected by the detector as

$$P' = b(1-\rho_I-\rho_{II}) \tag{A.13}$$

where $\rho_I = \frac{2\pi}{b}\int_0^{\theta_3(0)} \beta(\theta)\sin\theta d\theta$ and $\rho_{II} = \frac{2\pi}{b}\frac{\sin\theta_3(0)}{\theta_4(0)-\theta_3(0)}\int_{\theta_3(0)}^{\theta_4(0)} \beta(\theta)\sin\big(\theta_4(0)-\theta\big)d\theta$.

Note that Eq. A.11 is the only approximation in this evaluation. The numerical evaluation of these two integrals agree to 10 significant figures for the different expected $\beta(\theta)$ of 4 μm and 40 μm diameter polystyrene spheres. Therefore, not considered a significant source or error in our calculations.

APPENDIX B

TECHNICAL DRAWINGS FOR CAVITY PIECES

This section contains all the technical drawings for the cavity holder, the PTFE cavities and the quartz aperture pieces as they were designed in the final stage to enable the characterization of the backward and total scattering meter via the measurement of θ and ϕ.

First, the aluminum base is presented, followed by the PVC clamp. In both cases the first page shows the image overview, and then the dimensions are shown. all dimensions are in inches, since this is how it the images were presented to the machine shop.

The subsequent drawings are specific to the PTFE cavity design. A single "cavity bottom" is presented, and used for both the total and backward scattering coefficient meter. Then, the teflon top and quartz piece used for each meter is presented.

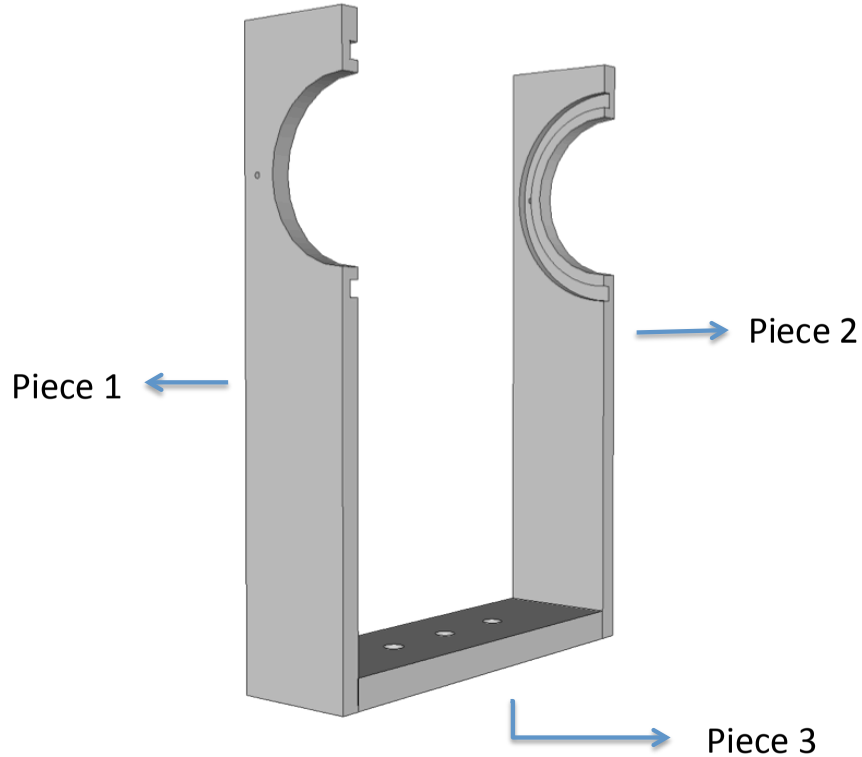

Name	Eleonora Figueroa		
Material	Aluminum	Title	Metal Base
Page	1/4	Piece	All

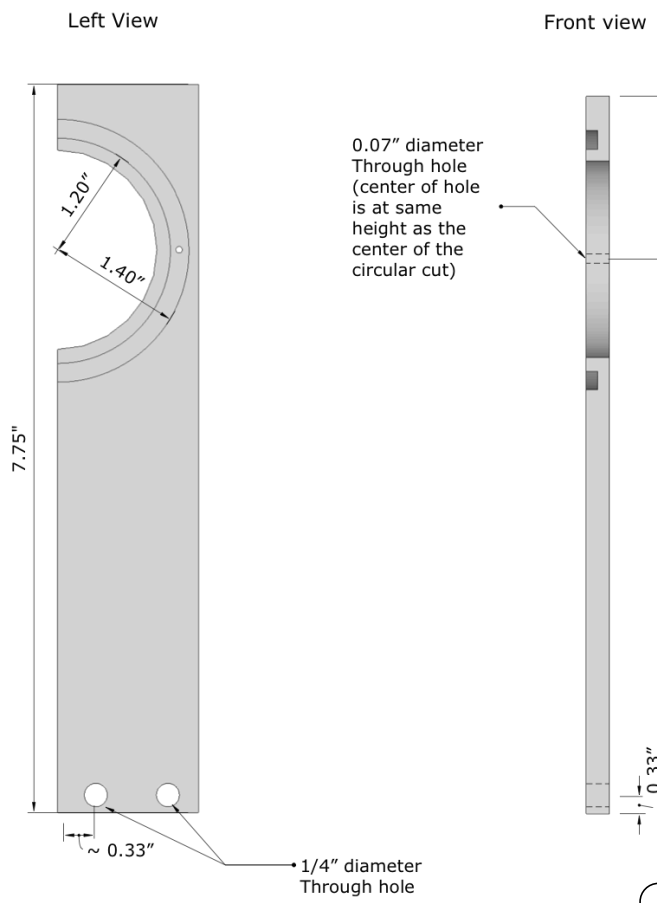

Name	Eleonora Figueroa				
Material	Aluminum			Title	Metal Base
Tolerance	+/- 0.01”	Page	2/4	Piece	1

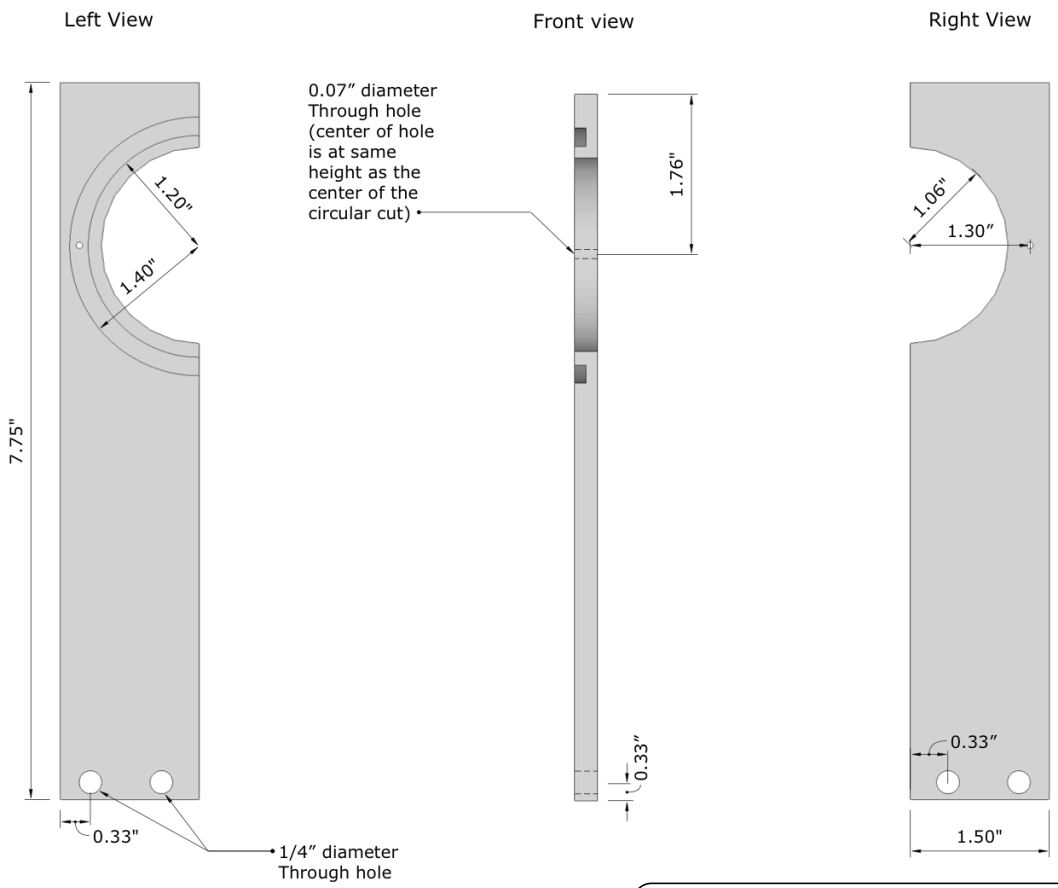

Name	Eleonora Figueroa				
Material	Aluminum			Title	Metal Base
Tolerance	+/- 0.01"	Page	3/4	Piece	2

Top View

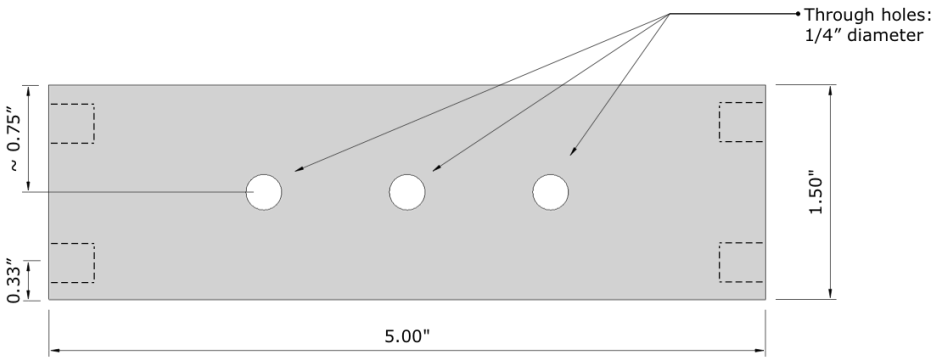

Front View

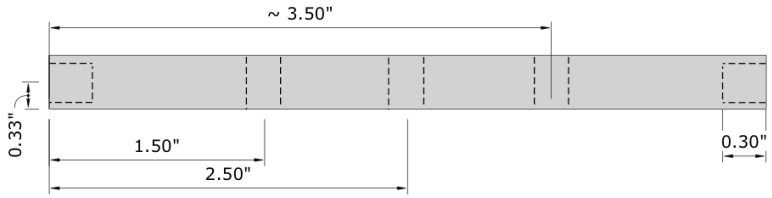

Side View

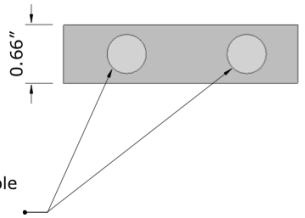

Name	Eleonora Figueroa				
Material	Aluminum			Title	Metal Base
Tolerance	+/- 0.01"	Page	4/4	Piece	3

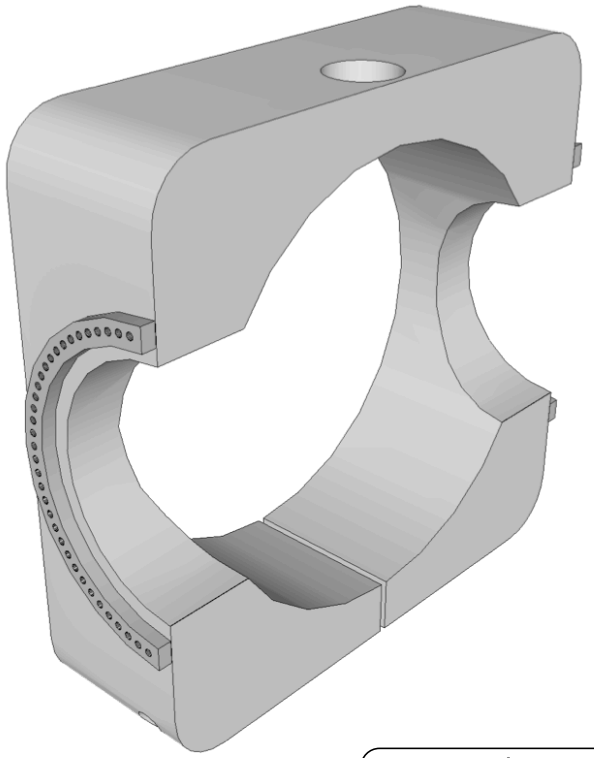

Name	Eleonora Figueroa		
Material	Black PVC	Title	PVC Clamp
Page	1/2	Piece	Overview

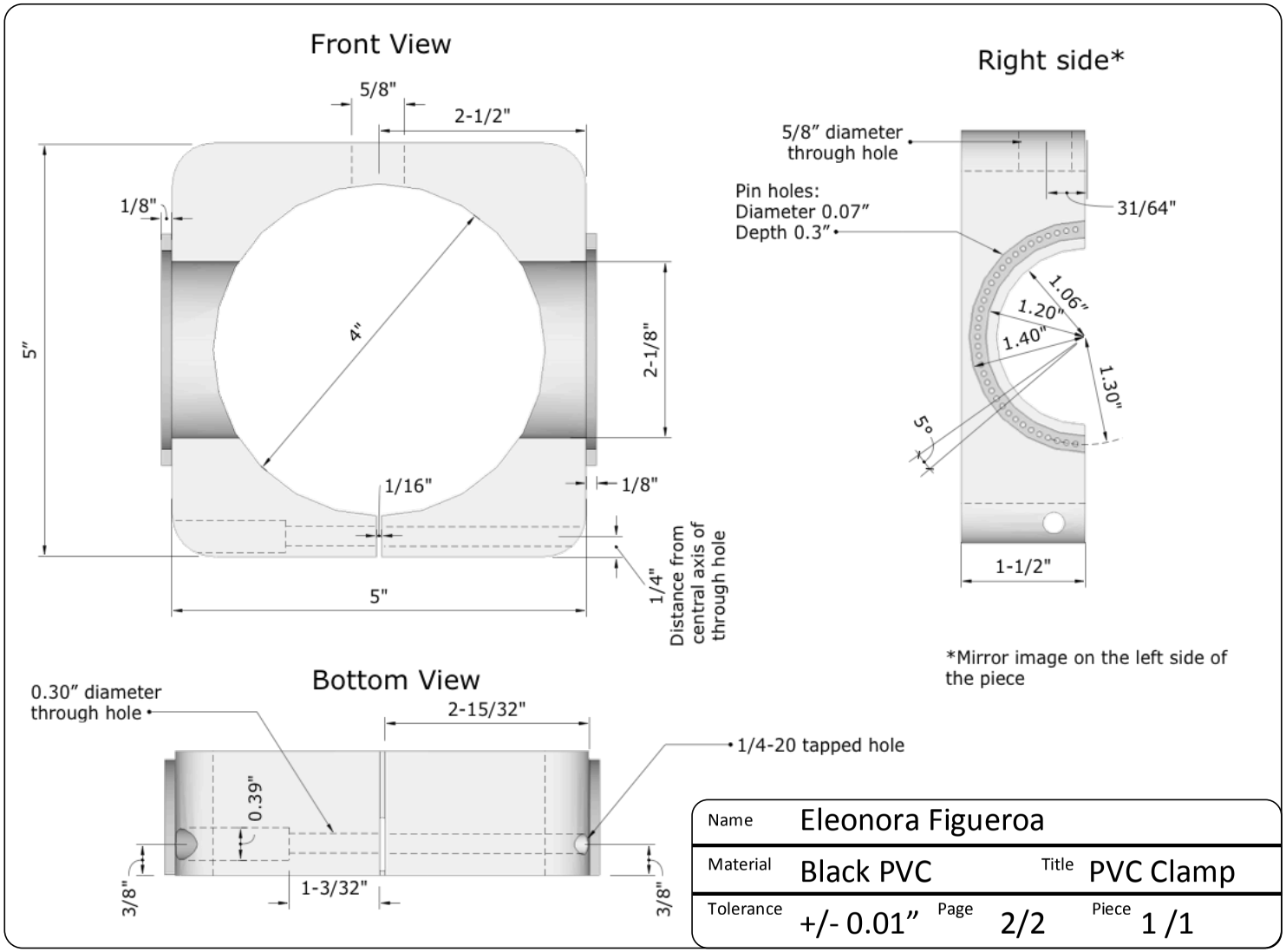
Front View
5/8"
2-1/2"
1/8"
5"
4"
2-1/8"
1/16"
1/8"
1/4"
Distance from central axis of through hole
5"
Right side*
5/8" diameter through hole
Pin holes:
Diameter 0.07"
Depth 0.3"
31/64"
1.06"
1.20"
1.40"
1.30"
5°
1-1/2"
*Mirror image on the left side of the piece
Bottom View
0.30" diameter through hole
2-15/32"
1/4-20 tapped hole
0.39"
3/8"
1-3/32"
3/8"
Name Eleonora Figueroa
Material Black PVC
Title PVC Clamp
Tolerance +/- 0.01"
Page 2/2
Piece 1 /1

Top View

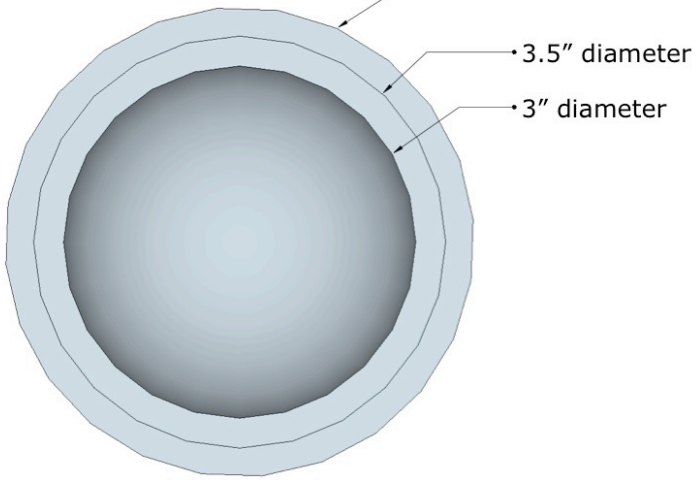

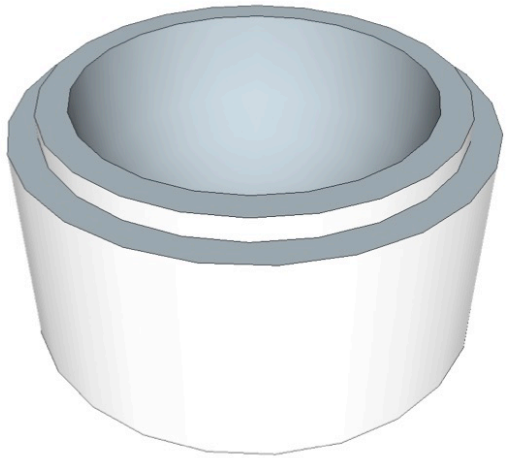

Side View

Name	Eleonora Figueroa		
Material	PTFE	Title	Cavity Bottom
Tolerance	+/- 0.005″	Page 1/1	Piece 1/1

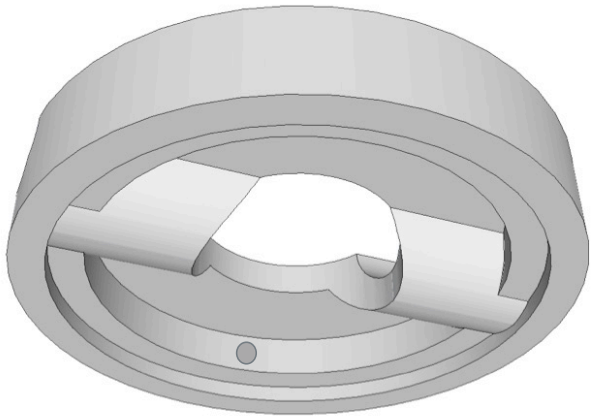

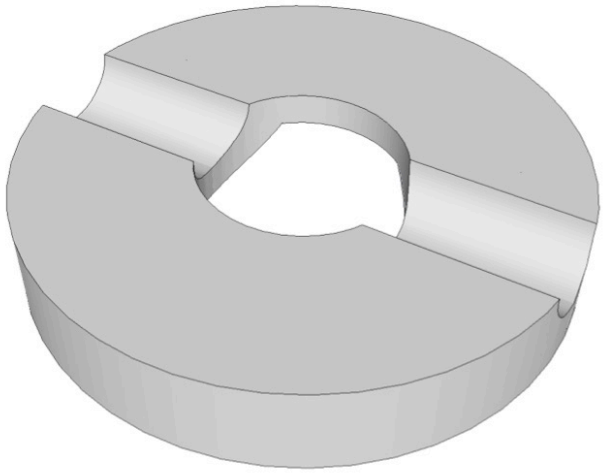

Name	Eleonora Figueroa		
Material	PTFE	Title	Backscattering Top
Page	1/2	Piece	Overview

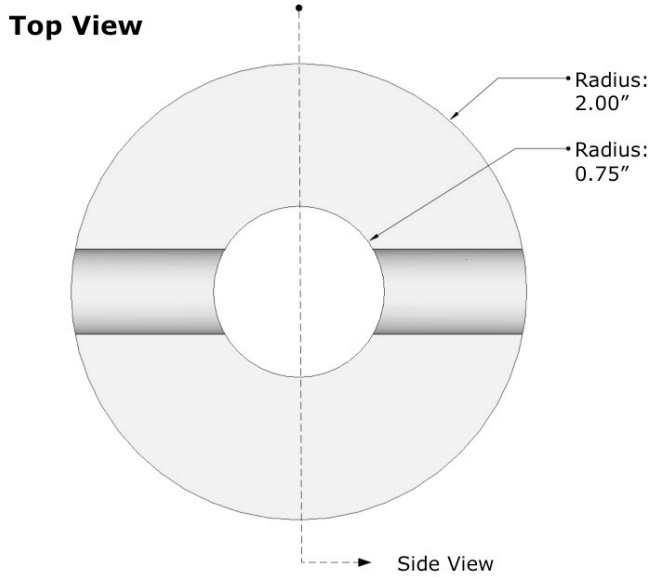

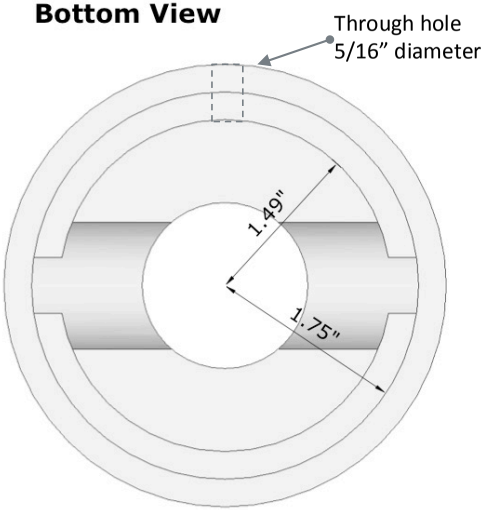

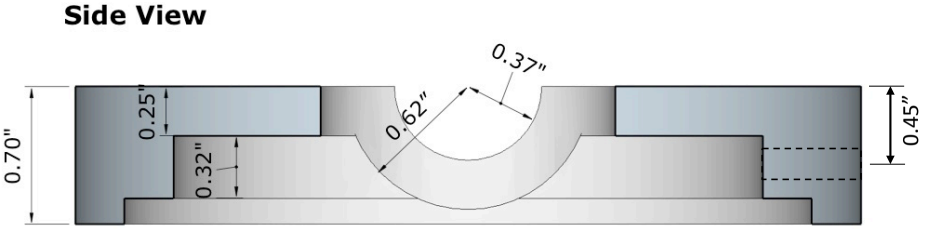

Name	Eleonora Figueroa				
Material	PTFE	Title	Backscattering Top		
Tolerance	+/- 0.005”	Page	2/2	Piece	1/1

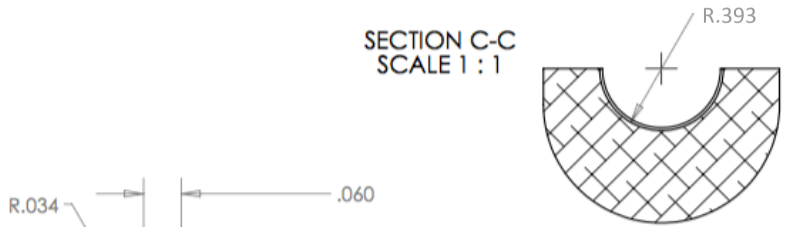

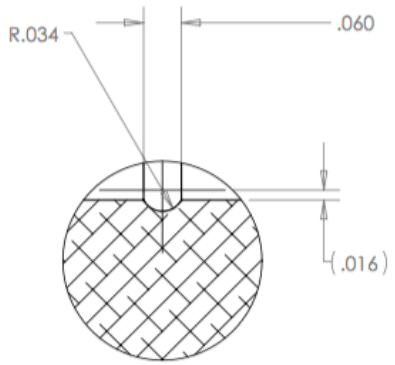

DETAIL B
SCALE 4 : 1

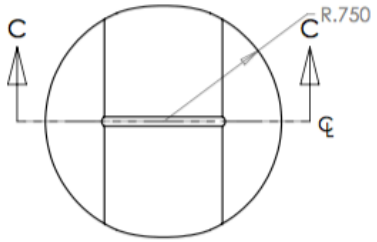

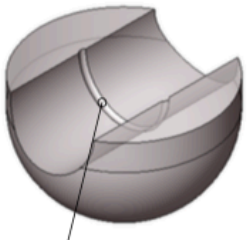

Must be optically polished

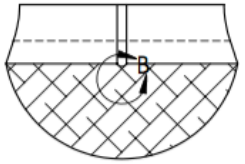

SECTION A-A
SCALE 1 : 1

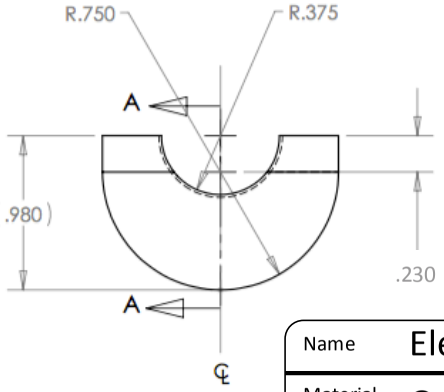

Name	Eleonora Figueroa		
Material	Quartz	Title	b_b Aperture Piece
Tolerance	+/- 0.005”	Units inches	Piece 1/1

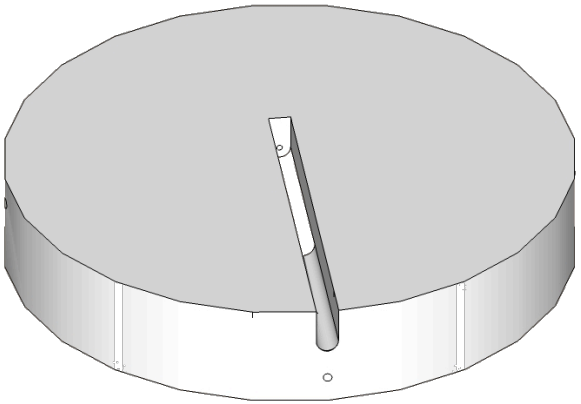

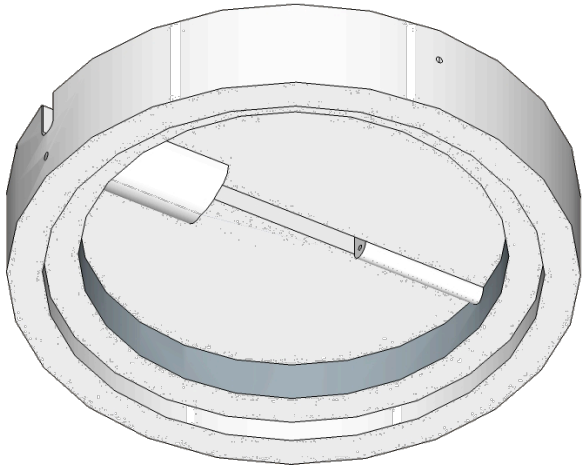

Name	Eleonora Figueroa		
Material	PTFE	Title	Total Scattering Coef. Top
Page	1/2	Piece	Overview

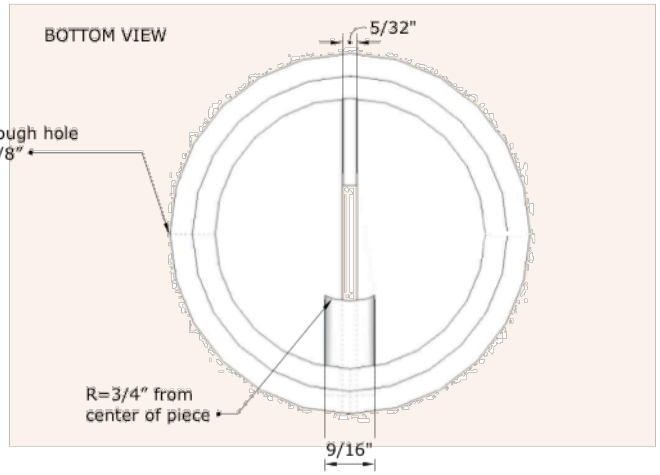

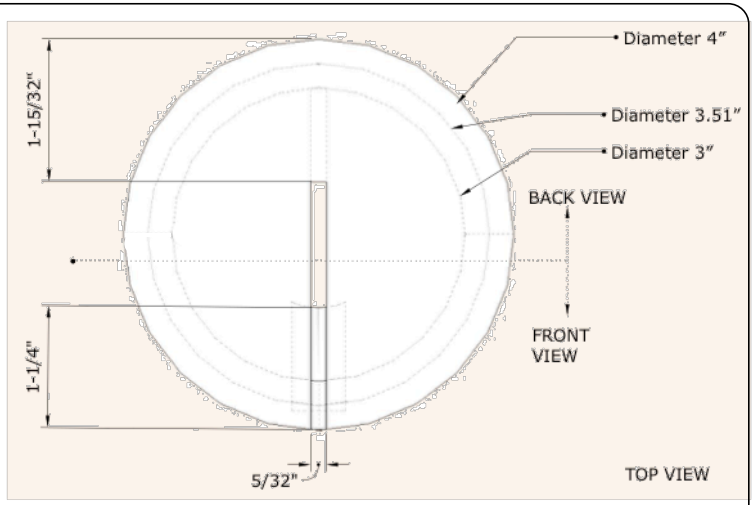

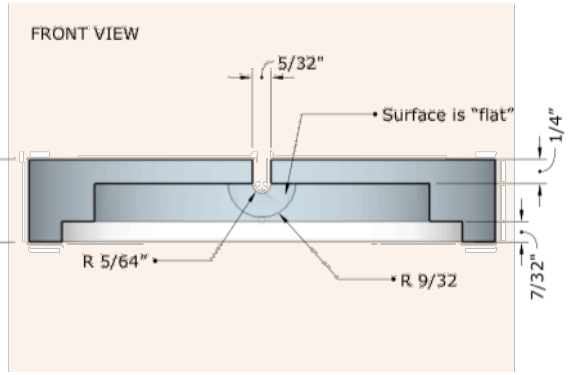

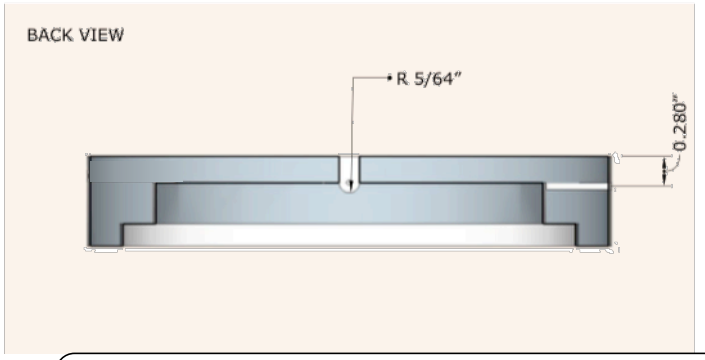

Name	Eleonora Figueroa				
Material	PTFE	Title	Total Scattering Coef. Top		
Tolerance	+/- 0.01"	Page	2/2	Piece	1 /1

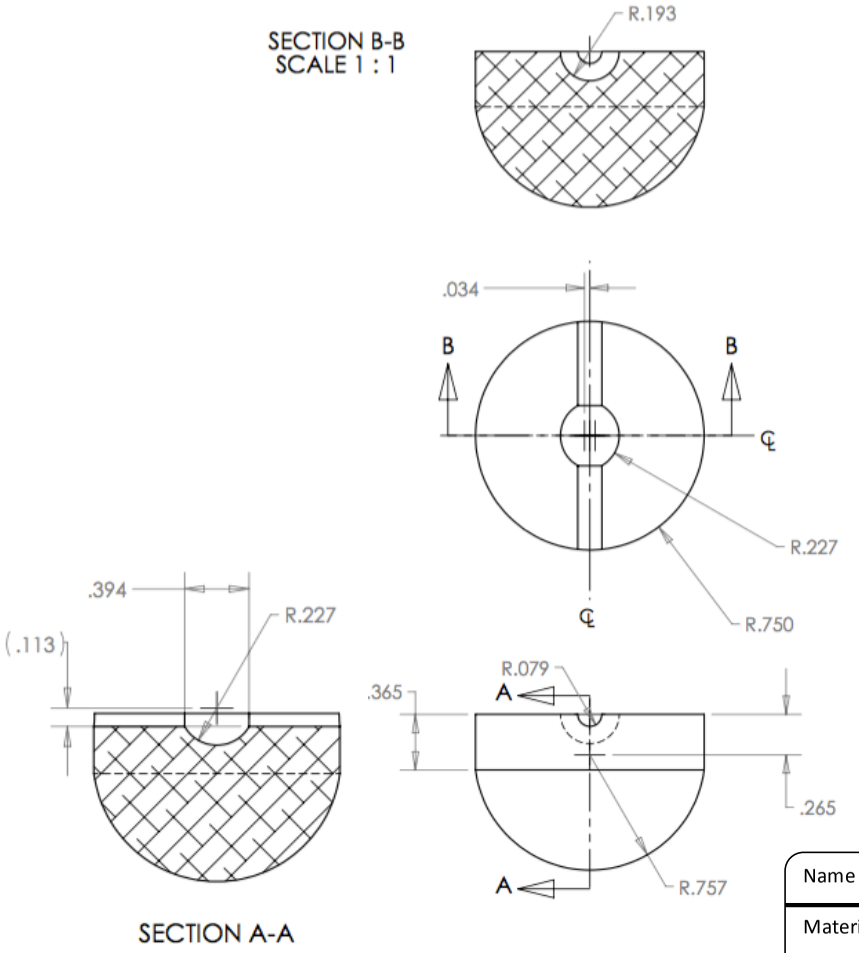

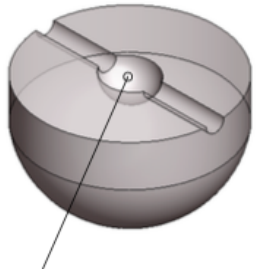

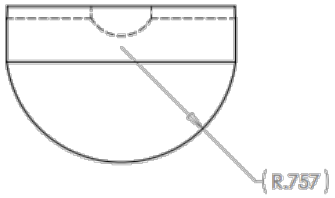

Name	Eleonora Figueroa		
Material	Quartz	Title	*b* Aperture Piece
Tolerance	+/- 0.005”	Units inches Piece	1/1

APPENDIX C

SOURCE CODE

C.1 Fresnel equations for light transmission

This section shows the Python code to simulate the Fresnel equations for reflection and transmission when light is incident on a surface of different index of refraction. The code takes into account multiple parameters, including the index of refraction of both environments, the size of the aperture and the depth of the aperture depression. The program simulates the behavior of the reflected and refracted rays.

```
#!/usr/bin/python
import math


def a2(a1):
value = math.asin(n1*math.sin(a1)/n2)
return value


def A(a1):
return (n2*math.cos(a2(a1))/n1/math.cos(a1))


def avg(x):
return sum(x[1:])/float(len(x[1:]))


def QuadEq(a,b,c,x0,I):
dis= b**2-4*a*c
```

```
if dis<0:
print("ERROR in QF:", x0, dis)

print("  b, a, c, b^2,4ac",b,a,c,b**2,4*a*c)
return x0
elif dis == 0:
print("Just one hit")
return x0
else:
xp=(-b+math.sqrt(dis))/(2*a)
xm=(-b-math.sqrt(dis))/(2*a)

#print("  x values",xp,xm)

if I==’’:
return xp
elif format(x0,’.10f’)==format(xp,’.10f’):  #Fixes rounding errors in math

return xm
else:
return xp

def slope(ai,t,x,I):        #Calculate m,  b and y for equation of line
if ai==t or ai==0:
mtemp=1e+6
ytemp = -math.cos(t)*R
```

```
else:
mtemp=1/math.tan(ai-t) # CHECK PLUS SIGN
#Method 1 for calculating y
ytemp = -math.cos(t)*R
#Method 2 :
#ytemp=-math.sqrt(R**2-x**2)
if I == '':
if ai!=0:
mtemp=-1/math.tan(ai)
else: mtemp=-mtemp

ytemp=-y0
# print("  Slope1", mtemp)
#calculate b
btemp=ytemp-mtemp*x
#print("  Slope2", mtemp)
xnew=QuadEq(1+mtemp**2,2*mtemp*btemp,btemp**2-R**2,x,I)
ynew=(xnew-x)*mtemp+ytemp

return (mtemp,xnew,btemp, ynew)

"""
n1=input("n of water: ")
n2=input("n of detector (glass):")
d=input("Diameter of detector (mm):")
R=input("Radius of curvature (mm):")
```

```
"""
FileName = "TranDet.py"

n1= 1.342 #n of water
n2= 1.4607 #n of detector
d=1.5 #Diameter of detector face (mm)
R=.866 #Radius of curvature of detector (mm)

y0=d/2/math.tan(math.asin(d/2/R))

step = 1000# Points on surface of detector to consider
end=100000 # Max number of reflections calculated
astart=0
astep=5 #step for angle intervals  (MAKE SURE NOT SMALLER THAN SCALE)
aend=90 #last angle(from laser) to check
scale=1 # For decimal points

#Initializing variables needed
acount=0
data=[]
Avg_array=[]


for alpha0 in range(astart*scale,int(aend*scale),int(astep*scale)):
x=[] #Distance from center of detector to edge of detector (e.g -0.1 to 0.1)
```

```
theta=[] #Angle between normal and vertical direction
alpha1=[]  #Alpha prime (angle seen by the surface at different parts
#in the detector)
t_p=[]
t_s=[]
T=[]
NRef=[]
blank=0
Z=[]

alpha0=alpha0/scale
print(alpha0)

for i in range(0,step):

x1=(d/step*i-d/2)
(m,X,b,Y)=slope(math.radians(alpha0), math.atan((d/2-x1)/R),x1,'')

Theta=math.asin(X/R)
Alpha1=math.radians(alpha0)-Theta

#Record values
T_s=A(Alpha1)*(2*n1*math.cos(Alpha1)/
(n1*math.cos(Alpha1)+n2*math.cos(a2(Alpha1))))**2
T_p=A(Alpha1)*(2*n1*math.cos(Alpha1)/
(n1*math.cos(a2(Alpha1))+n2*math.cos(Alpha1)))**2
```

```
#Find m, y2 and b inteceptions for equatino of line
(m,x2,b,y2)=slope(Alpha1,Theta,X,'i')

counter =0
y1 = -math.cos(Theta)*R

while y2<-math.sqrt(R**2-(d/2)**2) and X!=x2 and counter <end:
#same alpha1 because of iso triangles in unit circle
theta1=math.asin(x2/R)
(m,x2,b, y2)=slope(Alpha1,theta1,x2,'i')

T_s = T_s+A(Alpha1)*(2*n1*math.cos(Alpha1)/(n1*math.cos(Alpha1)+\
n2*math.cos(a2(Alpha1))))**2*(1-T_s)
T_p = T_p+A(Alpha1)*(2*n1*math.cos(Alpha1)/(n1*math.cos(a2(Alpha1))+\
n2*math.cos(Alpha1)))**2*(1-T_p)
counter = counter +1

#Save values
x.append(X)
theta.append(math.degrees(Theta))
alpha1.append(math.degrees(Alpha1))

t_s.append(T_s)
t_p.append(T_p)
```

```
NRef.append(counter)

T.append((T_s+T_p)/2)

Z.append(x1)


acount=acount+1

#Add title to columns


x.insert(0,"x for "+str(alpha0)+" degrees")

t_s.insert(0,"T_s for "+str(alpha0)+ " degrees")

t_p.insert(0,"T_p for "+ str(alpha0)+" degrees")

T.insert(0, "Total Transmission for "+ str(alpha0)+" deg")

NRef.insert(0,"Number of reflections")

alpha1.insert(0,"alpha1")

theta.insert(0,"Theta")


Z.insert(0,"Original x")


print("zipping data")


data=list(zip(*data))  #turn columns into rows


print("writing TestDataAngles.csv")

Data=open("TestDataAngles.csv","w")


intro="Index of refraction of water: "+str(n1)+"\nIndex of refraction "\

+"of detector: "+ str(n2)+"\nRadius of curvature = "+str(R)+'\n'+\
```

```
"Aperture of detector="+str(d)+'\n'+'\n'


Data.write(FileName+"\n\n")

Data.write(intro)

for line in data:

for dat in line:

value='{},'.format(dat)

Data.write(value)

Data.write('\n')

Data.close()


print("Writing AvgsSum.csv")


Avg_array.insert(0,('',"Total T","T_s","T_p"))


Data=open("AvgsSum.csv","w")

Data.write(intro)

for line in Avg_array:

for dat in line:

value='{}, '.format(dat)

Data.write(value)

Data.write('\n')

Data.close()


print()
```

C.2 Theoretical Coefficient Calculations

This section shows the Python code used to calculate the expected b and b_b values of each respective meter. The code relies on the interpolated data found in "InterpData.csv" and the VSF values of the environmental data found in "VSFValues.csv" (also shown in Appendix F). Our cavity's weight function at each scattering angle θ of the provided VSF is used to calculate the values for b, b_b, and b_f that the cavity is expected to give and compared to the values that would be found with a perfect collector whose weight function is $\sin\theta$ (i.e. a cosine collector)

```
#!/usr/bin/python


#The b values "MyBVal"
#Ideal font: Calibri


#The idea is to measure different ba and bb measurements based on the
# pre-existing VSF
#values from NLR.


import csv
import os
import numpy as np
from math import pi, radians, degrees, ceil, floor, atan, cos


#VSF information:
Set=3   #Columns per body of water
Rad=1   #Column with angle in radians
```

```
Beta=2  #Column with Beta value
Deg=0   #Column with angles in degrees
ImportData="InterpData.csv"     #Import Data
R=9.53 #mm
Z=1.1/2

T10=ceil(degrees(atan(R*2/Z)))
T20=180-T10

##ITEMS TO SHOW:
SHOWbActual='y'
SHOWbbActual='y'
SHOWbfActual='y'
SHOWExpb='n'
SHOWExpbb='y'
SHOWMybb='y'
SHOWErrorExp='y' #Error because of number of points
SHOWErrorCav='y'#Error because between cavity and expected value

bf=0
bb=0
bActual= 0 #The closest value to the real number
bbActual=0
MyData=[]
countbb=0
countb=0
```

```
Mybb=0

Myb=0

Mybf=0

Expbf=0

Expbb=0

Expb=0

data=[]

AngleSummary=[]


g=csv.reader(open(ImportData,"rU"))

for item in g:

    MyData.append(item)

    if item[0]=='90' or item[0]=='90.':

        MyDataBB=item

        BBIndex=len(MyData)-1

        print("read in 90.  BBIndex: ", BBIndex)


MyData=np.array(MyData) #Change from list to array

MyTitle=MyData[0]

MyData[MyData==''']=0

MyData=MyData.astype(float)  ###FIX!!!


f=csv.reader(open("VSFValues.csv", "rU"))  #Load known VSF


        #INITIALIZE TEMP VARIABLES

first= True
```

```
Trapz= False
First=True
MyDataFirst=True
MybbFirst=True

for item in f:
    if first == True:
        cols=len(item)      #define number of columns
        sample=item[::Set]  #Define title from .csv
        N=cols/Set          #Define number of sets
        first=False
        continue
    if item[0]=="Scattering (deg)": continue

    #   PULL ANGLE AND BETA VALUE AS FLOAT
    angleR=np.array(item[Rad::Set]).astype(float)
    angleD=np.array(item[Deg::Set]).astype(float)
    AngleSummary.append(angleD.astype(float))
    beta=np.array(item[Beta::Set]).astype(float)

    bval=np.sin(angleR)*beta

    MySignal=[]
    MyAngleR=[]
    #   Look at My Data
```

```
for x in angleD:
    (index,zero)= np.where(MyData==float(format(x, '.5f')))

    #print(MySignal)
    if len(index)==0: break
    MySignal.append(MyData[index[0],1])
    MyAngleR.append(radians(MyData[index[0],0]))
if len(index)==0: break
MySignal=np.asarray(MySignal)
MyAngleR=np.asarray(MyAngleR)

if MyDataFirst == True:
   MyDataFirst = False
   MyAngleRPrev=MyAngleR
   ExpAngleR=angleR
   MyBVal=MySignal*beta
   ExpBVal=bval
else:
    #MyAngleR=MyAngleR
    #print(MySignal)
    MyBVal=MySignal*beta
    ExpAngleR=angleR
    ExpBVal=bval

    Myb+=(MyBVal+MyBValPrev)/2*(MyAngleR-MyAngleRPrev)
    Expb+=(ExpBVal+ExpBValP)/2*(ExpAngleR-ExpAngleRP)
```

```
    if angleR[0]<radians(90):  #changes depending on bf measurements
        Mybf+=(MyBVal+MyBValPrev)/2*(MyAngleR-MyAngleRPrev)
        Expbf+=(ExpBVal+ExpBValP)/2*(ExpAngleR-ExpAngleRP)

countb+=1

if format(angleR[0], '.4f')==format(radians(T10),'.4f'):
    BT10=beta*MyBVal
    bT10=beta

if format(angleR[0],'.4f')>=format(radians(90),'.4f'):
        #Enters only if angles on both sets match
    if format(angleR[0], '.4f')==format(radians(float(\
    MyData[BBIndex][0])), '.4f'):

        #Only enters at angle = 90°
        MybbFirst=False
        B90=beta*MyBVal
        b90=beta

    elif MybbFirst==False:

        if format(angleR[0], '.4f')==format(radians(T20),'.4f'):
            BT20=beta*MyBVal
            Mybb+=1/4*((B90+BT10)*radians(90-T10)-\
```

```
            (BT20+B90)*radians(T20-180))
            Mybb+=-R/(2*Z)*radians(T20-T10)*(beta*cos(radians(T20))\
            +bT10*cos(radians(T10)))
            print("new Mybb:", Mybb)

        Mybb+=(MyBVal+MyBValPrev)/2*(MyAngleR-MyAngleRPrev)
        Expbb+=(ExpBVal+ExpBValP)/2*(ExpAngleR-ExpAngleRP)

    countbb+=1

    if countbb+BBIndex == len(MyData):
        print("bb data points: ",countbb)
        print("b data points: ",countb)
        countbb=countb=0

MyAngleRPrev=MyAngleR
MyBValPrev=MyBVal
ExpAngleRP=ExpAngleR
ExpBValP=ExpBVal

if format(angleR[0],'.4f')>format(radians(float(MyData\
[countb][0]))) and MyDataFirst==True:
    print("No data was recognized from ",ImportData)
    print(MyData)
    break
```

```
    if Trapz==True:      #Applies the trapizoidal rule to find b
        bActual += (bval+bvalPrev)/2*(angleR-angleRPrev)

    if angleR[0] >1.58: bbActual += (bval+bvalPrev)/2\
    *(angleR-angleRPrev)

    Trapz=True

    angleRPrev=angleR
    bvalPrev=bval

bActual=bActual*2*pi
bbActual=bbActual*2*pi
bfActual=bActual-bbActual
Mybb=Mybb*2*pi
Mybf=Mybf*2*pi
Expbf=Expbf*2*pi
Expbb=Expbb*2*pi
Myb=Myb*2*pi
Expb=Expb*2*pi

bErrorExp=(bActual-Expb)/bActual*100
bErrorCav=(-Expb+Myb)/Expb*100
bbErrorExp=(bbActual-Expbb)/bbActual*100
bbErrorCav=(-Expbb+Mybb)/Expbb*100
bfErrorExp=(bfActual-Expbf)/bfActual*100
```

```
bfErrorCav=(-Expbf+Mybf)/Expbf*100

        #Prepare to print

PrintText = '\n{:20} => {:10}; {:10}; {:}; {:}'
WriteText = '{0:20},{1:6},{2:10},{3:6},{4:10},{5:10},{6:},{7:}'
PrintData= '{:20} => {:.4e}; {:.4e}; \t{:.2f}; \t\t{:.2f}'

print('\n{:20} =>   {:15} {:14} {:6}'.format("Sample location",\
"Real b", "Real bb", "Real bf"))
for i in range(len(sample)):
    print('{:20} => {:.4e}; \t{:.4e}; \t{:.4e}'.format(\
    sample[i],bActual[i], bbActual[i], bfActual[i]))

print(PrintText.format("Sample location","Expected b", "Cavity b",\
 "Expected b Error", "Cavity b errors"))
for i in range(len(sample)):
    print(PrintData.format(sample[i],Expb[i], Myb[i], bErrorExp[i], \
    bErrorCav[i]))

print(PrintText.format("Sample location","Expected bb", "Cavity bb",\
"Expected bb Error", "Cavity bb Error" ))
for i in range(len(sample)):
    print(PrintData.format(sample[i],Expbb[i], Mybb[i],\
     bbErrorExp[i],bbErrorCav[i]))
```

```
print(PrintText.format("Sample location","Expected bf", \
"Cavity bf","Expected bf Error",
                        "Cavity bf Error" ))
for i in range(len(sample)):
    print(PrintData.format(sample[i],Expbf[i], Mybf[i], \
    bfErrorExp[i],bfErrorCav[i]))

titles=["Sample location","Real b", "Real bb", "Real bf",
        "Expected b", "Cavity b", "Expected b Error", "Cavity b errors",
                        "Expected bb", "Cavity bb","Expected bb Error",
                        "Cavity bb Error", "Expected bf", "Cavity bf",
                        "Expected bf Error", "Cavity bf Error" ]

for i in range(len(sample)):

    data.append((sample[i],bActual[i], bbActual[i], bfActual[i],
                Expb[i], Myb[i], bErrorExp[i], bErrorCav[i],
                Expbb[i], Mybb[i], bbErrorExp[i],bbErrorCav[i],
                Expbf[i], Mybf[i], bfErrorExp[i],bfErrorCav[i]
                ))


with open("BValues.csv",'w') as file:
    writer = csv.writer(file)
    writer.writerow(titles)
    writer.writerows(data)
```

```
with open("TotalAngles.csv",'w') as file:
    writer = csv.writer(file)
    writer.writerow(sample)
    writer.writerows(AngleSummary)
```

APPENDIX D

PHOTODIODE AMPLIFIER

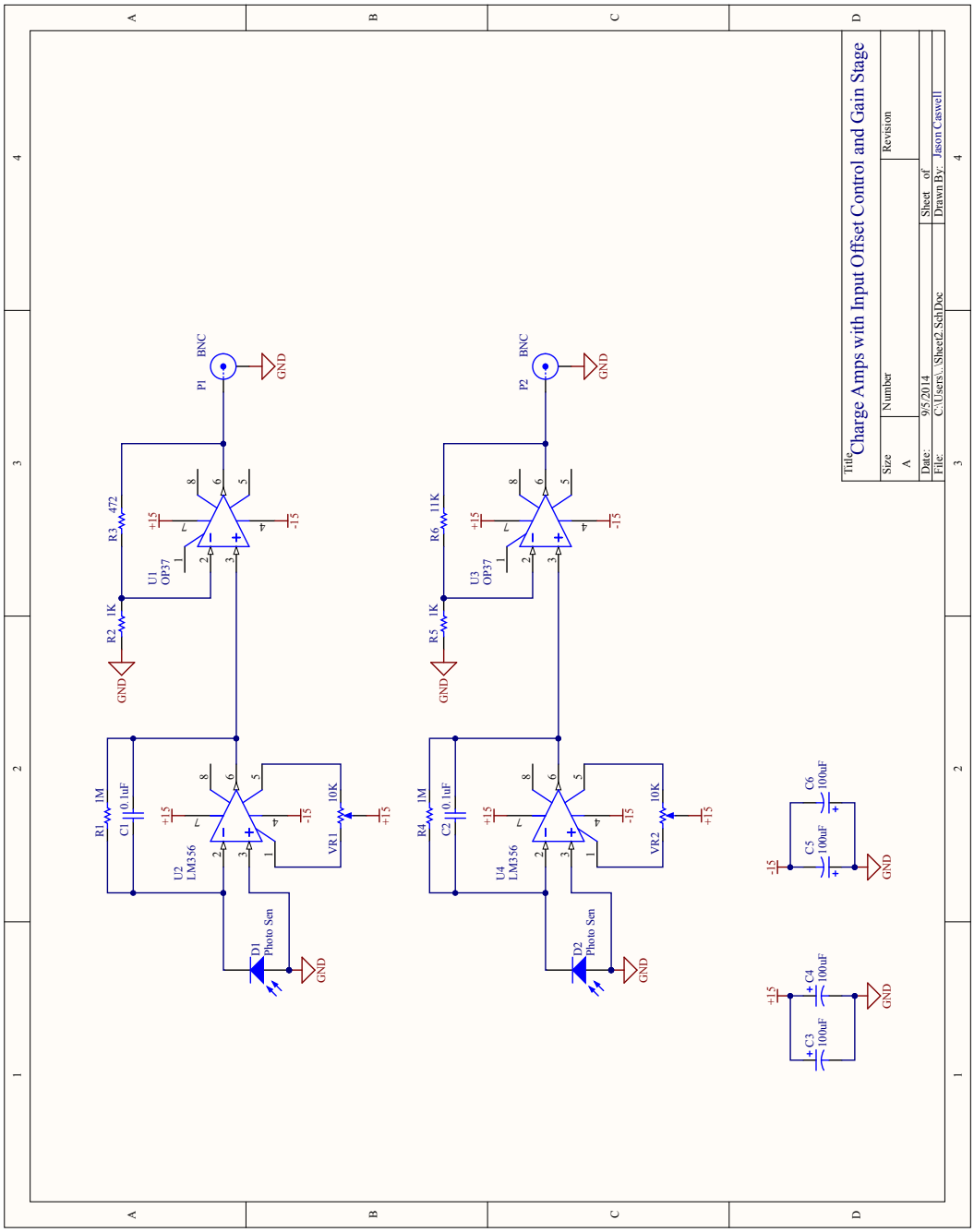

APPENDIX E

CAVITY CHARACTERIZATION

E.1 b_b Meter

E.1.1 Raw values

b_b **Meter Signal (Raw)**						
Scattering angle, θ (°)	Sin(θ)	$\phi = -40°$	$\phi = -20°$	$\phi = 0°$	$\phi = 20°$	$\phi = 40°$
90°	1.000	2.07	2.03	1.97	1.94	2.03
100°	0.985	2.05	2.01	1.94	1.92	2.00
110°	0.940	1.97	1.92	1.84	1.83	1.89
120°	0.866	1.81	1.75	1.70	1.68	1.71
130°	0.766	1.60	1.55	1.50	1.48	1.49
140°	0.643	1.35	1.29	1.24	1.22	1.22
150°	0.500	1.04	1.00	0.974	0.949	0.93
160°	0.342	0.71	0.69	0.668	0.643	0.604
165°	0.259	0.542	0.527	0.504	0.488	0.447
170°	0.174	0.367	0.359	0.331	0.312	0.28
180°	0	0	0	0	0	0

E.1.2 Average and normalized values

b_b **Meter Signal**			
Scattering angle, θ (°)	Sin(θ)	Average value (V)	Normalized average (V)
90°	1.000	2.008	1.000
100°	0.985	1.984	0.988
110°	0.940	1.89	0.941
120°	0.866	1.73	0.862
130°	0.766	1.524	0.759
140°	0.643	1.264	0.629
150°	0.500	0.9786	0.487
160°	0.342	0.663	0.330
165°	0.259	0.5016	0.250
170°	0.174	0.3298	0.164
180°	0	0	0

E.2 b Meter

b **Meter Signal**					
Scattering angle (°)	Normalized signal (mV)	Scattering angle (°)	Normalized signal (mV)	Scattering angle (°)	Normalized signal (mV)
0.14	0.00278	0.74	0.013	15.58	0.278
0.18	0.00327	0.78	0.0138	20.58	0.362
0.22	0.00378	0.98	0.0167	30.58	0.508
0.26	0.00457	1.18	0.0197	40.58	0.638
0.3	0.00545	1.38	0.0233	50.58	0.74
0.34	0.0062	1.58	0.0268	60.58	0.808
0.38	0.007	2.58	0.0407	70.58	0.862
0.42	0.00788	3.58	0.0595	80.58	0.89
0.46	0.00867	4.58	0.0818	90.58	0.9
0.5	0.00925	5.58	0.0973	100.58	0.878
0.54	0.00983	6.58	0.119	110.58	0.832
0.58	0.0103	7.58	0.137	120.58	0.763
0.62	0.0112	8.58	0.154	130.58	0.665
0.66	0.0117	9.58	0.172		
0.7	0.0123	10.58	0.192		

APPENDIX F

VSF VALUES

A list of volume scattering function values at specific scattering angles of light as measured by NRL at Monterrey Bay, Mobile Bay, Monterrey Normal, Possession Sound, Ligurian Sea, Snohomish and Chesapeake Bay. These values were provided by the National Research Laboratories (NRL)[32]

Monterrey Bay					
Scattering angle (deg)	Scattering angle (rad)	Phase function, β	Scattering angle (deg)	Scattering angle (rad)	Phase function, β
0.95288	0.016631	127.56744	90	1.570796	0.0014613
1.12437	0.019624	105.71834	91	1.58825	0.0010913
1.84681	0.032233	45.779317	92	1.605703	0.0012511
2.1787	0.038026	31.239981	93	1.623156	0.0012208
3.03094	0.0529	14.79849	94	1.640609	0.0011504
4.21259	0.073524	7.8553588	95	1.658063	0.0012098
4.96338	0.086627	5.6763607	96	1.675516	0.0013392
5.84443	0.102004	4.0333034	97	1.692969	0.0010784
6.87613	0.120011	2.8904513	98	1.710423	0.0010375
8.08068	0.141034	2.0557038	99	1.727876	0.0011765
9.48137	0.165481	1.5816848	100	1.745329	0.0010454
10	0.174533	1.5178204	101	1.762783	0.0009942
11	0.191986	1.2033916	102	1.780236	0.0009828
12	0.20944	0.815563	103	1.797689	0.0010714

Monterrey Bay (cont.)					
Scattering angle (deg)	Scattering angle (rad)	Phase function, β	Scattering angle (deg)	Scattering angle (rad)	Phase function, β
13	0.226893	0.8595644	104	1.815142	0.0010098
14	0.244346	0.662626	105	1.832596	0.0010381
15	0.261799	0.5736277	106	1.850049	0.0008764
16	0.279253	0.4450394	107	1.867502	0.0010545
17	0.296706	0.3386313	108	1.884956	0.0009025
18	0.314159	0.3387033	109	1.902409	0.0009205
19	0.331613	0.3051953	110	1.919862	0.0009383
20	0.349066	0.2784575	111	1.937315	0.0009361
21	0.366519	0.2318798	112	1.954769	0.0008637
22	0.383972	0.2040521	113	1.972222	0.0008913
23	0.401426	0.1706845	114	1.989675	0.0008388
24	0.418879	0.138857	115	2.007129	0.0008662
25	0.436332	0.1302596	116	2.024582	0.0008235
26	0.453786	0.1127523	117	2.042035	0.0008808
27	0.471239	0.101105	118	2.059489	0.0008779
28	0.488692	0.0824879	119	2.076942	0.0008951
29	0.506145	0.0817207	120	2.094395	0.0008121
30	0.523599	0.0647237	121	2.111848	0.0008291
31	0.541052	0.0628267	122	2.129302	0.0008261
32	0.558505	0.0569898	123	2.146755	0.0009829
33	0.575959	0.0486229	124	2.164208	0.0008998
34	0.593412	0.045516	125	2.181662	0.0008766

Monterrey Bay (cont.)					
Scattering angle (deg)	Scattering angle (rad)	Phase function, β	Scattering angle (deg)	Scattering angle (rad)	Phase function, β
35	0.610865	0.0395192	126	2.199115	0.0009333
36	0.628319	0.0343125	127	2.216568	0.0008
37	0.645772	0.0350658	128	2.234021	0.0008067
38	0.663225	0.0299091	129	2.251475	0.0008434
39	0.680678	0.0286224	130	2.268928	0.00077
40	0.698132	0.0275558	131	2.286381	0.0008066
41	0.715585	0.0232592	132	2.303835	0.0008232
42	0.733038	0.0204226	133	2.321288	0.0008398
43	0.750492	0.019166	134	2.338741	0.0008363
44	0.767945	0.0201395	135	2.356194	0.0009229
45	0.785398	0.0141729	136	2.373648	0.0008495
46	0.802851	0.0122563	137	2.391101	0.000776
47	0.820305	0.0137898	138	2.408554	0.0010226
48	0.837758	0.0116332	139	2.426008	0.0008792
49	0.855211	0.0104266	140	2.443461	0.0010158
50	0.872665	0.0099	141	2.460914	0.0008624
51	0.890118	0.0101634	142	2.478368	0.0008791
52	0.907571	0.0088067	143	2.495821	0.0008158
53	0.925025	0.00765	144	2.513274	0.0008725
54	0.942478	0.0066133	145	2.530727	0.0009192
55	0.959931	0.0074566	146	2.548181	0.000866
56	0.977384	0.0067298	147	2.565634	0.0009629

Monterrey Bay (cont.)					
Scattering angle (deg)	Scattering angle (rad)	Phase function, β	Scattering angle (deg)	Scattering angle (rad)	Phase function, β
57	0.994838	0.0059029	148	2.583087	0.0009698
58	1.012291	0.0055561	149	2.600541	0.0009967
59	1.029744	0.0051091	150	2.617994	0.0009037
60	1.047198	0.0043921	151	2.635447	0.0009607
61	1.064651	0.0045151	152	2.6529	0.0009779
62	1.082104	0.0052779	153	2.670354	0.000995
63	1.099557	0.0045008	154	2.687807	0.0009523
64	1.117011	0.0042635	155	2.70526	0.0009896
65	1.134464	0.0037362	156	2.722714	0.000967
66	1.151917	0.0040188	157	2.740167	0.0008345
67	1.169371	0.0040813	158	2.75762	0.0008421
68	1.186824	0.0031937	159	2.775074	0.0009198
69	1.204277	0.0032661	160	2.792527	0.0010475
70	1.22173	0.0028483	161	2.80998	0.0008753
71	1.239184	0.0025005	162	2.827433	0.0009433
72	1.256637	0.0025925	163	2.844887	0.0010113
73	1.27409	0.0025245	164	2.86234	0.0009094
74	1.291544	0.0025364	165	2.879793	0.0010277
75	1.308997	0.0022381	166	2.897247	0.000966
76	1.32645	0.0017998	167	2.9147	0.0009344
77	1.343904	0.0021214	168	2.932153	0.000973
78	1.361357	0.0021428	169	2.949606	0.0009016

Monterrey Bay (cont.)					
Scattering angle (deg)	Scattering angle (rad)	Phase function, β	Scattering angle (deg)	Scattering angle (rad)	Phase function, β
79	1.37881	0.0020042	170	2.96706	0.0009704
80	1.396263	0.0019354	171	2.984513	0.0009893
81	1.413717	0.0019365	172	3.001966	0.0011183
82	1.43117	0.0015175	173	3.01942	0.0012074
83	1.448623	0.0015884	174	3.036873	0.0011966
84	1.466077	0.0015992	175	3.054326	0.001256
85	1.48353	0.0019098	176	3.071779	0.0013954
86	1.500983	0.0015904	177	3.089233	0.001235
87	1.518436	0.0014208	178	3.106686	0.0010647
88	1.53589	0.0015011	179	3.124139	0.0013145
89	1.553343	0.0013013	180	3.141593	0.00132

Mobile Bay					
Scattering angle (deg)	Scattering angle (rad)	Phase function, β	Scattering angle (deg)	Scattering angle (rad)	Phase function, β
0.95288	0.016631	135.04588	90	1.570796	0.004474636
1.12437	0.019624	117.39749	91	1.58825	0.004444576
1.84681	0.032233	48.290279	92	1.605703	0.004164396
2.1787	0.038026	37.28928	93	1.623156	0.004090763
3.03094	0.0529	21.43862	94	1.640609	0.004070345
4.21259	0.073524	10.907722	95	1.658063	0.00401314
4.96338	0.086627	7.4703393	96	1.675516	0.003592485

Mobile Bay (cont.)					
Scattering angle (deg)	Scattering angle (rad)	Phase function, β	Scattering angle (deg)	Scattering angle (rad)	Phase function, β
5.84443	0.102004	5.4818335	97	1.692969	0.003465045
6.87613	0.120011	3.9491313	98	1.710423	0.003394156
8.08068	0.141034	3.0088375	99	1.727876	0.003379818
9.48137	0.165481	2.3868206	100	1.745329	0.003128699
10	0.174533	1.898710348	101	1.762783	0.003097468
11	0.191986	1.497671579	102	1.780236	0.003192792
12	0.20944	1.266126255	103	1.797689	0.003198006
13	0.226893	0.947827707	104	1.815142	0.003266446
14	0.244346	0.816085934	105	1.832596	0.00292478
15	0.261799	0.656674267	106	1.850049	0.00289301
16	0.279253	0.55222937	107	1.867502	0.003077806
17	0.296706	0.496801241	108	1.884956	0.003105835
18	0.314159	0.404986545	109	1.902409	0.003040433
19	0.331613	0.35236528	110	1.919862	0.002938271
20	0.349066	0.318670776	111	1.937315	0.003122683
21	0.366519	0.274766364	112	1.954769	0.003043673
22	0.383972	0.284735374	113	1.972222	0.00298791
23	0.401426	0.234811137	114	1.989675	0.003095397
24	0.418879	0.208586983	115	2.007129	0.00298947
25	0.436332	0.181049577	116	2.024582	0.003200133
26	0.453786	0.162962247	117	2.042035	0.003110722
27	0.471239	0.144368325	118	2.059489	0.00334124

Mobile Bay (cont.)					
Scattering angle (deg)	Scattering angle (rad)	Phase function, β	Scattering angle (deg)	Scattering angle (rad)	Phase function, β
28	0.488692	0.129794473	119	2.076942	0.003218358
29	0.506145	0.115624022	120	2.094395	0.00311208
30	0.523599	0.1067803	121	2.111848	0.003065741
31	0.541052	0.099096639	122	2.129302	0.002916013
32	0.558505	0.088146367	123	2.146755	0.002956232
33	0.575959	0.080632815	124	2.164208	0.003009735
34	0.593412	0.072272645	125	2.181662	0.002856527
35	0.610865	0.067412519	126	2.199115	0.002829945
36	0.628319	0.062399102	127	2.216568	0.002919992
37	0.645772	0.055052388	128	2.234021	0.00290334
38	0.663225	0.051862374	129	2.251475	0.002949991
39	0.680678	0.047805722	130	2.268928	0.003019952
40	0.698132	0.043275762	131	2.286381	0.003056558
41	0.715585	0.040199156	132	2.303835	0.002903147
42	0.733038	0.038202566	133	2.321288	0.002919724
43	0.750492	0.034542656	134	2.338741	0.002886292
44	0.767945	0.031806088	135	2.356194	0.002969523
45	0.785398	0.029972857	136	2.373648	0.002872754
46	0.802851	0.027516292	137	2.391101	0.002999323
47	0.820305	0.025983057	138	2.408554	0.0030159
48	0.837758	0.023853147	139	2.426008	0.002995822
49	0.855211	0.022559891	140	2.443461	0.003072428

Mobile Bay (cont.)					
Scattering angle (deg)	Scattering angle (rad)	Phase function, β	Scattering angle (deg)	Scattering angle (rad)	Phase function, β
50	0.872665	0.021189952	141	2.460914	0.002942389
51	0.890118	0.019133325	142	2.478368	0.002912374
52	0.907571	0.018486673	143	2.495821	0.002819055
53	0.925025	0.017453325	144	2.513274	0.002979102
54	0.942478	0.016376612	145	2.530727	0.002942519
55	0.959931	0.014993194	146	2.548181	0.002885978
56	0.977384	0.014449735	147	2.565634	0.002946148
57	0.994838	0.013499565	148	2.583087	0.002936367
58	1.012291	0.012472679	149	2.600541	0.002896639
59	1.029744	0.012035741	150	2.617994	0.002943634
60	1.047198	0.011135413	151	2.635447	0.003200688
61	1.064651	0.010591692	152	2.6529	0.003057806
62	1.082104	0.00992124	153	2.670354	0.003094992
63	1.099557	0.009747388	154	2.687807	0.003045581
64	1.117011	0.008933466	155	2.70526	0.003126243
65	1.134464	0.00833947	156	2.722714	0.003076983
66	1.151917	0.008092063	157	2.740167	0.00315447
67	1.169371	0.007724576	158	2.75762	0.003388707
68	1.186824	0.007277006	159	2.775074	0.003269697
69	1.204277	0.00736935	160	2.792527	0.003340776
70	1.22173	0.007071604	161	2.80998	0.003431947
71	1.239184	0.006820433	162	2.827433	0.003343212

Mobile Bay (cont.)					
Scattering angle (deg)	Scattering angle (rad)	Phase function, β	Scattering angle (deg)	Scattering angle (rad)	Phase function, β
72	1.256637	0.006512501	163	2.844887	0.003487908
73	1.27409	0.006314472	164	2.86234	0.003522703
74	1.291544	0.00611301	165	2.879793	0.003594267
75	1.308997	0.006021447	166	2.897247	0.003602601
76	1.32645	0.006006446	167	2.9147	0.003757707
77	1.343904	0.005484673	168	2.932153	0.003789588
78	1.361357	0.005239458	169	2.949606	0.003754912
79	1.37881	0.005110801	170	2.96706	0.003933681
80	1.396263	0.005195366	171	2.984513	0.003902562
81	1.413717	0.004966484	172	3.001966	0.004024891
82	1.43117	0.004820822	173	3.01942	0.004170668
83	1.448623	0.004915045	174	3.036873	0.004336562
84	1.466077	0.004702485	175	3.054326	0.004525906
85	1.48353	0.004689807	176	3.071779	0.005045369
86	1.500983	0.004267011	177	3.089233	0.004711617
87	1.518436	0.004470763	178	3.106686	0.00440465
88	1.53589	0.004404396	179	3.124139	0.005401137
89	1.553343	0.004521243	180	3.141593	0.00540114

Monterrey Normal					
Scattering angle (deg)	Scattering angle (rad)	Phase function, β	Scattering angle (deg)	Scattering angle (rad)	Phase function, β
0.95288	0.016631	113.12462	90	1.570796	0.001605
1.12437	0.019624	83.247787	91	1.58825	0.001485
1.84681	0.032233	37.199619	92	1.605703	0.00151
2.1787	0.038026	28.318924	93	1.623156	0.001635
3.03094	0.0529	15.597864	94	1.640609	0.00146
4.21259	0.073524	7.7251019	95	1.658063	0.001475
4.96338	0.086627	5.5780993	96	1.675516	0.00139
5.84443	0.102004	3.8529947	97	1.692969	0.0014
6.87613	0.120011	2.829704	98	1.710423	0.00135
8.08068	0.141034	1.985868	99	1.727876	0.00128
9.48137	0.165481	1.5110065	100	1.745329	0.00137
10	0.174533	1.248925	101	1.762783	0.00138
11	0.191986	1.11454	102	1.780236	0.00132
12	0.20944	0.86082	103	1.797689	0.001225
13	0.226893	0.68326	104	1.815142	0.00136
14	0.244346	0.5416	105	1.832596	0.001395
15	0.261799	0.562305	106	1.850049	0.001295
16	0.279253	0.46168	107	1.867502	0.0012
17	0.296706	0.37254	108	1.884956	0.00116
18	0.314159	0.30619	109	1.902409	0.00123
19	0.331613	0.274125	110	1.919862	0.00118
20	0.349066	0.23948	111	1.937315	0.001175

Monterrey Normal (cont.)					
Scattering angle (deg)	Scattering angle (rad)	Phase function, β	Scattering angle (deg)	Scattering angle (rad)	Phase function, β
21	0.366519	0.19583	112	1.954769	0.00119
22	0.383972	0.211575	113	1.972222	0.00117
23	0.401426	0.151675	114	1.989675	0.001145
24	0.418879	0.13321	115	2.007129	0.00111
25	0.436332	0.118055	116	2.024582	0.00108
26	0.453786	0.103475	117	2.042035	0.001185
27	0.471239	0.093655	118	2.059489	0.00114
28	0.488692	0.082595	119	2.076942	0.00112
29	0.506145	0.07694	120	2.094395	0.00112
30	0.523599	0.06819	121	2.111848	0.0011
31	0.541052	0.061495	122	2.129302	0.00109
32	0.558505	0.056315	123	2.146755	0.00112
33	0.575959	0.05114	124	2.164208	0.00108
34	0.593412	0.04507	125	2.181662	0.00112
35	0.610865	0.0425	126	2.199115	0.001085
36	0.628319	0.03747	127	2.216568	0.001055
37	0.645772	0.034655	128	2.234021	0.001165
38	0.663225	0.03142	129	2.251475	0.00118
39	0.680678	0.02887	130	2.268928	0.001085
40	0.698132	0.026595	131	2.286381	0.001095
41	0.715585	0.02363	132	2.303835	0.00114
42	0.733038	0.022145	133	2.321288	0.001145

Monterrey Normal (cont.)					
Scattering angle (deg)	Scattering angle (rad)	Phase function, β	Scattering angle (deg)	Scattering angle (rad)	Phase function, β
43	0.750492	0.02037	134	2.338741	0.001155
44	0.767945	0.018505	135	2.356194	0.001135
45	0.785398	0.016955	136	2.373648	0.00116
46	0.802851	0.015845	137	2.391101	0.00116
47	0.820305	0.01444	138	2.408554	0.001165
48	0.837758	0.01409	139	2.426008	0.001165
49	0.855211	0.01312	140	2.443461	0.00117
50	0.872665	0.01215	141	2.460914	0.00117
51	0.890118	0.011285	142	2.478368	0.00111
52	0.907571	0.01075	143	2.495821	0.001185
53	0.925025	0.010335	144	2.513274	0.001205
54	0.942478	0.009445	145	2.530727	0.001125
55	0.959931	0.00883	146	2.548181	0.001195
56	0.977384	0.00825	147	2.565634	0.00124
57	0.994838	0.00768	148	2.583087	0.001125
58	1.012291	0.00747	149	2.600541	0.001225
59	1.029744	0.006675	150	2.617994	0.001135
60	1.047198	0.00621	151	2.635447	0.001215
61	1.064651	0.005725	152	2.6529	0.001185
62	1.082104	0.005285	153	2.670354	0.001165
63	1.099557	0.00497	154	2.687807	0.00122
64	1.117011	0.00472	155	2.70526	0.00127

Monterrey Normal (cont.)					
Scattering angle (deg)	Scattering angle (rad)	Phase function, β	Scattering angle (deg)	Scattering angle (rad)	Phase function, β
65	1.134464	0.004485	156	2.722714	0.00128
66	1.151917	0.004275	157	2.740167	0.001335
67	1.169371	0.004175	158	2.75762	0.001175
68	1.186824	0.00398	159	2.775074	0.001305
69	1.204277	0.0038	160	2.792527	0.001345
70	1.22173	0.00364	161	2.80998	0.00119
71	1.239184	0.003455	162	2.827433	0.001245
72	1.256637	0.00329	163	2.844887	0.001255
73	1.27409	0.00341	164	2.86234	0.00128
74	1.291544	0.003225	165	2.879793	0.00132
75	1.308997	0.00295	166	2.897247	0.001335
76	1.32645	0.00282	167	2.9147	0.00125
77	1.343904	0.002665	168	2.932153	0.001305
78	1.361357	0.002525	169	2.949606	0.00134
79	1.37881	0.00259	170	2.96706	0.001325
80	1.396263	0.00248	171	2.984513	0.00137
81	1.413717	0.002335	172	3.001966	0.00133
82	1.43117	0.002215	173	3.01942	0.00141
83	1.448623	0.00207	174	3.036873	0.001425
84	1.466077	0.002005	175	3.054326	0.00154
85	1.48353	0.001925	176	3.071779	0.00164
86	1.500983	0.001895	177	3.089233	0.00159

Monterrey Normal (cont.)					
Scattering angle (deg)	Scattering angle (rad)	Phase function, β	Scattering angle (deg)	Scattering angle (rad)	Phase function, β
87	1.518436	0.00158	178	3.106686	0.001445
88	1.53589	0.00172	179	3.124139	0.00184
89	1.553343	0.001615	180	3.141593	0.0018

Possesion Sound					
Scattering angle (deg)	Scattering angle (rad)	Phase function, β	Scattering angle (deg)	Scattering angle (rad)	Phase function, β
0.95288	0.016631	276.7069993	90	1.570796	0.00366
1.12437	0.019624	231.5800009	91	1.58825	0.00338
1.84681	0.032233	96.88430007	92	1.605703	0.00333
2.1787	0.038026	68.80329997	93	1.623156	0.00338
3.03094	0.0529	30.02350006	94	1.640609	0.00341
4.21259	0.073524	14.14879999	95	1.658063	0.00338
4.96338	0.086627	9.760969994	96	1.675516	0.0034
5.84443	0.102004	6.858530003	97	1.692969	0.00321
6.87613	0.120011	4.861780009	98	1.710423	0.00314
8.08068	0.141034	3.407610011	99	1.727876	0.0031
9	0.15708	1.923330001	100	1.745329	0.00314
10	0.174533	1.895009999	101	1.762783	0.00298
11	0.191986	1.45454	102	1.780236	0.00281
12	0.20944	1.379390001	103	1.797689	0.00289
13	0.226893	0.98648	104	1.815142	0.00258

Possesdion Sound (cont.)					
Scattering angle (deg)	Scattering angle (rad)	Phase function, β	Scattering angle (deg)	Scattering angle (rad)	Phase function, β
14	0.244346	0.750789999	105	1.832596	0.00278
15	0.261799	0.87587	106	1.850049	0.00278
16	0.279253	0.68522	107	1.867502	0.00286
17	0.296706	0.446320001	108	1.884956	0.00269
18	0.314159	0.40984	109	1.902409	0.00263
19	0.331613	0.34043	110	1.919862	0.00241
20	0.349066	0.34491	111	1.937315	0.00245
21	0.366519	0.24614	112	1.954769	0.00252
22	0.383972	0.296750001	113	1.972222	0.00261
23	0.401426	0.20893	114	1.989675	0.00249
24	0.418879	0.1976	115	2.007129	0.0024
25	0.436332	0.16658	116	2.024582	0.00221
26	0.453786	0.15278	117	2.042035	0.00213
27	0.471239	0.14191	118	2.059489	0.00231
28	0.488692	0.12526	119	2.076942	0.00216
29	0.506145	0.10924	120	2.094395	0.00222
30	0.523599	0.09729	121	2.111848	0.00232
31	0.541052	0.09825	122	2.129302	0.00238
32	0.558505	0.08324	123	2.146755	0.00226
33	0.575959	0.0764	124	2.164208	0.00233
34	0.593412	0.06739	125	2.181662	0.00244
35	0.610865	0.05999	126	2.199115	0.0024

Possesdion Sound (cont.)					
Scattering angle (deg)	Scattering angle (rad)	Phase function, β	Scattering angle (deg)	Scattering angle (rad)	Phase function, β
36	0.628319	0.0577	127	2.216568	0.00245
37	0.645772	0.05004	128	2.234021	0.00251
38	0.663225	0.04335	129	2.251475	0.00246
39	0.680678	0.04083	130	2.268928	0.00233
40	0.698132	0.03583	131	2.286381	0.0024
41	0.715585	0.03421	132	2.303835	0.00242
42	0.733038	0.03051	133	2.321288	0.00246
43	0.750492	0.03036	134	2.338741	0.00246
44	0.767945	0.03288	135	2.356194	0.00246
45	0.785398	0.03383	136	2.373648	0.00242
46	0.802851	0.02847	137	2.391101	0.0025
47	0.820305	0.02695	138	2.408554	0.00244
48	0.837758	0.02421	139	2.426008	0.00246
49	0.855211	0.02249	140	2.443461	0.00246
50	0.872665	0.0201	141	2.460914	0.0026
51	0.890118	0.01929	142	2.478368	0.00249
52	0.907571	0.01879	143	2.495821	0.00251
53	0.925025	0.01755	144	2.513274	0.00247
54	0.942478	0.01493	145	2.530727	0.00244
55	0.959931	0.01315	146	2.548181	0.00239
56	0.977384	0.01163	147	2.565634	0.00249
57	0.994838	0.01087	148	2.583087	0.00252

Possesdion Sound (cont.)					
Scattering angle (deg)	Scattering angle (rad)	Phase function, β	Scattering angle (deg)	Scattering angle (rad)	Phase function, β
58	1.012291	0.01034	149	2.600541	0.00252
59	1.029744	0.00921	150	2.617994	0.00245
60	1.047198	0.0087	151	2.635447	0.00247
61	1.064651	0.00821	152	2.6529	0.00253
62	1.082104	0.00766	153	2.670354	0.00266
63	1.099557	0.00727	154	2.687807	0.00264
64	1.117011	0.00818	155	2.70526	0.0028
65	1.134464	0.00801	156	2.722714	0.0026
66	1.151917	0.00751	157	2.740167	0.00247
67	1.169371	0.00692	158	2.75762	0.00232
68	1.186824	0.00611	159	2.775074	0.00243
69	1.204277	0.00609	160	2.792527	0.00237
70	1.22173	0.00586	161	2.80998	0.00236
71	1.239184	0.00569	162	2.827433	0.00243
72	1.256637	0.00534	163	2.844887	0.00249
73	1.27409	0.00531	164	2.86234	0.00241
74	1.291544	0.00486	165	2.879793	0.00241
75	1.308997	0.00499	166	2.897247	0.00253
76	1.32645	0.00466	167	2.9147	0.00271
77	1.343904	0.00495	168	2.932153	0.0027
78	1.361357	0.00472	169	2.949606	0.00281
79	1.37881	0.00471	170	2.96706	0.00279

Possesdion Sound (cont.)					
Scattering angle (deg)	Scattering angle (rad)	Phase function, β	Scattering angle (deg)	Scattering angle (rad)	Phase function, β
80	1.396263	0.0043	171	2.984513	0.00317
81	1.413717	0.0044	172	3.001966	0.00316
82	1.43117	0.00416	173	3.01942	0.00334
83	1.448623	0.00446	174	3.036873	0.00331
84	1.466077	0.00403	175	3.054326	0.00336
85	1.48353	0.00437	176	3.071779	0.00363
86	1.500983	0.00417	177	3.089233	0.00378
87	1.518436	0.00403	178	3.106686	0.00318
88	1.53589	0.00393	179	3.124139	0.00417
89	1.553343	0.00391	180	3.141593	0.00417

Ligurian Sea					
Scattering angle (deg)	Scattering angle (rad)	Phase function, β	Scattering angle (deg)	Scattering angle (rad)	Phase function, β
0.5	0.008727	92.26955	90	1.570796	0.00233
0.75	0.01309	60.37593	91	1.58825	0.00213
1	0.017453	50.32526	92	1.605703	0.00212
2	0.034907	25.19488	93	1.623156	0.00209
3	0.05236	13.84616	94	1.640609	0.00198
4	0.069813	8.02717	95	1.658063	0.00191
5	0.087266	5.3043	96	1.675516	0.00207
6	0.10472	3.38681	97	1.692969	0.00193

Ligurian Sea (cont.)					
Scattering angle (deg)	Scattering angle (rad)	Phase function, β	Scattering angle (deg)	Scattering angle (rad)	Phase function, β
7	0.122173	2.41256	98	1.710423	0.00183
8	0.139626	1.74456	99	1.727876	0.00186
9	0.15708	1.24329	100	1.745329	0.00169
10	0.174533	0.82071	101	1.762783	0.00168
11	0.191986	0.68287	102	1.780236	0.00176
12	0.20944	0.57146	103	1.797689	0.00168
13	0.226893	0.47157	104	1.815142	0.00164
14	0.244346	0.36369	105	1.832596	0.00172
15	0.261799	0.29687	106	1.850049	0.0017
16	0.279253	0.27297	107	1.867502	0.00168
17	0.296706	0.22665	108	1.884956	0.00152
18	0.314159	0.18587	109	1.902409	0.0015
19	0.331613	0.15979	110	1.919862	0.00157
20	0.349066	0.13822	111	1.937315	0.00149
21	0.366519	0.13397	112	1.954769	0.00152
22	0.383972	0.13761	113	1.972222	0.00156
23	0.401426	0.11288	114	1.989675	0.00146
24	0.418879	0.10151	115	2.007129	0.00143
25	0.436332	0.09085	116	2.024582	0.00152
26	0.453786	0.08321	117	2.042035	0.0016
27	0.471239	0.07402	118	2.059489	0.00147
28	0.488692	0.06664	119	2.076942	0.00153

Ligurian Sea (cont.)					
Scattering angle (deg)	Scattering angle (rad)	Phase function, β	Scattering angle (deg)	Scattering angle (rad)	Phase function, β
29	0.506145	0.05984	120	2.094395	0.00153
30	0.523599	0.05424	121	2.111848	0.00154
31	0.541052	0.05035	122	2.129302	0.00153
32	0.558505	0.04576	123	2.146755	0.00141
33	0.575959	0.04153	124	2.164208	0.00143
34	0.593412	0.03875	125	2.181662	0.00145
35	0.610865	0.03505	126	2.199115	0.00137
36	0.628319	0.03231	127	2.216568	0.00148
37	0.645772	0.03026	128	2.234021	0.00145
38	0.663225	0.02827	129	2.251475	0.00145
39	0.680678	0.02611	130	2.268928	0.00153
40	0.698132	0.02354	131	2.286381	0.00162
41	0.715585	0.02226	132	2.303835	0.00141
42	0.733038	0.01994	133	2.321288	0.0014
43	0.750492	0.01867	134	2.338741	0.00148
44	0.767945	0.01717	135	2.356194	0.00139
45	0.785398	0.01619	136	2.373648	0.00143
46	0.802851	0.01468	137	2.391101	0.0015
47	0.820305	0.01425	138	2.408554	0.00145
48	0.837758	0.01302	139	2.426008	0.00141
49	0.855211	0.01223	140	2.443461	0.00141
50	0.872665	0.01185	141	2.460914	0.00146

Ligurian Sea (cont.)					
Scattering angle (deg)	Scattering angle (rad)	Phase function, β	Scattering angle (deg)	Scattering angle (rad)	Phase function, β
51	0.890118	0.01091	142	2.478368	0.00143
52	0.907571	0.01047	143	2.495821	0.00144
53	0.925025	0.00943	144	2.513274	0.00155
54	0.942478	0.00907	145	2.530727	0.00136
55	0.959931	0.00809	146	2.548181	0.0014
56	0.977384	0.00762	147	2.565634	0.00135
57	0.994838	0.00719	148	2.583087	0.0013
58	1.012291	0.00669	149	2.600541	0.0013
59	1.029744	0.00642	150	2.617994	0.00133
60	1.047198	0.006	151	2.635447	0.00134
61	1.064651	0.00561	152	2.6529	0.00131
62	1.082104	0.00571	153	2.670354	0.00134
63	1.099557	0.00549	154	2.687807	0.00132
64	1.117011	0.00544	155	2.70526	0.00128
65	1.134464	0.00504	156	2.722714	0.00137
66	1.151917	0.00476	157	2.740167	0.00138
67	1.169371	0.00459	158	2.75762	0.00137
68	1.186824	0.00446	159	2.775074	0.00126
69	1.204277	0.00425	160	2.792527	0.00125
70	1.22173	0.00416	161	2.80998	0.00132
71	1.239184	0.00402	162	2.827433	0.00144
72	1.256637	0.00381	163	2.844887	0.00129

Ligurian Sea (cont.)					
Scattering angle (deg)	Scattering angle (rad)	Phase function, β	Scattering angle (deg)	Scattering angle (rad)	Phase function, β
73	1.27409	0.00392	164	2.86234	0.00139
74	1.291544	0.00357	165	2.879793	0.00155
75	1.308997	0.00357	166	2.897247	0.00143
76	1.32645	0.00362	167	2.9147	0.00155
77	1.343904	0.00323	168	2.932153	0.00158
78	1.361357	0.00304	169	2.949606	0.00153
79	1.37881	0.00304	170	2.96706	0.00149
80	1.396263	0.00297	171	2.984513	0.00154
81	1.413717	0.00285	172	3.001966	0.00149
82	1.43117	0.00281	173	3.01942	0.00154
83	1.448623	0.00277	174	3.036873	0.00135
84	1.466077	0.00247	175	3.054326	0.00142
85	1.48353	0.00269	176	3.071779	0.00139
86	1.500983	0.00254	177	3.089233	0.0012
87	1.518436	0.00229	178	3.106686	0.00087
88	1.53589	0.00234	179	3.124139	0.00078
89	1.553343	0.00237	180	3.141593	0.00078

Snohomish					
Scattering angle (deg)	Scattering angle (rad)	Phase function, β	Scattering angle (deg)	Scattering angle (rad)	Phase function, β
0.95288	0.016631	82.80383663	90	1.570796	0.003185962

Snohomish (cont.)					
Scattering angle (deg)	Scattering angle (rad)	Phase function, β	Scattering angle (deg)	Scattering angle (rad)	Phase function, β
1.84681	0.032233	25.73999761	91	1.58825	0.003167808
2.1787	0.038026	19.29724507	92	1.605703	0.002841043
3.03094	0.0529	10.64368339	93	1.623156	0.002965092
4.21259	0.073524	5.853092443	94	1.640609	0.003049809
4.96338	0.086627	4.486396627	95	1.658063	0.002859196
5.84443	0.102004	3.386196059	96	1.675516	0.002898529
6.87613	0.120011	2.713117059	97	1.692969	0.002771454
8.08068	0.141034	1.919612939	98	1.710423	0.002844068
8.25	0.14399	1.535152393	99	1.727876	0.002816838
8.75	0.152716	1.493338542	100	1.745329	0.002668583
10	0.174533	0.928255465	101	1.762783	0.002559661
11	0.191986	0.81739429	102	1.780236	0.002405356
12	0.20944	0.736317166	103	1.797689	0.002547559
13	0.226893	0.585079299	104	1.815142	0.002487047
14	0.244346	0.502891777	105	1.832596	0.002514277
15	0.261799	0.423502941	106	1.850049	0.002411407
16	0.279253	0.398538678	107	1.867502	0.00245074
17	0.296706	0.342834273	108	1.884956	0.002332741
18	0.314159	0.291402022	109	1.902409	0.002384176
19	0.331613	0.257031155	110	1.919862	0.002223819
20	0.349066	0.221026461	111	1.937315	0.002317613
21	0.366519	0.205955925	112	1.954769	0.002217768

Snohomish (cont.)					
Scattering angle (deg)	Scattering angle (rad)	Phase function, β	Scattering angle (deg)	Scattering angle (rad)	Phase function, β
22	0.383972	0.196216504	113	1.972222	0.002235922
23	0.401426	0.142950736	114	1.989675	0.002287357
24	0.418879	0.124279731	115	2.007129	0.002317613
25	0.436332	0.117792835	116	2.024582	0.002317613
26	0.453786	0.10380244	117	2.042035	0.00225105
27	0.471239	0.093935943	118	2.059489	0.002244999
28	0.488692	0.084490006	119	2.076942	0.002257101
29	0.506145	0.075960827	120	2.094395	0.002269203
30	0.523599	0.073277116	121	2.111848	0.002266178
31	0.541052	0.066160894	122	2.129302	0.002235922
32	0.558505	0.057613561	123	2.146755	0.00227828
33	0.575959	0.054466932	124	2.164208	0.002208691
34	0.593412	0.051156921	125	2.181662	0.002193563
35	0.610865	0.046306877	126	2.199115	0.002241973
36	0.628319	0.043120916	127	2.216568	0.00225105
37	0.645772	0.039459934	128	2.234021	0.002181461
38	0.663225	0.037829133	129	2.251475	0.002193563
39	0.680678	0.034349688	130	2.268928	0.002172384
40	0.698132	0.0316569	131	2.286381	0.002257101
41	0.715585	0.030455735	132	2.303835	0.002151205
42	0.733038	0.026286452	133	2.321288	0.002266178
43	0.750492	0.024637498	134	2.338741	0.002190538

Snohomish (cont.)					
Scattering angle (deg)	Scattering angle (rad)	Phase function, β	Scattering angle (deg)	Scattering angle (rad)	Phase function, β
44	0.767945	0.023294129	135	2.356194	0.002145154
45	0.785398	0.022840288	136	2.373648	0.002166333
46	0.802851	0.02342423	137	2.391101	0.002172384
47	0.820305	0.020773801	138	2.408554	0.002139102
48	0.837758	0.020465189	139	2.426008	0.00207859
49	0.855211	0.018900951	140	2.443461	0.002096744
50	0.872665	0.017188459	141	2.460914	0.002127
51	0.890118	0.015282328	142	2.478368	0.002117923
52	0.907571	0.014395826	143	2.495821	0.002069513
53	0.925025	0.01373927	144	2.513274	0.001933361
54	0.942478	0.013122047	145	2.530727	0.00197572
55	0.959931	0.01248667	146	2.548181	0.001924284
56	0.977384	0.011575963	147	2.565634	0.001921259
57	0.994838	0.011158429	148	2.583087	0.001924284
58	1.012291	0.010722742	149	2.600541	0.001966643
59	1.029744	0.010296132	150	2.617994	0.001933361
60	1.047198	0.010193262	151	2.635447	0.00197572
61	1.064651	0.009155479	152	2.6529	0.001939412
62	1.082104	0.008644152	153	2.670354	0.001990848
63	1.099557	0.00830831	154	2.687807	0.002108846
64	1.117011	0.008244772	155	2.70526	0.001996899
65	1.134464	0.008039031	156	2.722714	0.002096744

Snohomish (cont.)					
Scattering angle (deg)	Scattering angle (rad)	Phase function, β	Scattering angle (deg)	Scattering angle (rad)	Phase function, β
66	1.151917	0.007890777	157	2.740167	0.002120949
67	1.169371	0.007657805	158	2.75762	0.002139102
68	1.186824	0.007064787	159	2.775074	0.002114898
69	1.204277	0.006356795	160	2.792527	0.002114898
70	1.22173	0.00593321	161	2.80998	0.002148179
71	1.239184	0.005939262	162	2.827433	0.002223819
72	1.256637	0.005760751	163	2.844887	0.002223819
73	1.27409	0.005745623	164	2.86234	0.002359972
74	1.291544	0.005576189	165	2.879793	0.0023751
75	1.308997	0.005337166	166	2.897247	0.002420484
76	1.32645	0.004995273	167	2.9147	0.002411407
77	1.343904	0.004644303	168	2.932153	0.002595969
78	1.361357	0.004583791	169	2.949606	0.002617148
79	1.37881	0.004368973	170	2.96706	0.002586892
80	1.396263	0.004486971	171	2.984513	0.002668583
81	1.413717	0.004390152	172	3.001966	0.002735146
82	1.43117	0.004142053	173	3.01942	0.002695814
83	1.448623	0.004111797	174	3.036873	0.002807761
84	1.466077	0.004042208	175	3.054326	0.002825915
85	1.48353	0.003860671	176	3.071779	0.002919708
86	1.500983	0.003518778	177	3.089233	0.002841043
87	1.518436	0.003488522	178	3.106686	0.002502175

Snohomish (cont.)					
Scattering angle (deg)	Scattering angle (rad)	Phase function, β	Scattering angle (deg)	Scattering angle (rad)	Phase function, β
88	1.53589	0.003403805	179	3.124139	0.003098219
89	1.553343	0.003288832	180	3.141593	0.00309822

Chesapeake Bay					
Scattering angle (deg)	Scattering angle (rad)	Phase function, β	Scattering angle (deg)	Scattering angle (rad)	Phase function, β
0.95288	0.016631	312.01845	90	1.570796	0.010987
1.12437	0.019624	266.62805	91	1.58825	0.010842
1.84681	0.032233	106.48949	92	1.605703	0.010982
2.1787	0.038026	81.703612	93	1.623156	0.010027
3.03094	0.0529	46.409104	94	1.640609	0.009691
4.21259	0.073524	24.191683	95	1.658063	0.009126
4.96338	0.086627	17.10033	96	1.675516	0.009495
5.84443	0.102004	12.644386	97	1.692969	0.009325
6.87613	0.120011	9.250423	98	1.710423	0.009174
8.08068	0.141034	6.955285	99	1.727876	0.009268
9.48137	0.165481	5.4515	100	1.745329	0.008982
10	0.174533	4.748139	101	1.762783	0.008866
11	0.191986	3.89586	102	1.780236	0.009169
12	0.20944	3.178567	103	1.797689	0.008853
13	0.226893	2.513428	104	1.815142	0.008682
14	0.244346	2.217259	105	1.832596	0.008665

Chesapeake Bay (cont.)					
Scattering angle (deg)	Scattering angle (rad)	Phase function, β	Scattering angle (deg)	Scattering angle (rad)	Phase function, β
15	0.261799	1.790531	106	1.850049	0.008833
16	0.279253	1.593408	107	1.867502	0.008837
17	0.296706	1.397119	108	1.884956	0.008345
18	0.314159	1.187746	109	1.902409	0.008353
19	0.331613	1.048068	110	1.919862	0.008601
20	0.349066	0.86894	111	1.937315	0.008354
21	0.366519	0.768667	112	1.954769	0.008267
22	0.383972	0.743744	113	1.972222	0.008259
23	0.401426	0.663377	114	1.989675	0.008222
24	0.418879	0.584194	115	2.007129	0.007864
25	0.436332	0.520471	116	2.024582	0.008057
26	0.453786	0.457604	117	2.042035	0.008129
27	0.471239	0.416352	118	2.059489	0.007912
28	0.488692	0.378084	119	2.076942	0.007924
29	0.506145	0.335937	120	2.094395	0.007816
30	0.523599	0.29789	121	2.111848	0.007889
31	0.541052	0.280872	122	2.129302	0.008116
32	0.558505	0.24929	123	2.146755	0.007958
33	0.575959	0.231418	124	2.164208	0.008085
34	0.593412	0.209996	125	2.181662	0.007917
35	0.610865	0.190329	126	2.199115	0.007824
36	0.628319	0.173142	127	2.216568	0.007921

Chesapeake Bay (cont.)					
Scattering angle (deg)	Scattering angle (rad)	Phase function, β	Scattering angle (deg)	Scattering angle (rad)	Phase function, β
37	0.645772	0.160605	128	2.234021	0.007913
38	0.663225	0.147063	129	2.251475	0.007995
39	0.680678	0.138931	130	2.268928	0.007931
40	0.698132	0.12633	131	2.286381	0.007928
41	0.715585	0.114178	132	2.303835	0.00777
42	0.733038	0.105091	133	2.321288	0.008017
43	0.750492	0.099944	134	2.338741	0.007764
44	0.767945	0.093602	135	2.356194	0.00768
45	0.785398	0.08456	136	2.373648	0.007837
46	0.802851	0.078604	137	2.391101	0.008089
47	0.820305	0.074392	138	2.408554	0.007831
48	0.837758	0.06851	139	2.426008	0.007798
49	0.855211	0.062088	140	2.443461	0.007765
50	0.872665	0.059511	141	2.460914	0.007966
51	0.890118	0.057245	142	2.478368	0.007853
52	0.907571	0.051728	143	2.495821	0.008025
53	0.925025	0.050106	144	2.513274	0.008117
54	0.942478	0.045879	145	2.530727	0.008194
55	0.959931	0.043777	146	2.548181	0.008036
56	0.977384	0.04244	147	2.565634	0.007898
57	0.994838	0.039653	148	2.583087	0.00809
58	1.012291	0.037861	149	2.600541	0.007827

Chesapeake Bay (cont.)					
Scattering angle (deg)	Scattering angle (rad)	Phase function, β	Scattering angle (deg)	Scattering angle (rad)	Phase function, β
59	1.029744	0.034379	150	2.617994	0.007805
60	1.047198	0.032966	151	2.635447	0.007792
61	1.064651	0.032384	152	2.6529	0.007884
62	1.082104	0.031377	153	2.670354	0.008197
63	1.099557	0.029624	154	2.687807	0.008159
64	1.117011	0.027537	155	2.70526	0.008416
65	1.134464	0.026484	156	2.722714	0.008454
66	1.151917	0.025017	157	2.740167	0.008822
67	1.169371	0.023344	158	2.75762	0.008804
68	1.186824	0.021617	159	2.775074	0.008702
69	1.204277	0.022069	160	2.792527	0.00893
70	1.22173	0.021366	161	2.80998	0.008873
71	1.239184	0.019433	162	2.827433	0.009216
72	1.256637	0.018825	163	2.844887	0.009399
73	1.27409	0.018292	164	2.86234	0.009728
74	1.291544	0.017508	165	2.879793	0.009666
75	1.308997	0.017685	166	2.897247	0.010319
76	1.32645	0.016712	167	2.9147	0.010258
77	1.343904	0.016703	168	2.932153	0.010527
78	1.361357	0.015219	169	2.949606	0.010975
79	1.37881	0.014896	170	2.96706	0.010934
80	1.396263	0.014402	171	2.984513	0.011048

Chesapeake Bay (cont.)					
Scattering angle (deg)	Scattering angle (rad)	Phase function, β	Scattering angle (deg)	Scattering angle (rad)	Phase function, β
81	1.413717	0.013583	172	3.001966	0.011132
82	1.43117	0.013334	173	3.01942	0.011106
83	1.448623	0.012765	174	3.036873	0.011211
84	1.466077	0.011975	175	3.054326	0.010805
85	1.48353	0.011716	176	3.071779	0.010905
86	1.500983	0.011756	177	3.089233	0.009499
87	1.518436	0.011772	178	3.106686	0.007964
88	1.53589	0.011227	179	3.124139	0.013179
89	1.553343	0.010962	180	3.141593	0.01318

APPENDIX G

EXPERIMENT DATA

This section shows the response of the b_b meter and the b meter in an environment with a known VSF. This step was used to calibrate and test each meter's response.

The meters were submerged in a tank filled with 22.8 L of highly purified water, free of organic elements, filtered through a with a 0.2 μm filter. The first test consisted of adding a solution of 1 ± 0.011 μm diameter polystyrene to the tank; in the second test 4 ± 0.043 μm diameter particles were added.

Each solution (described in the following sections) was pipetted into the tank until the entire solution was added to the tank. The pipetted amounts are indicated in the "Solution added" column of each table. The "CST reading" column displays the raw data collected by the C-Star Transmissometer (CST). This value is converted into particle concentration and used to calculate the expected scattering coefficients via Mie theory. Once the solution in the tank was homogeneous, the meter collected 125,000 data points over a 20 second interval. The values were averaged and the total indicated under the "Average PMT signal" column. The standard deviation of each the averaged value is indicated under "Standard deviation" . Since background noise was not completely eliminated for each test, each dataset set is shifted to 0V such that we only look at the difference in signal created by the change in particle concentration ("Signal minus background").

1μm diameter particle solution: 1230 μl of 1% concentration of 1 $\pm$ 0.011 μm diameter particle in 10 ml of water.					
Solution added (μl)	CST reading (counts)	Calculated b_b from particles (m^{-1})	Average PMT signal (V)	Signal minus background (V)	Standard deviation (V)
0	0.022	0.00E+00	0.068	0.000	0.001
44	0.037	1.88E-04	0.069	0.001	0.002
44	0.052	3.75E-04	0.069	0.001	0.001
44	0.068	5.75E-04	0.070	0.002	0.001
44	0.084	7.75E-04	0.070	0.002	0.001
44	0.1	9.75E-04	0.070	0.003	0.001
1090	0.49	5.85E-03	0.084	0.017	0.001
1090	0.89	1.09E-02	0.098	0.031	0.002
1090	1.28	1.57E-02	0.112	0.044	0.001
1090	1.68	2.07E-02	0.126	0.058	0.001
1090	2.07	2.56E-02	0.139	0.072	0.001
1090	2.46	3.05E-02	0.153	0.085	0.002
1090	2.85	3.54E-02	0.167	0.099	0.002
1090	3.23	4.01E-02	0.178	0.110	0.002
1090	3.59	4.46E-02	0.191	0.123	0.002
850	3.88	4.82E-02	0.202	0.134	0.002

4μm diameter particle solution: 5000 μl of a 1% concentration of 4 $\pm$ 0.043 μm diameter particles in 10 ml of water.					
Solution added (μl)	CST reading (counts)	Calculated b_b from particles (m^{-1})	Average PMT signal (V)	Signal minus background (V)	Standard deviation (V)
0	0.059	0.00E+00	0.094	0.000	0.001
100	0.065	3.14E-04	0.095	0.000	0.001
100	0.071	6.13E-04	0.095	0.001	0.001
100	0.077	8.79E-04	0.096	0.002	0.001
100	0.084	1.21E-03	0.096	0.002	0.001
100	0.09	1.54E-03	0.097	0.003	0.001
720	0.138	3.87E-03	0.104	0.009	0.002
720	0.185	6.18E-03	0.109	0.015	0.002
720	0.232	8.49E-03	0.116	0.021	0.002
720	0.279	1.08E-02	0.122	0.027	0.002
720	0.326	1.31E-02	0.128	0.033	0.002
720	0.373	1.54E-02	0.134	0.039	0.003
720	0.419	1.77E-02	0.140	0.046	0.003
720	0.466	2.00E-02	0.146	0.052	0.003
720	0.512	2.23E-02	0.153	0.059	0.003
720	0.559	2.46E-02	0.159	0.065	0.003
720	0.604	2.68E-02	0.165	0.071	0.003
720	0.65	2.91E-02	0.172	0.077	0.003
720	0.695	3.13E-02	0.177	0.083	0.003
720	0.74	3.35E-02	0.183	0.089	0.004

4μm diameter particle solution (cont.)					
Solution added (μl)	CST reading (counts)	Calculated b_b from particles (m^{-1})	Average PMT signal (V)	Signal minus background (V)	Standard deviation (V)
720	0.785	3.57E-02	0.190	0.096	0.004
720	0.829	3.79E-02	0.196	0.102	0.004
720	0.874	4.01E-02	0.202	0.107	0.004
720	0.917	4.22E-02	0.208	0.113	0.004
720	0.963	4.45E-02	0.214	0.120	0.004
720	1.002	4.64E-02	0.219	0.125	0.004

1 μm diameter particle solution: 80 μl of 1% concentration of 1 $\pm$ 0.011 μm diameter particle solution in 10ml of water					
Solution added (μl)	CST reading (counts)	Calculated b from particles (m^{-1})	Average PMT signal (V)	Signal minus background (V)	Standard deviation (V)
0	-0.018	0	0.075	0	0.063
800	-0.014	3.74E-03	0.079	0.005	0.074
800	-0.010	7.78E-03	0.084	0.01	0.078
800	-0.007	1.12E-02	0.088	0.014	0.082
800	-0.003	1.49E-02	0.094	0.019	0.090
500	0.005	2.32E-02	0.104	0.029	0.102
500	0.014	3.20E-02	0.113	0.039	0.098
1000	0.030	4.82E-02	0.136	0.062	0.126
1000	0.046	6.46E-02	0.157	0.082	0.150
1000	0.063	8.15E-02	0.178	0.103	0.158
1000	0.080	9.83E-02	0.195	0.121	0.186
1000	0.096	1.15E-01	0.215	0.14	0.208
1000	0.113	1.32E-01	0.235	0.16	0.228
1000	0.129	1.48E-01	0.254	0.179	0.240
1000	0.146	1.65E-01	0.271	0.197	0.240
1000	0.162	1.82E-01	0.289	0.215	0.272

4 μm diameter particle solution: 1500 μl of 1% concentration of 4 ± 0.043 μm diameter particle solution in 10ml of water					
Solution added (μl)	CST reading (counts)	Calculated b from particles (m^{-1})	Average PMT signal (V)	Signal minus background (V)	Standard deviation (V)
0	-0.014	0.00E+00	0.059	0	0.004
200	-0.009	5.18E-03	0.065	0.005	0.004
200	-0.007	8.10E-03	0.07	0.01	0.004
200	-0.003	1.23E-02	0.074	0.015	0.004
200	0.001	1.60E-02	0.08	0.02	0.005
200	0.005	2.10E-02	0.083	0.024	0.004
1000	0.020	3.79E-02	0.105	0.046	0.006
1000	0.037	5.64E-02	0.13	0.071	0.007
1000	0.053	7.34E-02	0.15	0.091	0.007
1000	0.069	9.07E-02	0.175	0.116	0.008
1000	0.085	1.08E-01	0.196	0.136	0.009
1000	0.101	1.27E-01	0.222	0.163	0.010
1000	0.117	1.44E-01	0.243	0.184	0.010
1000	0.133	1.61E-01	0.264	0.205	0.010
1000	0.149	1.79E-01	0.285	0.226	0.011
1000	0.165	1.97E-01	0.305	0.246	0.012
500	0.171	2.03E-01	0.312	0.253	0.011